Dissertation
submitted to the
Combined Faculties for the Natural Sciences and for Mathematics
of the Ruperto-Carola University of Heidelberg, Germany
for the degree of
Doctor of Natural Sciences

presented by
Jörg Bajorat, M.Sc.
born in Wiesbaden, Germany

Oral examination:……

Vitamin D_3-upregulated protein 1 (VDUP1), a crucial regulator of the redox equilibrium, controls aging of *Drosophila*

Referees: Prof. Dr. Walter Nickel, Biochemistry Center Heidelberg (BZH)
Prof. Dr. Peter H. Krammer, German Cancer Research Center (DKFZ), Heidelberg

DANKSAGUNG

Ganz herzlich möchte ich mich bei folgenden Personen bedanken:

- Prof. Dr. Peter H. Krammer, dass er mir ermöglicht hat unter seiner Aufsicht an diesem spannenden Projekt zu arbeiten. Mit seinem grenzenlosen Optimismus und der Fähigkeit zur Motivation hat er mir immer das Gefühl gegeben, auf dem richtigen Weg zu sein. Sehr genossen habe ich auch die zahlreichen Exkurse in die Geschichte der Immunologie.
- Prof. Dr. Walter Nickel für die unkomplizierte Betreuung, den Input während der TAC-Meetings und die Übernahme der Rolle des Erstgutachters.
- PD Dr. Karsten Gülow, dass er zu jederzeit ansprechbar war und für (fast) jedes Problem eine Lösung parat hatte. Mit seiner Motivation und seinem Engagement konnte er mir auch in schwierigen Situationen weiterhelfen, sodass ich mich stets gut betreut fühlte.
- Prof. Dr. Bruce Edgar, dass er mir die Möglichkeit gegeben hat, die Fliegenexperimente in seinem Labor durchzuführen. Ferner danke ich für die Bereitstellung notwendiger Materialien, sowie den wissenschaftlichen Input.
- Dr. Aurelio Teleman für die Zurverfügungstellung von Fliegen und seine Hilfe bei der Planung von Experimenten.
- Den Korrekturlesern: Karsten, Tina, Daniel, Selcen, Michael und Heiko.
- Der gesamten Abteilung D030. In dieser Abteilung ist die Arbeitsatmosphäre einfach einzigartig. Neben den fachlichen Diskussionen habe ich auch die sehr freundschaftliche Atmosphäre geschätzt, sodass ich hier viele neue Freunde kennengelernt habe.
- Meiner „Mit-Drosophilistin“ Tina, die mir unermüdlich bei fachlichen Fragen, gerade beim Anfertigen der Doktorarbeit, fast Tag und Nacht zur Verfügung stand. Du hast uns außerdem die notwendige Fachexpertise zum Durchführen der Fliegenexperimente gegeben.
- Meinen Azubis Gawan, Nadine und Yvonne, die immer eine große Hilfe für mich waren und maßgeblich zum Gelingen der Arbeit beigetragen haben.

- Meiner Familie, insbesondere meinen Eltern, die mich auch in schwierigen Phasen während meiner Zeit als Doktorand aufgemuntert und auch finanziell unterstützt haben.
- Meinen Freunden außerhalb des Labors. Ihr habt mir den notwendigen Ausgleich zum manchmal stressigen Laboralltag gegeben.

ABSTRACT

Aging of higher organisms is a complex biological process characterized by progressive deterioration of cellular functions and a higher risk to die within a given time period. Age-related loss of cellular functions can be attributed to damage of macromolecules like DNA, proteins and lipids. In the “free radical theory of aging” Denham Harman claimed that reactive oxygen species (ROS) arising from normal metabolic processes are responsible for accumulation of damage and, therefore, represent the main cause of aging.

Thioredoxin-interacting protein (TXNIP) has been described as a negative regulator of the cellular redox equilibrium, which is attributed to functional inhibition of thioredoxin (Trx). TXNIP overexpression leads to an increased sensitivity towards oxidative damage. In humans, TXNIP was shown to be expressed in an age-dependent manner in various tissues including T cells, hepatocytes and hematopoietic stem cells.

To elucidate the underlying mechanism of TXNIP-induced disturbance of the cellular redox equilibrium a *Drosophila* model was established. For this purpose, Schneider S2 cells were used as an *in vitro* model to overexpress the *Drosophila* TXNIP homologue vitamin D_3-upregulated protein 1 (VDUP1). In this thesis, I show that VDUP1 overexpression leads to increased basal ROS levels and, thus, to a higher sensitivity towards oxidative stress. In addition, to investigate a potential effect of VDUP1 on aging in an *in vivo* model, VDUP1-overexpressing and VDUP1 knockdown flies were generated. High expression of VDUP1 in flies is correlated to a lower resistance to oxidative stress and to a shortened lifespan. Upon VDUP1 knockdown, female flies show a prolonged healthy lifespan in conjunction with an increased oxidative stress resistance.

Taken together, experiments performed in this thesis characterize VDUP1 as an essential regulator in joining oxidative stress resistance to lifespan regulation in *Drosophila*.

ZUSAMMENFASSUNG

Der Alterungsprozess in höheren Organismen ist ein komplexer biologischer Vorgang, welcher durch eine progressive Verschlechterung zellulärer Funktionen sowie ein erhöhtes Sterberisiko gekennzeichnet ist. Diese fortwährende funktionelle Beeinträchtigung im Laufe des Lebens stellt einen Hauptrisikofaktor für verschiedene altersbedingte Erkrankungen dar. Der altersabhängige Funktionsverlust kann auf eine Schädigung von zellulären Makromolekülen, wie zum Beispiel DNA, Proteine und Lipide, zurückgeführt werden. In der so genannten „Theorie der freien Radikale“ formulierte Denham Harman, dass reaktive Sauerstoffspezies (ROS) maßgeblich für die Akkumulation zellulärer Schäden, und damit auch für den Alterungsprozess selbst, verantwortlich sind. Die ROS entstehen hierbei als Nebenprodukte im Rahmen von physiologischen Stoffwechselprozessen. Das Protein Thioredoxin-interacting protein (TXNIP) wurde als ein negativer Regulator der zellulären Redoxbalance beschrieben. Diese Funktion basiert auf der funktionellen Hemmung von Thioredoxin (Trx), welches sich in einer erhöhten Anfälligkeit der Zelle gegenüber oxidativem Stress äußert. Bei Versuchen im humanen System konnte eine altersabhängige Expression von TXNIP in verschieden Zelltypen nachgewiesen werden. Um den Mechanismus der von TXNIP induzierten Beeinträchtigung der zellulären Redoxbalance zu untersuchen, wurde ein *Drosophila*-Modell etabliert. Hierzu wurden Schneider S2-Zellen als ein *in vitro* Modell verwendet, um eine Überexpression des TXNIP-Homologs VDUP1 zu generieren. Es konnte gezeigt werden, dass eine VDUP1-Überexpression zu einer erhöhten basalen Konzentration von reaktiven Sauerstoffspezies führt. Dies wiederum resultierte in einer erhöhten Anfälligkeit gegenüber oxidativem Stress. Zusätzlich zu den *in vitro*-Versuchen wurden *in vivo*-Versuche durchgeführt, die den Zusammenhang zwischen einer Expression von VDUP1 auf Alterungsprozesse klären sollen. Fliegen mit einer erhöhten Expression von VDUP1 waren hierbei durch eine geringere Resistenz gegenüber oxidativem Stress und einer reduzierten Lebensdauer gekennzeichnet. Eine verringerte VDUP1-Expression in weiblichen Fliegen führte hingegen zu einer Verlängerung der Lebensspanne in Verbindung mit einer erhöhten Resistenz gegenüber oxidativem Stress. Zusammenfassend konnte in dieser Arbeit dargelegt werden, dass VDUP1 in *Drosophila* einen zentralen Regulator darstellt, welcher eine verminderte Resistenz gegenüber oxidativem Stress mit einer reduzierten Lebensspanne verbindet.

TABLE OF CONTENTS

1 INTRODUCTION

1.1 Aging

1.1.1 Theories of aging

Aging is a complex mechanism which is determined by a progressive loss of physiological integrity leading to deterioration of cellular function and eventually higher mortality of an organism (López-Otín *et al.* 2013). This lifelong impairment of cellular functions represents a major risk for diverse human pathologies such as diabetes, cardiovascular diseases, neurodegenerative disorders and cancer (López-Otín *et al.* 2013). To date more than 300 different theories of aging have been developed. In general, these can be differentiated into two main categories: **programmed theories and damage theories**.

Programmed theories describe aging as a process which follows an intrinsic preassigned biological schedule. Regulation of this schedule is dependent on gene expression changes in systems which are responsible for maintenance, repair and defense mechanisms. The damage theories describe environmental influences as the primary reason for aging. These extrinsic influences result in an accumulation of damage at various levels of aging (Jin 2010). A summary of the most common aging theories is depicted in Table 1.

Table 1: Overview of different aging theories (adapted from Jin 2010).

Category	Theory	Description
Programmed theories	Programmed longevity	Aging is the result of switching on and off of genes. Age-associated deficits are expressed in the state of senescence (Davidovic *et al.* 2010).
	Endocrine theory	Determination of age by hormonal levels that control aging progression (van Heemst 2010).
	Immunological theory	Programmed decline of the immune system over time which leads to a higher susceptibility to infectious diseases and eventually aging and death (Cornelius 1972).
Damage theories	Wear and tear theory	Cellular components wear out over time which results in aging (Weismann 1882).
	Rate of living theory	The life time of an organism is determined by the rate of oxygen-dependent metabolism (Brys *et al.* 2007).
	Cross-linking theory	Accumulation of cross-linked proteins over time results in a slowdown of cellular processes (Bjorksten 1968).
	Free radical theory	Free radicals damage cellular macromolecules which leads to malfunction of cells and organs (Harman 1956).
	Somatic DNA damage theory	Accumulation of naturally occurring DNA damage due to functionally-declining repair mechanisms (Freitas & de Magalhães 2011).

1.1.1.1 Hayflick limit theory of aging

One of the most popular aging theories is the so called Hayflick limit theory of aging. The theory was first described in 1961 by the American anatomist Leonard Hayflick, who observed that human cells were only able to undergo a certain number of cell divisions (Hayflick & Moorhead 1961). After approximately 50 divisions the cells stopped dividing resulting in replicative senescence. A prolonged state of senescence led to death of the cell which contributed to the aging process. According to the Hayflick limit, the cell division rate needs to be slowed down to avoid cellular damage and prolong the lifespan of the individual. Although Hayflick correlated cellular damage to cell division, he did not further specify the nature of damage. Later, telomere erosion was identified as the reason for the limited rate of cell divisions. Telomeres are shortened with each new round of cell division until induction of replicative senescence (Campisi 2000).

1.1.1.2 Free radical theory of aging

Harman first considered oxidative damage as a cause of aging in 1956. He claimed that aging and degenerative diseases are results of damage by free radicals on cellular components and on connective tissue. Origins of these free radicals are endogenous cellular enzymes catalyzing reactions which involve molecular oxygen (O_2). Moreover, connective tissue contains low amounts of metals which lead to generation of free radicals by the Fenton reaction (Harman 1956). 16 years later, Harman redefined his concept that mitochondria are the origin of free radicals. This theory is today known as the mitochondrial free radical theory of aging (MFRTA) (Harman 1972b). There is much experimental evidence in support of Harman's theory. For instance, age-dependent increase in oxidation of macromolecules could be demonstrated in several animal models (Stadtman 1992). Possible reasons for age-dependent increase in oxidative damage were contributed to a higher sensitivity of tissue towards oxidative damage (Agarwal & Sohal 1996). In addition, age-dependent enhanced mitochondrial ROS production due to a defective complex IV of the electron transport chain (ETC) could be demonstrated for multiple model

organisms such as *C. elegans*, *Drosophila*, mice and humans (Benzi *et al.* 1992; Bowling *et al.* 1993; Schwarze *et al.* 1998). Higher levels of oxidative damage are correlated to multiple age-related diseases (Beckman & Ames 1998). Furthermore, upregulation of the anti-oxidative defense, particularly Cu/Zn-superoxide dismutase and catalase, is correlated with a prolonged lifespan in *Drosophila* (Orr & Sohal 1994). External treatment with antioxidants was shown to prolong lifespan in *Drosophila* (Miquel *et al.* 1980; Viña *et al.* 1992). Besides its function as an adapter protein for various tyrosine kinases p66shc was shown to target the mitochondrial matrix where it regulated generation of oxidative stress. More precisely, in mitochondria, p66shc is bound to heat shock protein 70 (HSP70) under physiological conditions (Orsini *et al.* 2004). Upon oxidative stress p66shc was released allowing interaction witch cytochrome c (Cyt c). Thereby, it exerted oxidoreductase function which mediated transfer of electrons from Cyt c to molecular oxygen. During this process, ROS were generated which led to permeabilization of the mitochondria and induction of apoptosis *via* Cyt c release (Orsini *et al.* 2004; Giorgio *et al.* 2005). Loss of p66shc in mice caused enhanced resistance towards oxidative stress and increased lifespan by 30 % (Migliaccio *et al.* 1999). Therefore, p66shc was shown to be an essential mediator of the oxidative stress response which might be also implicated in aging (Galimov *et al.* 2014).

There were also reports showing no effect on lifespan prolongation in flies after overexpression of Mn-superoxide dismutase (MnSOD) and catalase. Nevertheless, the flies displayed enhanced oxidative stress resistance. As a consequence, this suggested that lifespan was not only dependent on oxidative stress resistance but also on influencing the antioxidant pool (Bayne *et al.* 2005). Other studies showed no connection of oxidative stress or a higher ROS production with lifespan. For instance, mice expressing an impaired mitochondrial DNA (mtDNA) polymerase accumulated DNA damage in mtDNA. Mutations in mtDNA then led to expression of defective proteins which resulted in dysfunctional mitochondria and, therefore, an aging phenotype in the mice. However, it could be shown that mitochondrial dysfunction was not due to an increased ROS production. Anti-oxidative defense enzymes were also unchanged indicating that a defective ETC per se contributed to the aging process (Larsson 2010; Trifunovic *et al.* 2005). Over time, more of these reports occurred which at the end question the MFRTA in its original iteration. Yet, research related to the MFRTA contributed to a new view of ROS as mediators of cellular

signaling (Stuart *et al.* 2014). ROS are known to play a role in diverse cellular processes like cell cycle, proliferation, differentiation, survival and death, which are all linked to aging. For example, mitochondrial ROS are implicated in regulation of the T cell immune response by controlling gene expression (Krammer *et al.* 2007; Kaminski *et al.* 2007). Furthermore, several other factors were shown to interfere with ROS- mediated T cell signaling such as MnSOD, dynamin-related protein 1 (Drp1)-mediated mitochondrial fission or ADP-dependent glucokinase (ADPGK) (Kamiński *et al.* 2012; Kamiński *et al.* 2012; Röth *et al.* 2014). Age-related changes in these factors but also a general increase in oxidative stress could, therefore, lead to deterioration of the ROS signal, which eventually results in a malfunctioning immune system. In the future, MFRTA should be adapted recognizing specific properties of individual ROS, identifying ROS-modulated proteins and considering interaction of ROS with different cell types and cellular processes (Stuart *et al.* 2014).

1.1.2 Molecular mechanisms of aging

1.1.2.1 Genomic instability

Cellular dysfunction due to lifelong accumulation of cellular damage is a characteristic sign of aging (Moskalev *et al.* 2013). Over time this damage leads to DNA mutations as well as diverse chromosomal aberrations and damage due to integrated viral transposons. Altogether, damage could have extrinsic and intrinsic causes. Extrinsic damage is mainly related to chemical, physical as well as diverse biological agents. The source of internal damage is attributed to defective DNA replication and endogenous ROS (Hoeijmakers 2009). The cell has developed efficient mechanisms to repair occurring DNA damage (Lord & Ashworth 2012). However, these repair mechanisms become increasingly insufficient upon aging, which becomes apparent by DNA oxidation. For instance, aging correlated with the occurrence of high amounts of 8-oxoguanosine in nuclear as well as the mitochondrial DNA in flies (Agarwal & Sohal 1994).

1.1.2.2 Epigenetic alterations

Epigenetic changes during the aging process are related to a changed DNA methylation pattern, different histone modifications and remodeling of chromatin. For instance, loss of methylation of lysine 4 in histone 3 (H3K4) or lysine 27 (H3K27) prolonged lifespan in *C. elegans* and *Drosophila* (Greer *et al.* 2010; Siebold *et al.* 2010). Furthermore, many efforts were made in investigating the function of histone deacetylases on lifespan. The silent information regulator 2 (SIR) protein family was extensively studied in the past. SIR2 proteins, or briefly sirtuins, are nicotinamide adenine dinucleotide (NAD)-dependent protein deacetylases and adenosine diphosphate (ADP) ribosyltransferases which regulate gene expression of various transcription factors like nuclear factor kappa-light-chain-enhancer of activated B cells (NF-κB), p53 or heat shock factor 1 (HSF-1). Interestingly, overexpression of Sir2 was correlated to lifespan prolongation. The sirtuin-mediated effect on lifespan is conserved in yeast, nematodes and flies (Kaeberlein *et al.* 1999; Rogina & Helfand 2004; Tissenbaum & Guarente 2001). The mammalian homologue of Sir2, SIRT1, is induced by cellular stress, particularly heat shock, unfolded proteins, hypoxia or ROS (Canto & Auwerx 2009; Westerheide *et al.* 2009). However, although improving healthy aging, an effect on lifespan could not be observed (Herranz *et al.* 2010). In contrast to SIRT1, a beneficial effect of SIRT6 on lifespan in mice could be observed. Loss of SIRT6 expression in mice correlated with signs of enhanced aging whereas SIRT6 overexpression led to prolongation of lifespan. Thereby, beneficial effects of SIRT6 manipulation arose from a reduced insulin-like growth factor-1 (IGF-1) serum levels and an altered IGF-1 signaling (see chapter 1.1.2.5, Mostoslavsky *et al.* 2006; Kanfi *et al.* 2012). There were also reports stating a role of heterochromatin in aging processes. In this connection, heterochromatin domains were lost during aging which results in activation of otherwise silenced genes and, therefore, in aberrant gene expression (Villeponteau 1997). In *Drosophila*, an age-dependent decrease in heterochromatin levels could be demonstrated. In addition, flies showing reduced heterochromatin levels have a significantly shortened lifespan whereas high heterochromatin levels prolong fly lifespan (Larson *et al.* 2012).

1.1.2.3 Telomere erosion

Another well-known age-related molecular change is erosion of telomeres. This process is marked by the inability of somatic cells to sustain their terminal chromosomal region called telomeres (Harley *et al.* 1990). Normally, telomeres are replicated and restored by the enzyme telomerase. However, this restoration is only incomplete leading to shortened telomeres with increasing age (Blasco 2007). Also, it could be demonstrated that the telomere length correlated with replicative capacity (Allsopp *et al.* 1992; Cawthon *et al.* 2003). Advanced telomere erosion leads to critically short telomeres, which induce a senescence response. Each cell type can undergo a certain number of cell divisions before replicative senescence is induced. This limitation is known as the Hayflick limit named after its discoverers Hayflick & Moorhead (1961). In humans, defects in telomerase activity are linked to a loss of tissue regenerative capacity, which is found in aplastic anemia, dyskeratosis, congenital and pulmonary fibrosis (Armanios & Blackburn 2012). In a mouse model of premature aging, genetic telomerase reactivation was shown to reverse aging effects (Jaskelioff *et al.* 2011). Enhanced telomerase expression might be a potential method to slow down or even reverse aging. Yet, there are also studies proving a tumorigenic potential of a higher telomerase activity (Artandi *et al.* 2002). Nonetheless, later it could be shown that systemic viral transduction of adult mice with telomerase resulted in a delayed age phenotype without elevated incidence of cancer (Bernardes de Jesus *et al.* 2012).

1.1.2.4 Loss of protein homeostasis

Maintaining cellular protein homeostasis is crucial for cellular function. On the one hand, the cell possesses several mechanisms to stabilize correctly folded proteins like heat shock proteins. On the other hand, efficient mechanisms to degrade proteins, for example by lysosomes or the proteasome, are required (Hartl *et al.* 2011; Koga *et al.* 2011; Mizushima *et al.* 2008). Defects in the mentioned systems lead to a changed protein homeostasis, which is linked to aging and neurodegenerative diseases such as Alzheimer's or Parkinson's disease (Koga *et al.*

2011; Powers *et al.* 2009). Many studies aimed at modulation of cellular chaperons. Thereby, enhanced chaperon expression in various model organisms was correlated to prolonged lifespan (Morrow *et al.* 2004; Walker & Lithgow 2003). Furthermore, reduced activity in lysosome-mediated autophagy as well as in proteasomal degradation upon aging was reported (Rubinsztein *et al.* 2011; Tomaru *et al.* 2012). For example, mice overexpressing the autophagy receptor lysosome-associated membrane protein 2 (LAMP2a) maintained autophagic activity until old age which was accompanied by ameliorated hepatic function (Zhang & Cuervo 2008). Regarding proteasomal function, pharmacological activation of the proteasome improved the removal of toxic proteins and led to extension of replicative lifespan in yeast (Lee *et al.* 2010; Kruegel *et al.* 2011).

1.1.2.5 Sensing of nutrients

Different pathways are implicated in aging in relation to sensing of cellular nutrients. One of the most studied pathways is the insulin and IGF-1 signaling pathway (IIS pathway), which is shared by insulin as well as by IGF-1. The IIS pathway is highly conserved from worms to humans. Ligand binding induces activation of phosphatidylinositol-3-kinase (PI3K) and protein kinase B (PKB/AKT), which ends in inhibition of forkhead box O (FOXO) proteins. FOXO proteins themselves act as a transcription factor regulating genes involved in proliferation, differentiation, and longevity. Whereas in nematodes and flies a direct involvement of FOXO proteins in regulation of longevity could be shown, an effect in mammals such as mice could not be conclusively demonstrated (Kenyon *et al.* 1993; Slack *et al.* 2011)**.** However, a correlation between certain variants of *FOXO3A* in humans and longevity were reported (Kuningas *et al.* 2007; Willcox *et al.* 2008; Flachsbart *et al.* 2009). Besides manipulation of FOXO proteins, inhibition of upstream components of the IIS pathway is also implicated in lifespan prolongation. In *Drosophila*, the insulin receptor together with the downstream insulin receptor substrate CHICO were described to prolong lifespan up to 50 % (Tatar *et al.* 2001; Clancy *et al.* 2001). Furthermore, *Pten* overexpression and a defective PI3K in mice were also linked to reduced IIS signaling and a prolonged lifespan (Foukas *et al.* 2013; Ortega-Molina *et al.* 2012).

However, null mutants in PI3K or AKT are embryonic lethal (Renner & Carnero 2009).

The Target of Rapamycin (TOR) pathway is another nutrient-sensing pathway, which is highly conserved among all species. Under physiological conditions, the TOR pathway is activated in the presence of high amino acid concentrations whereas low nutrient conditions lead to inactivation (Houtkooper *et al.* 2010). The key protein of the TOR pathway is the serin/threonin kinase mTOR which comprises two protein complexes mTORC1 and mTORC2 (Laplante & Sabatini 2012). Genetic downregulation of mTORC1 as well as pharmacological inhibition by rapamycin are implicated in lifespan extension (Harrison *et al.* 2009; Johnson *et al.* 2013). Furthermore, mice displaying a loss of ribosomal S6 protein kinase 1 (S6K1), a downstream target of mTORC1, also show a long-lived phenotype (Selman *et al.* 2009). Despite the conserved effect on lifespan, TOR inhibition also had undesired effects like insulin resistance and impaired wound healing (Wilkinson *et al.* 2012).

Whereas the TOR pathway is activated by high amounts of nutrients, the AMP-activated protein kinase (AMPK) is activated under starvation conditions in particular by high adenosine monophosphate/adenosine triphosphate (AMP/ATP) ratios (Houtkooper *et al.* 2010). Induction of AMPK leads to both stimulation of catabolic processes to generate ATP and inhibition of anabolic processes, which would otherwise further deplete the cell of nutrients. Therefore, AMPK activation was reported to prolong lifespan in diverse model organisms. Interestingly, AMPK induction also led to mTORC1 inhibition (Alers *et al.* 2012).

In addition, sirtuins are implicated in sensing cellular NAD^+ levels. Besides their function as regulator of heat shock factor expression, sirtuins are also able to modulate activation of the transcriptional coactivator peroxisome proliferator-activated receptor γ (PPARγ) coactivator 1α (PGC-1α) (Rodgers *et al.* 2005). In turn, PGC-1α is crucial for upregulation of genes involved in energy metabolism, mitochondrial biosynthesis and fatty acid (Wu *et al.* 1999; Fernandez-Marcos & Auwerx 2011). An overview of the nutrient sensing pathways involved in aging and dietary restriction is depicted in Figure 1.

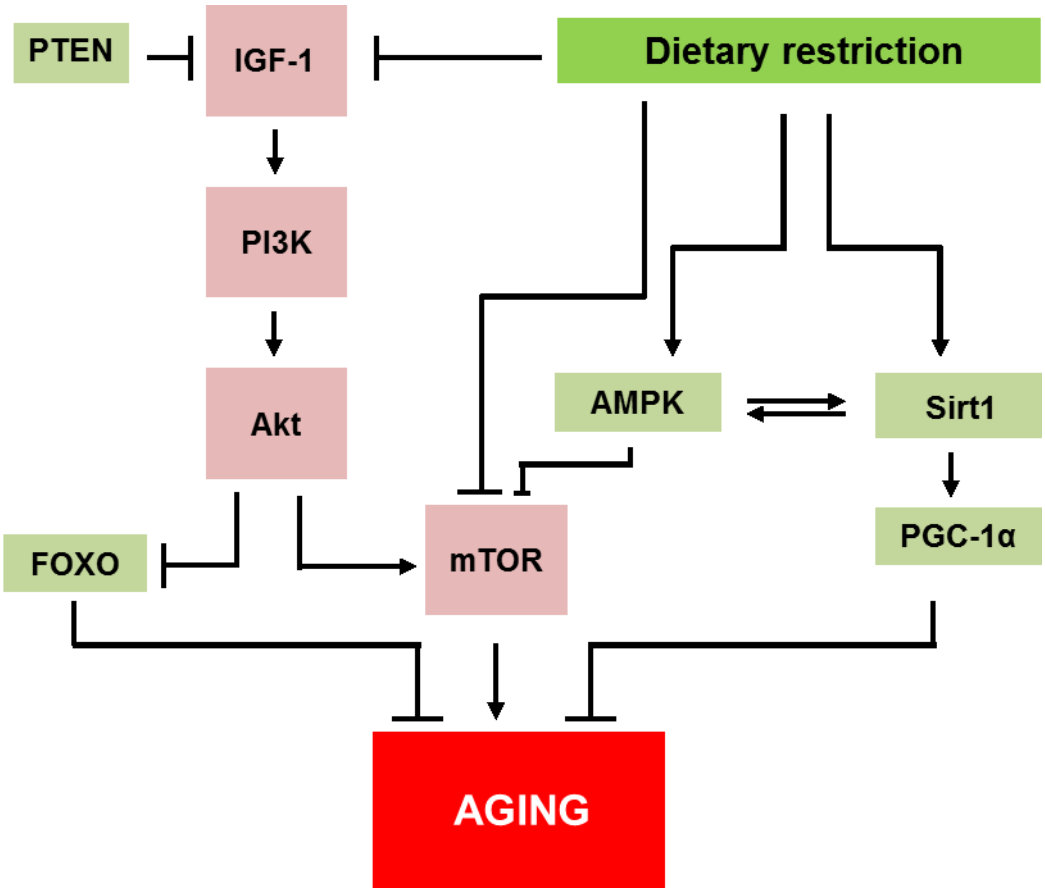

Figure 1: Summary of nutrient sensing pathways involved in aging.
Schematic overview of the insulin/insulin growth factor 1 (IGF-1) signaling pathway (IIS pathway) and its involvement in dietary restriction and aging. Stimulation of IIS pathway leads to mTOR activation and inhibition of FOXO proteins, which favor the aging process. Induction of PTEN or dietary restriction downregulate IIS signaling promoting longevity. Besides direct inhibition of mTOR, dietary restriction accelerates the aging process by activation of AMPK. Furthermore, dietary restriction disfavors aging by upregulation of Sirt1 and enhanced mitochondrial biogenesis *via* PGC-1α. Age-promoting molecules are depicted in red, and molecules with anti-aging properties are shown in green (adapted from López-Otín *et al.* 2013).

1.1.2.6 Mitochondrial dysfunction

Upon aging mitochondria undergo several deteriorating changes which are mostly related to a defective ETC. Defects in the ETC are eventually expressed as enhanced ROS generation due to electron leakage or impaired ATP production (Benzi *et al.* 1992; Bowling *et al.* 1993; Schwarze *et al.* 1998; Green *et al.* 2011). Because mitochondria were described as the primary source of cellular ROS, changes in the mitochondrial redox equilibrium had the most striking impact on aging.

For instance, MnSOD was shown to play a critical role in maintaining the mitochondrial redox balance. Heterozygous knockout of MnSOD resulted in reduced activity of complex I and III in liver mitochondria, whereas homozygous knockout led to reduced activity of complex II (Williams *et al.* 1998; Melov *et al.* 1999). Importantly, MnSOD knockout resulted in $O_2^{-\bullet}$-mediated defects in proteins containing iron-sulfur clusters like the citric acid cycle enzyme aconitase or complex I and II of the ETC. Thereby, iron-sulfur clusters were oxidized which led to Fe^{2+} liberation. In turn, free Fe^{2+} might participate in the Fenton reaction which generates even more $O_2^{-\bullet}$ from H_2O_2 (Melov *et al.* 1999). The importance of MnSOD-mediated mitochondrial redox balance was underpinned in a fly model. Here, MnSOD overexpression led to lifespan prolongation (Sun *et al.* 2002).

In the mitochondrial free radical theory of aging, Harman described that mitochondrial dysfunction results in an increased mitochondrial ROS production and, thereby, accumulation of damage in various macromolecules. Consequently, this cellular damage is responsible for the aging process (Harman 1972b). However, it has been shown that increased mitochondrial ROS levels and oxidative damage in mice do not affect aging (Van Remmen *et al.* 2003; Zhang *et al.* 2009). Moreover, also a physiological role of mitochondrial ROS production was discussed (Sena & Chandel 2012). Hekimi *et al.* (2011) proposed a model of the physiological role of ROS. Here it was stated that basal ROS production, which is part of the cellular homeostasis, acted as a signaling molecule inducing a compensatory stress response, which was beneficial for the organism. However, with increasing age cellular damage accumulates through ROS-independent mechanisms which eventually induce an increasing ROS-mediated stress response. Beyond a certain threshold, the ROS signal itself becomes toxic to cells exacerbating age-dependent damage. In addition to functional damage, an impaired mitochondrial biogenesis could be observed with increasing age. As mentioned before, age-dependent changes in biogenesis are mainly caused by aberrant expression of the transcriptional cofactor PGC-1α or by reduced autophagic activity. Importantly, both mechanisms are regulated by the sirtuin SIRT1 (Rodgers *et al.* 2005; Lee *et al.* 2008).

1.1.2.7 Cellular senescence

Cellular senescence describes a state of a permanent cell cycle arrest which was shown to be increased in cells upon aging (Campisi & d'Adda di Fagagna 2007; Collado *et al.* 2007; Kuilman *et al.* 2010; Wang *et al.* 2009).

In parallel to telomere erosion and DNA damage, other mechanisms exist which contribute to a cellular senescent phenotype. The most prominent example is the age-dependent de-repression of the INK4/ARF locus (Collado *et al.* 2007; Krishnamurthy *et al.* 2004). $p16^{INK4A}$ was originally described as a tumor suppressor gene leading to G_1 cell cycle arrest by inhibition of cyclin-dependent kinase (CDK4)/cyclin D (Serrano 1997). Later an age-dependent expression of $p16^{INK4A}$ was proven in a mouse model and in humans rendering $p16^{INK4A}$ an aging marker (Krishnamurthy *et al.* 2004; Ressler *et al.* 2006). Physiologically, $p16^{INK4A}$-induced senescence could be considered as a beneficial compensatory mechanism in younger individuals leading to protection from cancer and maintenance of tissue homeostasis by removal of damaged cells. However, in older individuals, upregulation of $p16^{INK4A}$ may also be deleterious as cells encounter high levels of cellular damage together with a deficiency in clearance of damaged cells. This potential exhaustion of regenerative capacity eventually results in accumulation of senescent cells and, thereby, accelerates aging (López-Otín *et al.* 2013). In addition, age-dependent increase in cellular ROS levels was also reported to induce cellular senescence in hematopoietic stem cells (Shao *et al.* 2011). Sources of increased ROS levels are mitochondria and/or nicotinamide adenine dinucleotide phosphate (NADPH)-oxidases (NOX). Thereby, ROS induce senescence either *via* activation of ataxia telangiectasia mutated (ATM)-p53-p21 pathway by detection of DNA double strand breaks or *via* activation of p38. However, both pathways result in activation of $p16^{INK4A}$ which is important for senescence induction (Shao *et al.* 2011).

1.1.2.8 Stem cell exhaustion

Reduced replicative potential is a common feature of aged stem cells which impairs organ and tissue integrity (Sharpless & DePinho 2007). Again, stem cell deterioration correlated with DNA damage accumulation, telomere shortening and $p16^{INK4A}$ de-repression (Rossi *et al.* 2007; Janzen *et al.* 2006; Flores *et al.* 2005; Sharpless & DePinho 2007). Moreover, senescence of hematopoietic stem cells (HSC) was correlated to ROS-induced DNA damage as well as p38 activation which converged in $p16^{INK4A}$ de-repression (Shao *et al.* 2011). Conversely, excessive proliferation of the stem cells can be detrimental due to exhaustion of stem cell niches resulting in premature aging (Rera *et al.* 2011). Concerning this matter, $p16^{INK4A}$ de-repression as well as a deregulated IIS pathway could be considered as mechanisms to retain stem cell quiescence. Furthermore, a study from Chakkalakal *et al.* (2012) implicated a role of fibroblast growth factor 2 (FGF2) receptor signaling in preserving stem cell quiescence. Enhanced FGF2 signaling was correlated to stem cell depletion and, therefore, FGF2 inhibition could reverse the effects. Also, several studies pointed to a beneficial effect of stem cell transplantation on lifespan (Lavasani *et al.* 2012).

1.1.2.9 Altered intracellular communication

Another aspect, which is affected during aging, is deregulation of soluble factors involved in intercellular communication. For instance, an aged immune system exhibits a pro-inflammatory phenotype which arises from a process described as “inflammaging” (Salminen *et al.* 2012). Inflammaging is a complex situation which is characterized by a plethora of diverse causes such as an incomplete clearance of pathogens and dysfunctional cells, defective autophagy and accumulation of damaged tissue (Salminen *et al.* 2012). These changes lead to secretion of proinflammatory cytokines like interleukin-1β (IL-1β), tumor necrosis factor α (TNFα), and interferons (Green *et al.* 2011; Salminen *et al.* 2012). Simultaneously to inflammaging, aging in the immune system is marked by immunosenescence (Deeks 2011). Thereby, the function of the immune system declines upon aging which is reflected by impaired clearance of pathogens, infected and transformed, or

senescent cells (Davoli & de Lange 2011). Furthermore, over-activation of certain inflammatory pathways is a feature of aging immune cells. Particularly, constitutive NF-κB pathway activation is a common feature in diverse aging processes. Expression of the NF-κB inhibitor NFKB1$^{\Delta SP}$-ER in the skin of old mice could reestablish a young phenotype (Adler *et al.* 2007). More recently, a study provided a correlation between NF-κB activation and reduced release of gonadotropin-releasing hormone (GnRH) from the hypothalamus (Zhang *et al.* 2013). Here, impaired GnRH release accounted for the development of age-related alterations such as muscle weakness, reduced neurogenesis, and bone fragility. In addition, sirtuins were implicated in downregulation of pro-inflammatory pathways like NF-κB (Xie *et al.* 2013; Kawahara *et al.* 2009; Rothgiesser *et al.* 2010). Age-dependent decline of sirtuins contributed to a higher incidence and progression of inflammatory diseases (Zhang *et al.* 2010; Gillum *et al.* 2011).

Beyond inflammatory processes, there were also reports describing a senescent cell bystander effect which is mediated by gap-junctions and ROS (Nelson *et al.* 2012). More precisely, senescent cells were able to induce DNA damage as well as senescence itself in healthy neighboring cells. In the past, many efforts were made to overcome age-induced alterations in intercellular communication. These efforts include dietary restriction, parabiosis and manipulation of the gut microbiome (Piper *et al.* 2011; Conboy *et al.* 2005; Claesson *et al.* 2012).

1.1.2.10 T cell receptor signaling

Activation of the T cells requires engagement of the adapter proteins zeta chain-associated protein kinase 70 (ZAP70) and linker of activated T cells (LAT) which results in recruitment of phospholipase Cγ1 (PLCγ1) (Chan *et al.* 1991; Finco *et al.* 1998). In turn, PLCγ1 activation follows in the generation of inositol 3,4,5-triphosphate (IP_3) and diacylglycerol (DAG). Whereas IP_3 mediates Ca^{2+} release from the endoplasmatic reticulum (ER) into the cytosol, DAG activates protein kinase Cθ (PKCθ) which facilitates ROS release from the mitochondria. Ca^{2+} release together with the H_2O_2 signal from mitochondria act in concert to induce expression of genes such as cluster of differentiation 95 ligand (CD95L) (Devadas *et al.* 2002; Williamson

1986; Kaminski *et al.* 2007; Gulow *et al.* 2005). Age-related defects were described in nearly all components of the T cell receptor signaling machinery ultimately leading to reduced activation of gene transcription (Whisler *et al.* 1991; Whisler *et al.* 1998; Gupta 1989; Whisler *et al.* 1996). As T cell receptor signaling involves a ROS signal, a well-controlled cellular redox balance is essential for proper functionality. However, during aging, mitochondrial dysfunction resulted in enhanced oxidative signaling/stress which might contribute to a defective T cell function (see chapter 1.1.2.6). Several age-related diseases are correlated to enhanced activation of NOX (Wang *et al.* 2010; Aguirre & Lambeth 2010). Moreover, dual oxidase 1 (DUOX1) was demonstrated to be involved in generation of the ROS signal during T cell receptor activation (Kwon *et al.* 2010). This suggested enhanced generation of ROS due to activation of NOX upon aging and, therefore, an impaired T cell receptor signaling likewise to mitochondrial dysfunction. Beyond the role of mitochondria and NOX, it was shown that age-dependent upregulation of TXNIP inhibited Trx activity, which led to a pro-oxidative shift in T cells (Sass 2010). Figure 2 summarizes all nine hallmarks contributing to the aging process.

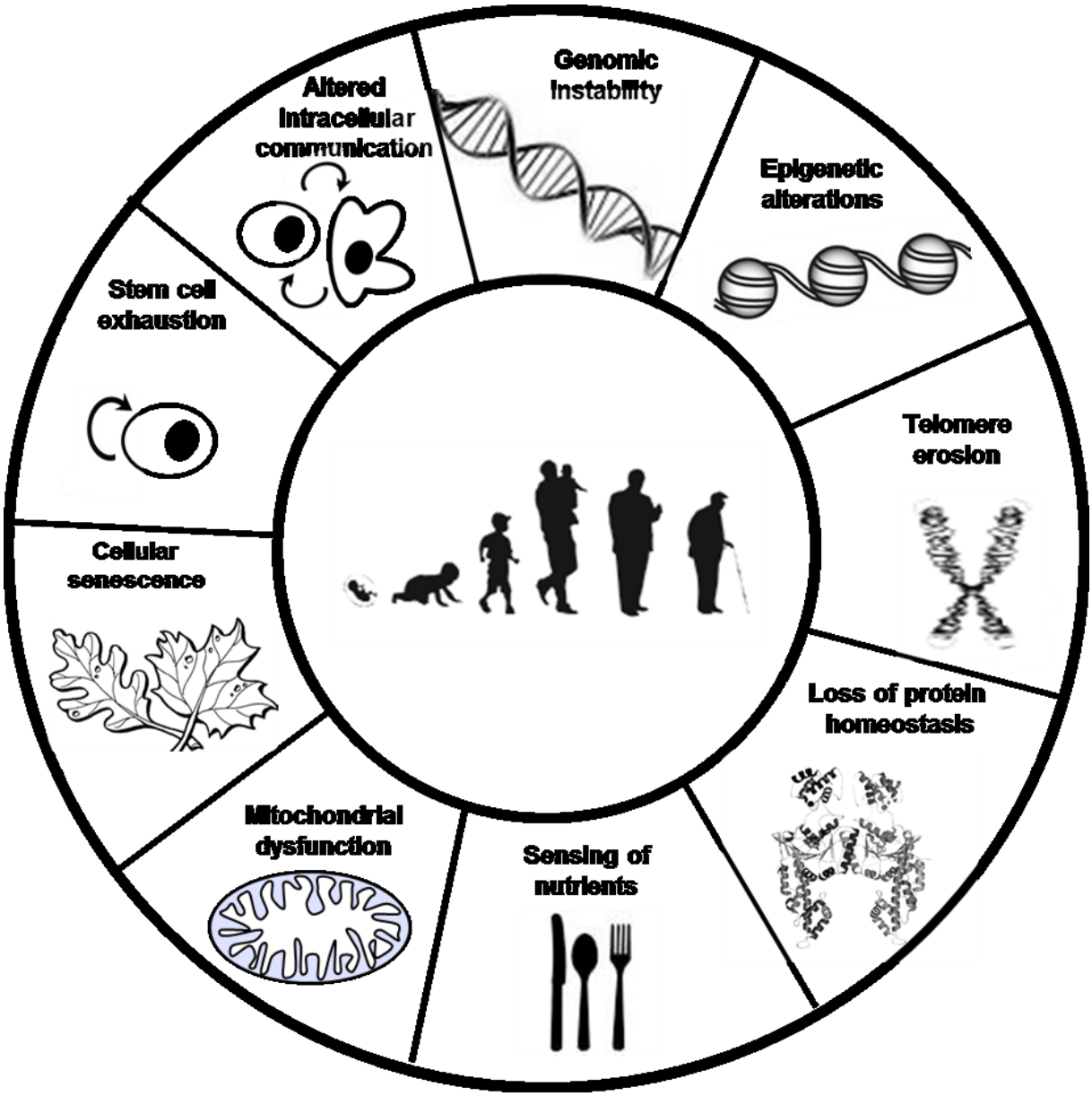

Figure 2: Schematic representation of the nine hallmarks of aging.
Aging processes can be classified into nine different categories which are generally implicated to determine the aging phenotype (adapted from López-Otín *et al.*, 2013).

1.1.3 Manipulation of the aging process

1.1.3.1 Caloric restriction

Caloric restriction (CR) or dietary restriction (DR) describes a diet which is marked by a reduced calorie intake without malnutrition. The aims of CR are general amelioration of health or even prolongation of lifespan. The earliest report of CR is attributed to Luigi Cornaro (1467–1565), a Venetian noble man, who switched to low calorie intake diet at the age of 35. Later, at the age of 83, he published a treatise in which he ascribed his good health conditions and old age to a low calorie intake diet (Speakman & Mitchell 2011). Experimental research on CR started in 20th century with Osborne *et al.* (1917) showing that food restriction in rats was able to prolong the mean as well as the maximum lifespan. To date, lifespan-prolonging effects of CR could be confirmed for a plethora of species including yeast, worms, flies, mice, and dogs. This fact renders CR the only reliable intervention which is able to result in a significant prolongation of lifespan in many diverse organisms (Masoro 2005). General effects of CR related to lifespan prolongation and reduced mortality are decreased blood glucose, improved insulin sensitivity, enhanced immunity, and a positive influence on various cognitive functions (Speakman & Mitchell 2011). Subsequently, also studies on CR in rhesus monkeys were established confirming an amelioration of general health coincided with an improved metabolic profile, reduced risk of cancer, and a better cognitive function (Lane *et al.* 1992; Kemnitz *et al.* 1994; Ingram *et al.* 1990; Colman *et al.* 2009). Many volunteers participate in various studies to investigate CR effects in humans. However, efficiency of CR in humans could not be conclusively demonstrated. Nevertheless, CR positively affected biomarkers of longevity such as insulin sensitivity, reduced risk for cardiovascular diseases, and lower risk of developing cancer (Speakman & Mitchell 2011; Fontana & Klein 2007).

On the molecular level, CR has different consequences, which are mostly tissue-specific. For instance, mitochondria isolated from mice under CR displayed a reduced superoxide radical production (Sohal & Weindruch 1996; Sohal *et al.* 1994) Furthermore, the ratio of reduced to oxidized glutathione (GSH/GSSG ratio) in the kidney was increased after CR. However, no changes in enzymes involved in anti-

oxidative defense like SOD, catalase or glutathione reductase could be observed (Cadenas *et al.* 1994). Consequently, the cellular mitochondrial ROS production was reduced which supersedes regulation of mediators of anti-oxidative defense. Also the influence of CR on mitochondrial metabolic rate gave conflicting results. Whereas in mice CR led to enhanced expression of PGC-1α indicating increased mitochondrial biogenesis, rats did not display an upregulation (Nisoli *et al.* 2005; Hancock *et al.* 2011). Although different studies confirmed that CR increased the expression of SIRT1 in multiple tissues (Kanfi *et al.* 2008; Masoro 2005), other studies showed a reduced SIRT1 activity in the liver, and even an activation of SIRT1 expression by a high-caloric diet (D. Chen *et al.* 2008). Despite the conflicting results, loss of SIRT1 in mice abrogated impact of lifespan underpinning a critical role for SIRT1 in mediating the lifespan-prolonging effect (Boily *et al.* 2008). Yet, the effects of SIRT1 on lifespan could be also explained by prevention of the age-dependent loss of autophagy (Morselli *et al.* 2010; Salminen & Kaarniranta 2009). Being a crucial sensor of cellular energy status, AMPK detected a CR-induced high AMP/ATP ratio and mediated several processes which are known to prolong lifespan. This includes mTOR inhibition, recruitment of sirtuins by increased NAD^+ levels and FOXO activation (Houtkooper *et al.* 2010). Additionally, AMPK-induced increase in NAD^+ levels shifted cellular redox balance towards a more pro-oxidative environment (Cantó *et al.* 2009).

1.1.3.2 Pharmacological intervention

Beyond the possibility to influence the aging process *via* a reduced calorie intake, several drugs were developed which promise to treat age-related diseases like diabetes, neurodegeneration, cancer, and aging itself (Ingram *et al.* 2006; Chen & Guarente 2007). Most of these drugs target cellular components mediating the effects of CR.

The most prominent example for pharmacological intervention is the polyphenol resveratrol. Resveratrol is naturally occurring in the skin of red wine grapes and peanuts. Mechanistically, resveratrol is able to activate sirtuins which modulate expression of genes involved in longevity (Chen & Guarente 2007). First evidence of lifespan prolongation was given in yeast where resveratrol extends replicative

lifespan up to 70 % (Howitz *et al.* 2003). Subsequent studies confirmed an effect in other model organisms like *C. elegans* and *Drosophila* (Wood *et al.* 2004; Greer & Brunet 2009). However, other studies questioned the role of resveratrol in lifespan prolongation in worms and flies (Bass *et al.* 2007; Zou *et al.*) In mice, resveratrol only exhibited reduced mortality under high-fat diet whereas no effect could be observed in mice fed with normal chow (Baur *et al.* 2006; Pearson *et al.* 2008; Miller *et al.* 2011). Besides the questionable effect on lifespan, resveratrol treatment unequivocally displayed improvement of age-related phenotypes in mice including increased aortic elasticity, increased insulin sensitivity, enhanced mitochondrial biogenesis, and improved motor coordination (Baur *et al.* 2006; Pearson *et al.* 2008). Resveratrol was first described as activating SIRT1 (Howitz *et al.* 2003). Yet, there were also reports describing a secondary effect of resveratrol on SIRT1 *via* AMPK or cyclooxygenase-1 (COX1) (Calamini *et al.* 2010). SIRT1 knockout mice were irresponsive to resveratrol treatment indicating that SIRT1 mediated the effects of resveratrol directly or indirectly (Boily *et al.* 2008). From a pharmaceutical point of view resveratrol is a critical compound as it has a low bioavailability and binds to diverse cellular targets. This promotes the search for more potent SIRT1 activators. In first studies these sirtuin-activating compounds (STAC) exerted positive effects on insulin sensitivity and mitochondrial function (Alcaín & Villalba 2009).

Another compound which can be used to mimic CR effects is the biguanide metformin. Metformin is a widely used antidiabetic drug which exerts its function by lowering blood glucose. Moreover, a protective role in cancer could be demonstrated (Anisimov 2010). The relevant function of metformin for lifespan extension is activation of AMPK and subsequent inhibition of mTOR and IGF-1 signaling (Rena *et al.* 2013; McCarty 2004; Sharp 2011). However, in mice, conflicting studies exist questioning the efficacy of metformin in lifespan prolongation (Anisimov *et al.* 2005; Anisimov 2010). In addition to its role in AMPK activation, metformin is also implicated in modulating mitochondrial ROS generation (Kaminski *et al.* 2007). Due to the function as a mild inhibitor of complex I of the mitochondrial ETC metformin reduced activation-induced ROS production after T cell receptor activation (El-Mir *et al.* 2000; Kaminski *et al.* 2007). This indicated a role of metformin in influencing the redox equilibrium and rendered metformin a drug that counteracts age-dependent increase in mitochondrial ROS production. However, ROS display an ambivalent function in the cellular processes. Whereas moderate amounts of ROS are

necessary for maintaining cellular function, high amounts of ROS are toxic to the cell (Hekimi *et al.* 2011). This equivocal function of ROS might explain the conflicting studies regarding the lifespan-prolonging effect of metformin (Anisimov *et al.* 2005; Anisimov 2010).

An alternative approach to interfere with aging is direct targeting of mTOR by rapamycin. Hereby, treatment of mice with rapamycin led to a profound extension of lifespan even when the treatment was started in older mice (Harrison *et al.* 2009; Miller *et al.* 2011). Very recently, pharmacological inhibition of the rat sarcoma (Ras)-extracellular-signal-regulated kinases (ERK)- E-twenty six (ETS) signaling pathway (Ras-Erk-ETS) in *Drosophila* by the mitogen/extracellular signal-regulated kinase (MEK) inhibitor trametinib showed an effect on lifespan extension (Slack *et al.* 2015).

1.1.4 Diseases of premature aging

To date many diseases are known which are related to premature aging. Most diseases share common features occurring in the normal aging process including cardiovascular disorder, organ dysfunction, or neurodegeneration. One possible reason for premature aging is connected to an error-prone DNA repair. For instance, Ataxia telangiectasia (A-T) patients carry a mutation in the *ATM* gene which leads to a defective detection of DNA damage and, thereby, defects in DNA repair (Savitsky *et al.* 1995). A more prominent disease is the so called Werner syndrome which affects the werner syndrome ATP-dependent helicase (WRN). WRN helicases are implicated in cellular mechanisms such as DNA double strand repair. Point mutations in the *WRN* gene lead to expression of an aberrant protein leading to accumulation of DNA damage (Ozgenc & Loeb 2006).

Another disease of premature aging is the Cockayne syndrome. Here, patients harbor a mutation in genes coding for the Cockayne syndrome type A (CSA) or Cockayne syndrome type B (CSB) proteins. In healthy individuals these proteins are responsible to control transcription-coupled repair, which is part of the cellular nucleotide excision repair (Hoeijmakers 2009). Interestingly, induced pluripotent stem

cells (iPSC) from CSB patients displayed higher intracellular levels of ROS which is accompanied by increased expression of TXNIP (Andrade *et al.* 2012).

There are also progeroid diseases which are not associated with DNA damage repair. One of these diseases is the so called Hutchinson-Gilford progeria syndrome (HGPS). Genetically, patients harbor a point mutation in the prelamin A (*LMNA*) gene leading to defective lamin A maturation and an altered nuclear morphology (Eriksson *et al.* 2003). Furthermore, T cells from rheumatoid arthritis (RA) patients have an age-related phenotype including a defective regenerative capacity and high amount of DNA double strand breaks. Both characteristics could be attributed to an impaired telomeric maintenance and a deficiency of the ATM-related DNA repair machinery eventually causing apoptosis of RA cells. In turn, enhanced apoptosis led to chronic proliferative stress which is accompanied by an exhaustion of the immune system (Weyand *et al.* 2009; Weyand *et al.* 2014). In addition, it could be demonstrated that T cells from RA patients showed upregulation of TXNIP expression (Sass 2010). This pointed to a TXNIP-mediated pro-oxidative shift of the cellular redox equilibrium in RA cells leading to impaired T cell signaling. Moreover, T cells from RA patients showed defective phosphorylation of LAT (Gringhuis *et al.* 2000)

1.1.5 *Drosophila* as a model organism to study aging

Drosophila is a widely used model organism to study aging and age-associated diseases. Aging research in flies started in 1916 with Loeb and Northrop who studied the influence of temperature on longevity (Loeb & Northrop 1916). In 1948, Gardner performed the first drug screening in flies to investigate the role of various compounds on lifespan. Here, a lifespan-prolonging effect of biotin, pantothenic acid, and pyridoxine could be demonstrated (Gardner 1948). Today, genetic and molecular tools allow knockout or overexpression of any gene of interest in flies. In particular, the GAL4-upstream activator sequence (UAS) system enables time-dependent and tissue-specific modulation of gene expression. Here, two different fly strains have to be crossed to establish functional modulation of gene expression in the progeny. On the one hand, a driver line harbors genetic information for the yeast-derived transcription factor GAL4 which is coupled to a tissue-specific promotor allowing

tissue-specific manipulation of gene expression. On the other hand, the responder line contains a gene of interest which is joined to an UAS to enable transcriptional activation. In case of knockdown, the gene of interest in the responder line encodes for a short hairpin RNA (shRNA) mediating degradation of a target mRNA by RNA interference (Muqit & Feany 2002). Furthermore, *Drosophila* provides other advantages such as a relatively short lifespan, convenient housing, and husbandry (Rogina 2011; Linford *et al.* 2013). Importantly, the aging process in *Drosophila* and mammals show similarities referring to age-related decline in functional and behavioral performance (Jones & Grotewiel 2011). Referring to Harman's free radical theory of aging, flies were shown to accumulate oxidative damage in DNA, proteins, and mitochondria during aging. Due to this fact, much research was performed to study mitochondrial function in aging. For instance, aging was shown to result in decline in mitochondrial ETC activity (Ferguson *et al.* 2005). In contrast, moderate knockdown, but not a complete knockdown, of genes coding for components of the ETC were demonstrated to prolong fly lifespan (Copeland *et al.* 2009). Additionally, complex IV of the mitochondrial ETC was shown to be critical for mediating the lifespan-prolonging effects of CR (Bahadorani *et al.* 2010). Mitochondrial function was also reported to be linked to age-related diseases such as Alzheimer's disease (Bonner & Boulianne 2011). In addition to mitochondria, *Drosophila* studies contribute to better understanding of processes like maintenance of tissue homeostasis and the influence of environmental factors on longevity (Wang & Jones 2011; Le Bourg 2011).

1.2 Oxidative stress resistance

The utilization of molecular oxygen to generate energy provides the evolutionary basis for the development of higher organisms. However, the use of oxygen also represents a potential risk to the cell as ROS are produced during diverse cellular processes. This requires potent strategies to detect and detoxify potentially harmful agents (Finkel & Holbrook 2000).

1.2.1 Sources of ROS

In most cell types mitochondria represent the main source of ROS. Under physiological conditions mitochondria produce ATP by using the ETC to generate a proton gradient. The mitochondrial ETC consists of four redox complexes which are supplemented by the two mobile electron carriers ubiquinone and Cyt c. Feeding of the ETC takes place either by NADH oxidation at complex I (NADH dehydrogenase) or at complex II (succinate dehydrogenase) *via* oxidation of flavin adenine dinucleotide ($FADH_2$). Subsequently, electrons are transferred to ubiquinone mediating electron transport to complex III (cytochrome c reductase). After reduction by complex III, cytochrome c transfers the electrons *via* complex IV (cytochrome c oxidase) to molecular oxygen. Throughout the ETC, the energy produced at complex I, II and IV is used to mediate translocation of protons from the mitochondrial matrix into the intermembrane space. This proton gradient is then used to induce ATP synthase (complex V), which produces ATP from ADP. The ETC is a well-controlled redox system. However, at complex I or complex III electrons can be directly transferred to molecular oxygen resulting in reduction to superoxide anions ($O_2^{\bullet-}$) (Murphy 2009). Altogether, it is estimated that 1-3 % of the oxygen in the mitochondria undergoes reduction to give rise to highly reactive $O_2^{\bullet-}$(McLennan & Degli Esposti 2000). Mitochondria also served as a redox signaling platform. For instance, activation of the T cell receptor resulted in recruitment of PKCθ which in turn mediated ROS release from complex I of the mitochondrial ETC (Kaminski *et al.* 2007). Furthermore, targeting complex I by metformin or ciprofloxacin reduced signs of inflammation in cells derived from atopic dermatitis patients (Kaminski *et al.* 2010). Moreover, MnSOD was shown to regulate T cell receptor-induced ROS generation by representing a shutdown mechanism induced by activation-induced expression (Kamiński *et al.* 2012). Beyond the role in T cell receptor activation, mitochondria also control other cellular processes such as proliferation. Thereby, it was demonstrated that mitochondrial- or NOX-derived ROS led to cellular senescence by activation of $p16^{INK4A}$. Activation of $p16^{INK4A}$ occurred *via* induction of the p53-mediated DNA damage response or *via* activation of p38 pathway (Shao *et al.* 2011). Moreover, ROS are involved in apoptosis induction *via* the mitochondrial pathway. Upon oxidative stress, induction p66shc translocated to the mitochondria promoting ROS generation by transferring electrons from Cyt c to oxygen (Galimov 2010). Due

to an incomplete reduction of oxygen, massive amounts of ROS were generated resulting in mitochondria degeneration and release of Cyt c.

In addition to mitochondria, NOX are other sources of cellular ROS. NOX2 was discovered in neutrophils as an important ROS source to inactivate phagocytosed pathogens (Hampton *et al.* 1998). Beyond NOX2 the NOX enzyme family comprises six other members NOX1, NOX3-5, as well as the two dual oxidases DUOX1 and DUOX2, which are all involved in host defense and signaling (Aguirre & Lambeth 2010). NOX also take part in diverse physiological signaling processes. During T cell stimulation, an activation of phagocytic NOX2 was described which acted in concert with mitochondria to promote ROS-dependent gene expression (Jackson *et al.* 2004). Later, DUOX1 was described to have a similar function in enhancing T cell signaling (Kwon *et al.* 2010)

Other enzymes involved in ROS production include xanthine oxidase, nitric oxide synthase, cyclooxygenases, cytochrome P450 enzymes and lipoxygenases (Holmström & Finkel 2014). Moreover, other organelles like peroxisomes or the endoplasmatic reticulum (ER) are capable of producing ROS. Yet, the mitochondrial ETC and the NOX enzymes present the major sources of cellular ROS (Holmström & Finkel 2014). An overview of different intracellular sources of ROS is depicted in Figure 3.

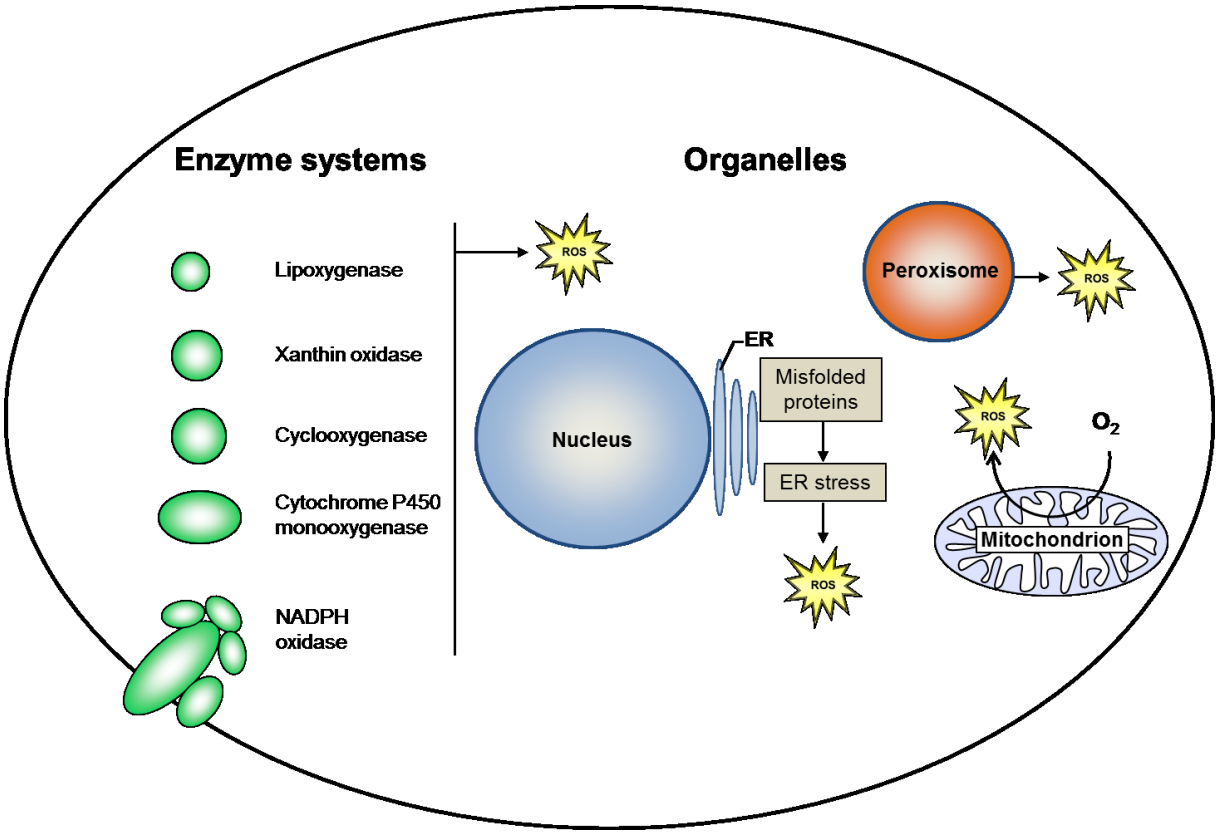

Figure 3: Sources of cellular ROS.
ROS are generated in different cellular organelles such as peroxisomes, mitochondria and the ER. In addition, various cellular enzyme systems including oxygenases and oxidases are considered to contribute sources of intracellular ROS production (adadpted from Holmström & Finkel 2014).

1.2.2 Maintenance of the redox balance

Not only during normal metabolism but also upon removal of pathogens ROS are produced in the cell. To eliminate the potential threat of oxidative damage as well as to maintain the cellular redox balance, efficient systems to neutralize oxidants have evolved. These include various detoxifying enzymes and small-molecule scavengers. The best studied anti-oxidative enzymes are SODs which eradicate highly reactive $O_2^{\bullet-}$ by dismutating it to H_2O_2 and molecular oxygen. SODs can be discriminated due to their subcellular localization and their reactive metal ions in the active center. Whereas CuZnSODs are localized in the cytosol (SOD1) or extracellularly (SOD3), expression of MnSOD (SOD2) is restricted to mitochondria. Three SOD isoforms are conserved in other metazoans such as in *Drosophila* (Blackney *et al.* 2014). MnSOD was described in regulation of T cell receptor signaling where it mediated shutdown

of the ROS signal *via* a feedback mechanism (Kamiński *et al.* 2012). Beyond the enzymatic detoxification by SODs, dismutation of $O_2^{\bullet-}$ also occurs spontaneously by reaction with protons (H^+). However, this process is slow compared to enzymatic dismutation by SODs. Defective removal of $O_2^{\bullet-}$ promotes the reaction with reactive nitrogen species (RNS) such as nitic oxide ($NO^{\bullet}$) resulting in peroxynitrite ($ONOO^{\bullet}$) formation (Fridovich 1995).

Although H_2O_2 is less reactive than $O_2^{\bullet-}$, it can still be converted to highly reactive hydroxyl radicals ($OH^{\bullet}$) by reaction with metal ions like iron (Fe^{2+}) or copper (Cu^{2+}) (Fenton 1894). To avoid further accumulation of H_2O_2 in the cell, other enzymes are needed. The enzyme catalase is a common enzyme catalyzing the reaction of H_2O_2 to oxygen and water. However, catalase is mainly located in peroxisomes demanding other factors to detoxify H_2O_2. One possibility are peroxiredoxins. During catalytic reaction the active center of peroxiredoxins is oxidized. This requires mechanisms to regenerate enzymatic functionality. Trx is able to reduce oxidized thiol groups in the active center of peroxiredoxins (Rhee *et al.* 2001). H_2O_2-induced damage on proteins is characterized by oxidation of thiol groups. To regenerate function, the two enzymatic systems glutathione peroxidase (Gpx)/glutathione reductase as well as Trx/Trx reductase are involved. More precisely, disulfide bridges are reduced back to –SH moieties, which restore protein function. Gpx exerts its function by using the tripeptide glutathione (GSH) as a substrate to reduce oxidized proteins or lipids. However, during this process GSH itself becomes oxidized leading to formation of dimeric glutathione disulfide (GSSG). Glutathione represents the most important redox buffer in the cell underlined by its high abundance in mammalian cells. In healthy cells the reduced form of glutathione is 10- to 100-fold higher than oxidized form. Upon oxidative stress, GSH/GSSG ratio decreases. However, the glutathione redox state is maintained by increased glutathione reductase activity or new synthesis of glutathione by γ-glutamyl cysteine synthetase (γ-GCS) (Filomeni *et al.* 2002). Furthermore, glutathione is associated with immune function. The GSH/GSSG ratio played an essential role in T cells. Whereas a high GSH/GSSG ratio resulted in activation and expression of NF-κB low ratios inhibited its DNA binding activity (Dröge *et al.* 1994). Also, a role of glutathione in sequestration of copper (Cu^{2+}) was reported. By binding of Cu^{2+} reduced GSH prevented the Fenton reaction and, thereby, massive generation of ROS (Ferreira *et al.* 1993). Besides the mentioned

enzymatic systems also non-enzymatic small molecules such as vitamin A, C and E are able to scavenge ROS.

1.2.3 The thioredoxin anti-oxidant system

The Trx anti-oxidant system comprises NADPH, Trx reductase (TrxR), and Trx. These three components build up a major disulfide reductase system, which provides electrons to diverse proteins. The interplay of these components contributes to the maintenance of the cellular redox equilibrium (Lu & Holmgren 2014). In their active center, thioredoxins harbor a CGPC motif which is responsible for catalyzing the protein dilsulfide/dithiol change. Moreover, the CGPC motif is shared with many other enzymes involved in thiol-dependent anti-oxidative defense such as glutaredoxin, peroxiredoxin, and glutathione peroxidase (Fernandes & Holmgren 2004; Wood *et al.* 2003; Ladenstein *et al.* 1979). Upon binding to oxidized proteins, Trx first reduces one thiol group by formation of an intermolecular disulfide bridge with the substrate. This mixed disulfide is cleaved in the second step which includes attack of the second thiol group within the target protein. Thereby, the second thiol group of the protein is reduced and both Trx thiols form a disulfide bridge (Kallis & Holmgren 1980). Formation of the intracellular disulfide bridge renders Trx inactive which necessitates NADPH-dependent recycling by TrxR. Aside from its crucial function in reducing oxidized proteins, the Trx system is also involved in peroxiredoxin-mediated scavenging of H_2O_2. Acting as a substrate, Trx provides electrons to enable recycling of oxidized peroxiredoxins. The mode of action of the Trx system is summarized in Figure 4.

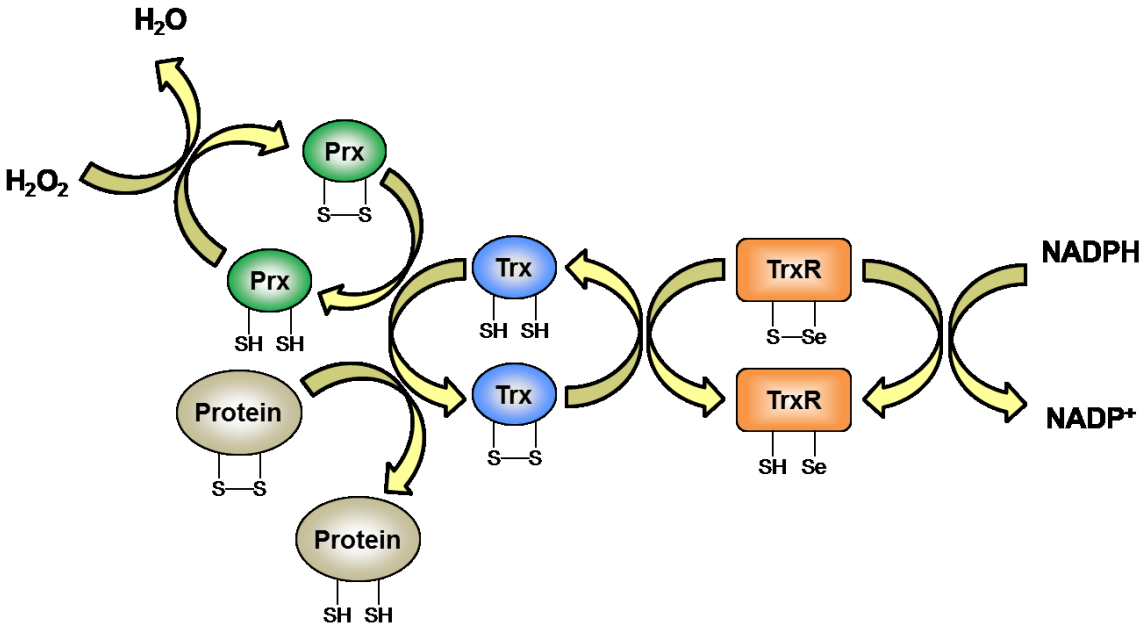

Figure 4: Mode of action of the thioredoxin system.
Reduced Trx catalyzes the reduction of oxidized proteins including Prx. During this process Trx is oxidized. Recycling of Trx function is achieved by TrxR using electrons from NADPH (adapted from Karlenius & Tonissen 2010).

A further functional role of Trx includes modulation of transcription factors such as NF-κB (Hirota *et al.* 1999). Whereas Trx inhibits IκBα degradation and, thereby, NF-κB activation in the cytosol, Trx reduces p50 subunit in the nucleus leading to enhanced DNA binding of NF-κB. Moreover, upregulation of Trx is associated with the development of various cancer types (Nakamura *et al.* 1992; Gasdaska *et al.* 1994; Berggren *et al.* 1996; Kawahara *et al.* 1996).

Regulation of Trx is achieved by various mechanisms. Besides transcriptional regulation by nuclear factor-erythroid 2 p45-related factor 2 (Nrf2) (Hawkes *et al.* 2014; Tebay *et al.* 2015), posttranslational modifications in the cysteine residues including thiol-oxidation, S-nitrosylation, and glutathionylation were described in modifying Trx activity (Haendeler 2006). Furthermore, activity of Trx can be reduced by binding of the endogenous inhibitor TXNIP (Nishiyama *et al.* 1999).

In contrast to the Trx system in mammals, the *Drosophila* system comprises three different thioredoxins including TRX-2, deadhead (DHD) and TrxT (Svensson *et al.* 2003). It has been shown that *dhd* and *TrxT* are organized as a gene pair sharing a common regulatory region Whereas TRX-2 is expressed in larvae, adults, and Schneider S2 cells, expression of DHD and TrxT is gender-specific. DHD is expressed only in female ovaries while TrxT expression is restricted to testis

(Svensson *et al.* 2003). Functional studies describe TRX-2 as a critical mediator of oxidative stress resistance and lifespan in *Drosophila* (Svensson & Larsson 2007). Despite high sequence homology of DHD and TRX-2, DHD is not able to serve as a substrate for thioredoxin peroxidase-1 (Bauer *et al.* 2002). In addition, DHD is an essential factor for early mitotic cell divisions. Loss of DHD led to female sterility (Salz *et al.* 1994). Importantly, Kanzok *et al.* (2001) demonstrated the absence of glutathione reductase in *Drosophila.* Trx reductase adopted the function of glutathione reductase underlining a critical role of the *Drosophila* Trx system in regulation of the cellular redox equilibrium.

1.2.4 Thioredoxin-interacting protein (TXNIP)

TXNIP (TBP-2/ VDUP1) is a 46 kDa protein structurally belonging to the family of α-arrestins. (Alvarez 2008). Originally, TXNIP was identified in HL-60 cells as a protein which was upregulated by vitamin D_3. Therefore, TXNIP is also known as Vitamin D_3-upregulated Protein 1 (Chen & DeLuca 1994). TXNIP was described as a binding partner of Trx (Nishiyama *et al.* 1999). The binding of TXNIP and Trx is dependent on establishment of a disulfide bridge between the oxidized cysteine 247 residue in TXNIP and reduced cysteine 32 in Trx (Patwari *et al.* 2006; Patwari *et al.* 2009). Recently, a disulfide bond-switching mechanism of binding was proposed leading to structural rearrangements in the TXNIP molecule (Hwang *et al.* 2014). Binding of TXNIP to Trx resulted in changes within the TXNIP structure referring to the head-to-tail interprotomer cysteine 63- cysteine 247 which switched to an interdomain cysteine 63- cysteine 190. Due to the new proposed disulfide switching mechanism, TXNIP differs from other members of the α- and β-arrestin family members (Hwang *et al.* 2014; Alvarez 2008). As Trx is an important scavenger of ROS, TXNIP overexpression in an *in vitro* system reduced free levels of Trx and contributed to enhanced cellular ROS levels (Nishiyama *et al.* 1999; Junn *et al.* 2000; Wang *et al.* 2002). In contrast, TXNIP knockout in mice did not show any significant changes in available Trx (Sheth *et al.* 2005; Sheth *et al.* 2006; Chutkow *et al.* 2008).

Overexpression of TXNIP in T cells led to higher activation-induced ROS production together with a reduced resistance towards oxidative stress. In contrast, TXNIP

knockdown resulted in reduced ROS production after T cell activation and a higher resistance towards oxidative stress (Sass 2010). Importantly, TXNIP expression was shown to be upregulated in an age-dependent manner. Therefore, enhanced expression of TXNIP upon aging contributes to the deterioration of T cell function which is associated with a decline of immune function. In addition, age-dependent upregulation of TXNIP was demonstrated in other cell types such as hepatocytes and hematopoietic stem cells (Sass unpublished data). This suggested a general function in regulation of the cellular redox balance.

Beyond the function in the regulation of cellular stress resistance, TXNIP was also implicated in the modulation of cell metabolism. For instance, in the Hcb-19 mouse model of familial combined hyperlipidemia (FCHL), a non-sense mutation in the TXNIP gene could be identified affecting Trx-TXNIP interaction (Bodnar *et al.* 2002). Hcb-19 mice have a metabolic phenotype displaying increased ketone body synthesis together with a decreased CO_2 production. This indicated that Trx inhibition by TXNIP led to changes in citric acid cycle and fatty acid utilization, which affects lipid metabolism (Donnelly *et al.* 2004). Later, a role of TXNIP in defective fatty acid utilization could be confirmed in TXNIP knockout mice. TXNIP knockout mice additionally displayed a higher mortality upon fasting which was attributed to a higher bleeding tendency and renal and hepatic dysfunction (Oka *et al.* 2006). Interestingly, this effect could be abrogated upon glucose feeding. Upon normal feeding, TXNIP knockout mice showed reduced levels of blood glucose compared to WT mice indicating a defective glucose metabolism (Oka *et al.* 2006; Sheth *et al.* 2005). In a genome-wide screen performed with human samples, TXNIP was found to be inhibited by insulin and stimulated upon glucose treatment. Glucose-mediated upregulation is regulated by Max-like protein (Mlx), MondoA and nuclear factor Y (NF-Y) by binding to a carbohydrate response elements (ChoRE) located in the TXNIP promoter (Minn *et al.* 2005; Yu & Luo 2009).

Furthermore, a role of TXNIP in glucose uptake could be confirmed as TXNIP was able to regulate surface expression of the Glut-1 glucose transporter by internalization *via* clathrin-coated pits. However, the internalization of Glut-1 was associated with a tight regulation of TXNIP expression by AMPK upon starvation (Wu *et al.* 2013). The crucial function of TXNIP in glucose metabolism is also reflected by its implication in metabolic diseases like diabetes. Here, glucose-induced expression

of TXNIP was shown to be correlated to disease progression (Schulze *et al.* 2004; Minn *et al.* 2005). TXNIP knockout mice were also described to be protected from glucose-induced toxicity. More precisely, the amount of β-cells in the pancreas and, therefore, their function was preserved (J. Chen *et al.* 2008). In a model of leptin-deficiency, TXNIP is highly expressed in various tissues such as pancreatic islets and skeletal muscles. Additionally, TXNIP knockout restored insulin sensitivity, β-cell function, and survival of the mice (Yoshihara, Fujimoto, *et al.* 2010).

Apart from its role in diabetes TXNIP is also implicated in cardiac metabolism. Upon experimental pressure overload, hearts from TXNIP-KO mice had diminished cardiac hypertrophy and preserved contractility which was attributed to enhanced glucose uptake (Yoshioka *et al.* 2007).

TXNIP is also shown to regulate inflammasome-mediated immune reactions. In macrophages and pancreatic islets, TXNIP is bound to Trx in the unstressed state. Upon oxidative stress, the TXNIP-Trx complex dissociates which allows TXNIP-mediated activation of non-obese diabetic (NOD)-like receptor family pyrin domain containing 3 (NLRP3) inflammasome. Subsequently, NLRP3 inflammasome activation drives caspase-1 recruitment and maturation of IL-1β (Zhou *et al.* 2010; Oslowski *et al.* 2012). However, activation of NLRP3 inflammasome by TXNIP is still a topic of debate as the interaction between TXNIP and NLRP3 could only be shown by one group and was never reproduced (Zhou *et al.* 2010).

As many functions of TXNIP are based on the interaction with Trx, Yoshihara *et al.* (2014) suggested the term “Trx/TXNIP redoxisome” describing the Trx-TXNIP complex as a redox-dependent signaling complex regulating multiple conditions and diseases such as autoimmune disease, diabetes and cancer (Watanabe *et al.* 2010; Masutani *et al.* 2012; Yoshihara, Chen, *et al.* 2010).

A function in apoptosis induction was reported by Saxena *et al.* (2010). After induction of oxidative stress TXNIP is shuttling from the nucleus to the mitochondria *via* an α-importin-mediated mechanism and disrupts Trx2- apoptosis signal-regulating kinase 1 (Trx2-ASK1) interaction. Released ASK1 in turn activates the intrinsic apoptosis pathway.

A recent report from Qiao *et al.* (2015) specified a role for TXNIP in autophagy induction. Together with the intrinsic mTOR inhibitor regulated in development and

DNA damage responses 1 (REDD1), TXNIP formed a complex which induced ROS-mediated autophagy. A loss of REDD1 prevented complex formation with TXNIP and led to failed autophagy due to accumulation of dysfunctional mitochondria.

TXNIP is described as an intrinsic inhibitor of constitutive photomorphogenesis 9 (COP9) Signalosome Subunit 5 (COPS5) mediating the nuclear export of $p27^{kip1}$ (cyclin-dependent kinase inhibitor 1B, CDKN1B) in the cytosol where it is degraded in the proteasome. TXNIP overexpression leads to an enhanced COPS5 inhibition and G_1 cell cycle arrest due to $p27^{kip1}$ accumulation in the nucleus (Jeon *et al.* 2005). In line with this observation, TXNIP was described as a tumor suppressor gene which is reflected by its relatively low expression in various tumors such as hepatocellular carcinoma, breast and gastrointestinal cancer (Ikarashi *et al.* 2002; Yang *et al.* 1998; Sheth *et al.* 2006).

Whereas human TXNIP is well characterized, the *Drosophila* homologue VDUP1 is much less investigated. The *vdup1* locus comprises 2330 bp encoding a protein of 342 amino acids (Figure 5A). VDUP1 is a 38 kDa protein possessing an arrestin C-terminal-like domain as well as N-terminal domains and, thereby, sharing similarities to the human homologue. VDUP1 has shown to be expressed in *Drosophila* brain where it represents an important regulatory target of reverse polarity (REPO) during gliogenesis (Mandalaywala *et al.* 2008). Moreover, higher expression levels could be detected in crop and the salivary gland (Figure 5B). Characterization of the VDUP1 *cis*-regulatory regions revealed homologies to neuronal enhancers such as neurogenin and E-boxes, which are described to mediate glucose-dependent upregulation of the human homologue TXNIP. Upregulation of VDUP1 by glucose resulted in a developmental arrest of the *Drosophila* nervous system pointing to a conserved mechanism between mammals and insects (Levendusky *et al.* 2009). In addition, VDUP1 was found to be downregulated in laminar precursor cells (LPC) which drives development of the *Drosophila* visual system. This downregulation was mediated in a Hedgehog (Hh)-dependent fashion by the transcription factor Cubitus interruptus (Ci). In contrast, in a Hh loss-of-function model, VDUP1 expression was stabilized inhibiting LPC proliferation as well as a proper neurogenesis (Chang *et al.* 2010).

A

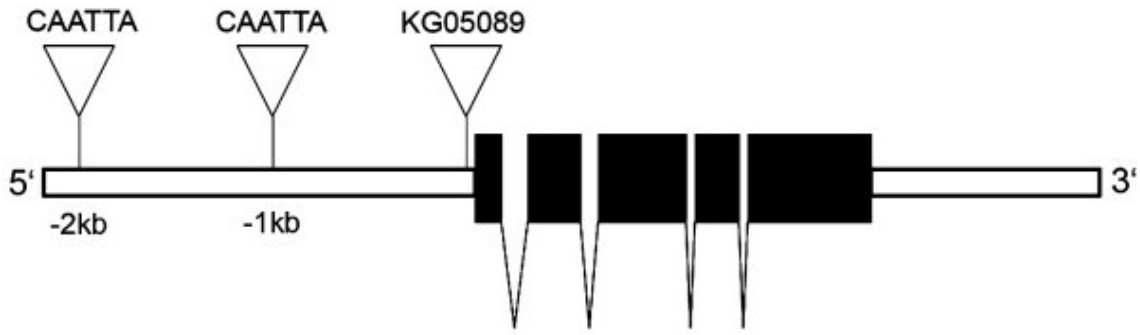

B

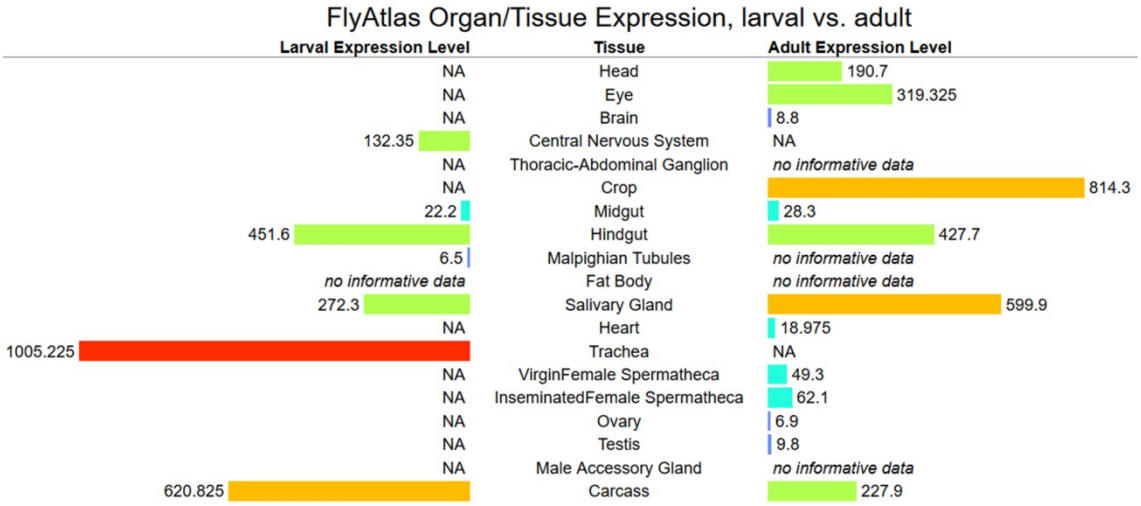

Figure 5: Genetic locus of and expression levels of *Drosophila vdup1.*
(A) The *vdup1* locus has a total length of 2330 bp and consists of five exons (black boxes) and four introns. Two REPO binding motifs (CAATTA) and a potential P-element insertion (KG05089) were identified. Translation yields a protein of 342 amino acids (Mandalaywala *et al.* 2008).
(B) Expression levels of *Drosophila* VDUP1 in diverse tissues from larva (left) and adult flies (right). From: http://www.flybase.org.

1.3 Aim of the study

In previous studies conducted in humans, TXNIP expression was found to be upregulated upon aging in various tissues (Sass 2010). Representing a negative regulator of the cellular redox equilibrium, TXNIP leads to a decreased age-dependent resistance towards oxidative damage. Therefore, this study aims at developing a suitable *in vivo* model to elucidate the underlying mechanism of TXNIP-induced disturbance of the cellular redox balance. Since *Drosophila* is a generally accepted model organism to study aging, the role of TXNIP in aging processes should be investigated in the fly system. After clarification of the mechanism, experiments have been complemented by lifespan data analyzing whether TXNIP expression in flies is part of a general mechanism affecting healthy aging and age-related stress resistance.

2 MATERIALS

2.1 Chemicals

Unless otherwise stated all chemicals were purchased from the companies Fluka (Neu-Ulm), Serva (Heidelberg), Sigma-Aldrich (Munich) or Roth (Karlsruhe).

2.2 Reagents

Reagent	Company
2'-7'- dichlorodihydrofluorescein diacetate (H_2DCFDA)	Life Technologies, Darmstadt, Germany
4-(2-Benzothiazolyl)-4-hydroxy-2,5-cyclohexadien-1-one (PMX 464)	R&D Systems, Wiesbaden, Germany
Amersham ECL Select Western Blotting Detection Reagent	GE Healthcare, Freiburg, Germany
Ampicillin	Sigma-Aldrich, Munich, Germany
BspQI	New England Biolabs, Frankfurt, Germany
Calf Intestinal Alkaline Phosphatase (CIP)	New England Biolabs, Frankfurt, Germany
CellROX® Green Reagent	Thermo Fisher Scientific, Braunschweig, Germany
Diethylpyrocarbonate (DEPC)-supplemented peqGOLD RNase free water	Peqlab, Erlangen, Germany
DNA loading buffer (5x)	Bioline, Luckenwalde, Germany
dNTPs (10 mM mix)	Life Technologies, Darmstadt, Germany
DpnI	New England Biolabs, Frankfurt, Germany
Hoechst® 33342 (10 mg/ml)	Thermo Fisher Scientific, Braunschweig, Germany
Hygromycin B	GERBU Biotechnik, Heidelberg, Germany
HyperLadder™ 1kb	Bioline, Luckenwalde, Germany

KOD buffer (10 x)	TOYOBO, Osaka, Japan
KOD polymerase (1 U/µl)	TOYOBO, Osaka, Japan
Magnesium sulfate ($MgSO_4$)	Life Technologies, Darmstadt, Germany
Mowiol 4-88	Sigma-Aldrich, Munich, Germany
MuLV reverse transcriptase	Life Technologies, Darmstadt, Germany
NEBuffer 4(10 x)	New England Biolabs, Frankfurt, Germany
Power SYBR® Green PCR Master Mix (2 x)	Life Technologies, Darmstadt, Germany
Precision Plus Protein™ All Blue Prestained Protein Standards (10-250 kDa)	Biorad, Munich, Germany
Prestained Protein Marker, Broad Range (7-175 kDa)	New England Biolabs, Frankfurt, Germany
Protein G Sepharose 4 Fast Flow	GE Healthcare, Freiburg, Germany
RNAse inhibitor (20 U/µl)	Life Technologies, Darmstadt, Germany
T4 DNA Ligase (400 U/µl)	New England Biolabs, Frankfurt, Germany
T4 DNA Ligase Buffer (10 x)	Life Technologies, Darmstadt, Germany
T4 polynucleotide kinase (10 U/µl)	Life Technologies, Darmstadt, Germany
TRIzol ® Reagent	Life Technologies, Darmstadt, Germany
Western Lightning™ Plus-ECL	Perkin Elmer, Rodgau, Germany

2.3 Consumables

Consumable	Company
Bacterial culture tubes	Greiner-Bio-One, Frickenhausen, Germany
Cell culture flasks	TPP, Trasadingen, Switzerland
Cell culture plates	TPP, Trasadingen, Switzerland
Costar® -96 well flat micro titer plates black	Sigma-Aldrich, Munich, Germany
Cryo.s™ 2 ml tubes	Greiner-Bio-One, Frickenhausen, Germany
Disposable cuvettes (1.5 ml)	Brand, Wertheim, Germany
Drosophila vials (50 ml)	nerbe plus, Winsen (Luhe), Germany
Dumont tweezers no. 5	Neolab, Heidelberg, Germany
Econo-Column® chromatography column, 1.0 × 30 cm	Biorad, Munich, Germany
FACS tubes	Becton Dickinson, Heidelberg, Germany
Micro pestle	Roth, Karlsruhe, Germany
MicroAmp® Optical 96 well Reaction Plate	Life Technologies, Darmstadt, Germany
Microscopy cover glasses	Langenbrinck, Emmendingen, Germany
Millex-AA Syringe Filter Unit, 0.80 µm	Merck Millipore, Darmstadt, Germany
Millex-GV Syringe Filter Unit, 0.22 µm	Merck Millipore, Darmstadt, Germany
Mite-proof plugs for *Drosophila* vials	Kuhnle, Karlsruhe, Germany
Nitrocellulose membrane Amersham Protran 0.45 NC	GE Healthcare, Freiburg, Germany
Optical Adhesive Covers for qRT-PCR plates	Life Technologies, Darmstadt, Germany
PCR tubes (0.2 ml)	Starlab, Hamburg, Germany
Pipette tips	Starlab, Hamburg, Germany
Pipettes	Gilson, Middleton, USA
Reaction tubes (1.5 ml, 2 ml)	Eppendorf, Hamburg, Germany

Reaction tubes (15 ml, 50 ml)	Becton Dickinson, Heidelberg, Germany
Serological pipets	Becton Dickinson, Heidelberg, Germany
Whatman paper	Biorad, Munich, Germany

2.4 Commercial Kits

Name	Purpose	Company
BCA Assay Kit	Determination of protein concentration	Pierce, Rockford, USA
GeneArt® Genomic Cleavage Detection Kit	Detection of CRISPR-Cas9-mediated genomic cleavage	Life Technologies, Darmstadt, Germany
MinElute Reaction Cleanup Kit	DNA cleanup from enzymatic reactions	QIAGEN, Hilden, Germany
Phusion® High-Fidelity PCR Kit	Polymerase chain reaction	New England Biolabs, Frankfurt, Germany
Plasmid Maxi Kit	Plasmid DNA purification	QIAGEN, Hilden, Germany
Plasmid Mini Kit	Plasmid DNA purification	QIAGEN, Hilden, Germany
QIAquick PCR Purification Kit	PCR product purification	QIAGEN, Hilden, Germany
RNeasy Mini Kit	RNA purification	QIAGEN, Hilden, Germany
Thioredoxin activity assay FkTRX-02	Analysis of thioredoxin activity	BIOZOL Diagnostica, Eching, Germany

2.5 Buffers and Solutions

Buffer	Composition
Annealing buffer (2 x)	20 mM Tris 2 mM EDTA 100 mM NaCl pH 8.0
Blocking solution (western blot)	PBS-T 5 % (w/v) skim milk powder
Coomassie destain solution	30 % ethanol 10 % acetic acid
Coomassie solution	0.26 % (w/v) coomassie brilliant blue R250 40 % (v/v) methanol 10 % (v/v) acetic acid
Elution buffer for antibody purification	0.1 M glycine pH 3.0
HEPES-buffered saline (2 x) (HBS)	50 mM HEPES 1.5 mM NA_2HPO_4 280 mM NaCl pH 7.1
Lysis buffer for cell cycle analysis	0.1 % (w/v) sodium citrate 0.1 % (w/v) Triton X-100 50 µg/ml propidium iodide
Non-reducing sample buffer (5 x)	50 % (v/v) glycerol 10 % (w/v) SDS 50 mM Tris (pH 6.8) 0.25 mg/ml bromphenol blue
PBS-T wash buffer (western blot)	PBS 0.05 % (w/v) Tween-20
PBS^{T++}	PBS 0.1 % Triton X-100 1 mM MgCl2 0.1 mM CaCl2

Phosphate-buffered saline (PBS)	137 mM NaCl 8.1 mM Na_2HPO_4 2.7 mM KCl 1.5 mM KH_2PO_4 pH 7.4
Ponceau S solution	0.1 % (w/v) ponceau S 5 % (v/v) acetic acid
Reducing sample buffer (5 x)	50 % (v/v) glycerol 10 % (w/v) SDS 50 mM Tris (pH 6.8) 25 % β-mercaptoethanol 0.25 mg/ml bromphenol blue
Resolving gel (SDS-PAGE)	24 mM Tris-HCl (pH 6.8) 5 % (w/v) acrylamide 0.1 % (w/v) SDS 0.1 % APS 0.1 % (w/v) TEMED
RF1 buffer	100 mM RbCl 50 mM $MnCl_2$ 30 mM KAc 10 mM $CaCl_2$ 15 % (v/v) glycerol pH 5.8
RF2 buffer	10 mM MOPS 10 mM RbCl 75 mM $CaCl_2$ 15 % (v/v) glycerol pH 6.8
S2 cell lysis buffer	50 mM Tris (pH 7.8) 150 mM NaCl 1 % (v/v) Nonidet P40
SDS extraction buffer (1 x) for protein lysates from fly heads	5 % SDS (w/v) 65 mM Tris-HCl pH 6.8

SDS running buffer	25 mM Tris 0.19 M glycine 1 % (w/v) SDS
Semi-dry transfer buffer	48 mM Tris 39 mM glycine 20 % (v/v) methanol
Stacking gel (SDS-PAGE)	37.5 mM Tris-HCl (pH 8.8) 10 % (w/v) acrylamide 0.1 % (w/v) SDS 0.03 % (w/v) APS 0.1 % (w/v) TEMED
TAE buffer	40 mM Tris acetate 1 mM EDTA pH 7.4
Thioredoxin activity assay lysis buffer	20 mM HEPES (pH 7.9) 100 mM KCl 300 mM NaCl 10 mM EDTA 0.1 % (v/v) Triton X-100
Wash buffer for antibody purification	0.1 M Tris pH 8.0
Western blot stripping buffer	62.5 mM Tris-HCl (pH 8.0) 100 mM β-mercaptoethanol 2 % (w/v) SDS
Western blot transfer buffer	25 mM Tris 190 mM glycine 20 % (v/v) methanol

2.6 Culture Media

2.6.1 Bacterial culture media

Media for bacterial culture were autoclaved at 125°C for 30 min and stored at 4°C until further use. To select for positive clones lysogeny broth (LB) medium was supplemented with ampicillin (100 µg/ml)

Medium	Content
Grape agar plates	0.3 % (w/v) agar 1.67 % (w/v) saccharose 1.33 % (v/v) nipagin (10% solution in EtOH) 33.3 % red grape juice
LB agar	20 g agar per 1 l LB medium
Lysogeny broth (LB) medium	10 g tryptone 5 g yeast extract 10 g NaCl pH 7.4 ad 1 l ddH_2O
Standard fly food (produced at DKFZ *Drosophila* Facility, Heidelberg, Germany)	0.8 % (w/v) agar 8 % (w/v) cornmeal 1 % (w/v) soy flour 1.8 % (w/v) brewer's yeast 8 % (w/v) malzin 2.2 % (w/v) Grafschafter Goldsaft 0.62 % (v/v) propionic acid 0.06 % (v/v) phosphoric acid 1 % (v/v) ethanol 0.24 % (w/v) nipagin

2.6.2 Media and supplements for eukaryotic cell culture

In general, media were supplemented with 10 % (v/v) heat-inactivated fetal calf serum (FCS) and stored at 4 °C until further use

Reagent	Company
FCS	Sigma-Aldrich, Munich, Germany
Freezing medium	90 % (v/v) FCS, 10 % (v/v) DMSO
Hygromycin B	GERBU Biotechnik, Heidelberg, Germany
Penicillin-Streptomycin (10,000 U/ml)	Life Technologies, Darmstadt, Germany
Puromycin	Sigma-Aldrich, Munich, Germany
Roswell Park Memorial Institute (RPMI)-1640 medium	Sigma-Aldrich, Munich, Germany
Schneider's Insect Medium	Sigma-Aldrich, Munich, Germany

2.7 Biological materials

2.7.1 Bacterial strains

Strain	Experimental purpose	Company
E. coli DH5α	Vector amplification and cloning	Life Technologies, Darmstadt, Germany

2.7.2 Eukaryotic cell lines

Strain	Characteristics	Medium
Hybridoma cells (generated at the Monoclonal Antibody Facility, DKFZ)	Secretion of α-Vdup1-specific antibody	RPMI-1640
Schneider's *Drosophila* Line 2 (S2)	late embryonic *Drosophila melanogaster* cell line	Schneider's Insect Medium

2.8 Antibodies

2.8.1 Primary antibodies for Western blotting

Primary antibodies for immunoblot were diluted in Western blot blocking solution as indicated in the following table:

Name	Antigen	Isotype	Dilution	Company
Anti (α)-Trx-2	TRX-2	Rabbit polyclonal	1:1000	K. Becker, University of Gießen, Gießen, Germany
α-V5	V5-tag	Mouse monoclonal immune globulin (Ig) G2A	1:5000	Life Technologies, Darmstadt, Germany
α-VDUP1	VDUP1	Mouse monoclonal IgG2B	1:1000	Monoclonal Antibody Facility, DKFZ, Heidelberg, Germany

α-β-tubulin E7	β -tubulin	Mouse monoclonal IgG1	1:1000	Developmental Studies Hybridoma Bank at the University of Iowa (DSHB), Iowa City, USA

2.8.2 Secondary HRP- conjugated antibodies

Horseradish peroxidase (HRP)-conjugated secondary antibodies were diluted 1: 10000 in Western blot blocking solution.

Specificity	Isotype	Company
Mouse IgG	Goat polyclonal	Santa Cruz, Heidelberg, Germany
Mouse IgG2A	Goat polyclonal	SouthernBiotech, Birmingham, USA
Mouse IgG2B	Goat polyclonal	SouthernBiotech, Birmingham, USA
Rabbit IgG	Goat polyclonal	Santa Cruz, Heidelberg, Germany

2.9 Materials for molecular biology

2.9.1 Polymerase chain reaction (PCR) primers

Primers were designed using Primer- Basic Local Alignment Search Tool (BLAST) online tool provided by the National Center for Biotechnology Information (Bethesda, USA). The tool is accessible online under the URL http://www.ncbi.nlm.nih.gov/tools/primer-blast. All primers were synthesized by Sigma-Aldrich (Munich, Germany).

Name	Primer orientation	Sequence (5'-3')
Oligo dT		TTTTTTTTTTTTTTT
Vdup1 fwd *EcoRV*	Forward	GCCGATATCATGCCGCGCAAGTTGC
Vdup1 rev *XhoI*	Reverse	CCGCTCGAGTGCCTCGATAGGCTTCTCG
Vdup1-C1-ol_fw	Forward	TGGATTCAGTTCTACGCAAAGGCGGCGCTCCG
Vdup1-C1-ol_rv	Reverse	CGGAGCGCCGCCTTTGCGTAGAACTGAATCCA
Vdup1-C2-ol_fw	Forward	GCACAACCGTTCACCGCCGAAGTTGAGCACAAG
Vdup1-C2-ol_rv	Reverse	CTTGTGCTCAACTTCGGCGGTGAACGGTTGTGC
Vdup1-C3-ol_fw	Forward	CAAGCTAGGCGTCGTCGCTGTTAGTGGAGGTCAG
Vdup1-C3-ol_rv	Reverse	CTGACCTCCACTAACAGCGACGACGCCTAGCTTG
Vdup1-C4-ol_fw	Forward	GTGGAGGTCAGATAAAGGCCAGAGTGTCCCTTGATC

Vdup1-C4-ol_rv	Reverse	GATCAAGGGACACTCTGGCCTTTATCTGACCTCCAC
Vdup1-C5-ol_fw	Forward	CGACCAATCTTCATGGCGCCCGCCTGATCAAAATATC
Vdup1-C5-ol_rv	Reverse	GATATTTTGATCAGGCGGGCGCCATGAAGATTGGTCG
Vdup1-cl_det-fw	Forward	CCATAATGACGCGTGCGGAG
Vdup1-cl_det-rv	Reverse	GTGGCAAGCCGAGTTTGAAG

2.9.2 Primers for quantitative RT-PCR

Primers for qRT-PCR were designed using the Primer-BLAST online tool provided by the National Center for Biotechnology Information (Bethesda, USA, http://www.ncbi.nlm.nih.gov/tools/primer-blast). In addition, primers were chosen to be exon-spanning. All primers were synthesized by Sigma-Aldrich (Munich, Germany).

Name	Primer orientation	Sequence (5'-3')
dhd-fw	Forward	GTAAGCGCGAGATGTGGGTA
dhd-rv	Reverse	CGCGCCACAAATCATAGCAT
drosCatalase-fw	Forward	CAACCCCTTCGATGTCACCA
drosCatalase-rv	Reverse	TCTGCTCCACCTCAGCAAAG
drosSOD2-fw	Forward	AGCGAAATAACGAGAACGTAAGC
drosSOD2-rv	Reverse	CCGCCAGGCTTGCAGTTTG
drosSOD3-fw	Forward	CTTAACTGGCAAGCTGGGGA
drosSOD3-rv	Reverse	CTGCATTGCCGGTCTTCTTG

drosSOD-fw	Forward	ACACGAGCTGAGCAAGTCAA
drosSOD-rv	Reverse	CAGTGGCCGACATCGGAATA
drosTrx-2A-fw	Forward	GCGACGTGCTCATTTTGGTAA
drosTrx-2A-rv	Reverse	GGATGGGAGATGTGGAGACG
drosTrx-2B-fw	Forward	GCATAGTGGCCAGCAAAACC
drosTrx-2B-rv	Reverse	ACAGGCTCACGCTTCTCATT
drosTrxT-fw	Forward	TGTACCCAGTGCGGAACAAG
drosTrxT-rv	Reverse	TCGTCCACGTTCACCTTGAG
Rp49-fw	Forward	CGGATCGATATGCTAAGCTGT
Rp49-rv	Reverse	CGACGCACTCTGTTGTCG
Vdup1_ex3-4-fw	Forward	AAGGCATCCCTCACTGAGAC
Vdup1_ex3-4-rv	Reverse	AGCTCCCGTTTTTCCGTTTG

2.9.3 Vectors

Plasmid	Description	Company
pAc5.1/V5-His A	Vehicle control vector	Life Technologies / B. Linke, DKFZ
pAc5.1/V5-His A Vdup1	VDUP1 overexpression vector for S2 cells	Generated during this study
pAc-sgRNA-Cas9-Puro	Expression of target sgRNA and Cas9 in S2 cells	Addgene / Dr. Ji-Long Liu, University of Oxford, Great Britain
pAc-sgRNA-Cas9-Puro-Vdup1-K1A	Expression of target Vdup1-K1A-sgRNA and Cas9 in S2 cells	Generated during this study

pAc-sgRNA-Cas9-Puro-Vdup1-K2D	Expression of target Vdup1-K2D-sgRNA and Cas9 in S2 cells	Generated during this study
pAc-sgRNA-Cas9-Puro-Vdup1-K1B	Expression of target Vdup1-K1B-sgRNA and Cas9 in S2 cells	Generated during this study
pCoHygro	Hygromycin B resistance plasmid	Life Technologies / B. Linke, DKFZ
PFLC1 cDNA (RE65532) Vdup1	Origin of VDUP1 cDNA for cloning	*Drosophila* Genomics Resource Center (DGRC), Bloomington, IN, USA

2.10 Instruments

Instrument	Company
7500 Real time PCR systems	Life Technologies, Darmstadt, Germany
Agarose gel electrophoresis chamber PerfectBlue Gel System Mini	Peqlab, Erlangen, Germany
Analysis Scale	Sartorius, Göttingen, Germany
Bacterial shaker Multitron Standard	Infors, Bottmingen, Switzerland
BioPhotometer	Eppendorf, Hamburg, Germany
C1000 Thermal cycler	Biorad, Munich, Germany
Centrifuge 5810R	Eppendorf, Hamburg, Germany
Centrifuge Megafuge 3.OR	Haereus, Hanau, Germany
Centrifuge Megafuge 3.ORS	Haereus, Hanau, Germany
FACS Canto II flow cytometer	Becton Dickinson, Heidelberg, Germany

Gel Doc™ XR+ System	Biorad, Munich, Germany
GeneAmp PCR system 9700	Life Technologies, Darmstadt, Germany
GloMax®-Multi+ Detection System	Promega, Mannheim, Germany
Heating block Thermostat 5320	Eppendorf, Hamburg, Germany
Heracell™ 240i CO2 incubator	Thermo Fisher Scientific, Braunschweig, Germany
Image acquisition system Chemi-Smart 5100	Vilber Lourmat, Eberhardzell, Germany
LSM 710 confocal microscope	Carl Zeiss Microscopy, Jena, Germany
Microscope Axiovert 25	Zeiss, Jena, Germany
Microwave oven	
Mini-PROTEAN II® electrophoresis chamber	Biorad, Munich, Germany
Mini-PROTEAN® Tetra cell	Biorad, Munich, Germany
Model 680 Microplate Reader	Biorad, Munich, Germany
NanoDrop ND-1000	Thermo Fisher Scientific, Braunschweig, Germany
neoMag Magnetic Stirrer	Neolab, Heidelberg, Germany
Neubauer counting chamber	Brand, Wertheim, Germany
Orbital Shaker 3015	GFL, Burgwedel, Germany
peqPOWER E300 power supply	Peqlab, Erlangen, Germany
PerfectBlue™ 'Semi-Dry' Electro Blotter	Peqlab, Erlangen, Germany
Peristaltic pump P-1	GE Healthcare, Freiburg, Germany
PH meter ProfiLine pH 3210	WTW, Weilheim, Germany
PIPETBOY acu	INTEGRA Biosciences, Zizers, Switzerland
Power supply Consort E865	Consort, Turnhout, Belgium

Refrigerator -20°C	Liebherr, Biberach, Germany
Refrigerator -80°C	ThermoLife Science, Egelsbach, Germany
Roller Cat. RM5	Neolab, Heidelberg, Germany
Safety cabinet place HeraSafe	Heraeus, Hanau, Germany
Sorvall Evolution RC	Thermo Fisher Scientific, Braunschweig, Germany
Tabletop centrifuge Fresco 17	Thermo Scientific, Braunschweig, Germany
Thermomixer compact	Eppendorf, Hamburg, Germany
Vortex mixer	Neolab, Heidelberg, Gemany
Water bath	Lauda, Lauda-Königshofen, Germany

2.11 Software

Software	Company
7500 Software version 2.0.1	Life Technologies, Darmstadt, Germany
Ammonium Sulfate Calculator	EnCor Biotechnology, Gainesville, USA
Chemi Capt version 15.01	Vilber Lourmat, Eberhardzell, Germany
E-CRISP-Version 4.0	Florian Heigwer, DKFZ Heidelberg, Germany
FACSDIVA™ 6.1.2	Becton Dickinson, Heidelberg, Germany
Flow Jo version 7.6.5	FlowJo LLC, Ashland, USA
Graph Pad Prism version 4.5	GraphPad Software, La Jolla, CA, USA
Image Lab 5.1 beta	Biorad, Munich, Germany
Instinct software version 3.1.3	Promega, Mannheim. Germany
Microplate Manager version 5.2.1	Biorad, Munich, Germany

Microsoft Office 2010	Microsoft, Unterschleißheim, Germany
NanoDrop 1000 version 3.7.1	Thermo Fisher Scientific, Langenselbold, Germany
PrimerX	Carlo Lapid, National Institute of Molecular Biology and Biotechnology (NIMBB) at the University of the Philippines, Diliman, Philippines
Sigma Plot version 13	Systat Software, Erkrath, Germany
ZEN 2012 version 8.1	Carl Zeiss Microscopy, Jena, Germany

2.12 Fly strains

Strain	Genotype	Company / Resource
Balancer strain for second chromosome	*w⁻; CyO (Cy)/lF;+*	A. Teleman, DKFZ Heidelberg, Germany
Balancer strain for third chromosome	*w⁻; CyO (Cy)/lF; MKRS (Sb)/TM6B (Tb)*	B. Edgar, ZMBH Heidelberg, Germany
Tub-GAL4 driver	*w⁻; + ; tub-GAL4/TM6B*	A. Teleman, DKFZ Heidelberg, Germany
UAS-Vdup1	*yw; +; P[UAS-Vdup1]*	Mandalaywala *et al.* (2008)
UAS-Vdup1-RNAi	*w^{1118}; P[UAS-Vdup1-RNAi];* +	Vienna *Drosophila* Resource Center (VDRC), Vienna, Austria
w⁻	*w⁻; +; +*	A. Teleman, DKFZ Heidelberg, Germany

3 METHODS

3.1 Cell culture

3.1.1 General culture conditions

Schneider's *Drosophila* Line 2 (S2) cells were cultivated in Schneider's *Drosophila* Medium (Sigma-Aldrich) supplemented with 10 % FCS (v/v) at room temperature (RT). Before use, FCS was heated in a water bath for 30 min at 56 °C to inactivate complement factors. If not otherwise stated the medium was supplemented with 1 % penicillin-streptomycin. The cells were passaged twice a week. For this purpose, cells were rinsed with medium to ensure complete detachment from the cell culture flask. Subsequently, cells were transferred to a new cell culture flask containing fresh medium. Hereby, the cell density was adjusted to 2 x 10^6 cells/ml. Harvesting of the cells was conducted by centrifugation at 1200 rpm for 10 min at RT. All cell culture work was carried out under sterile conditions using a laminar flow hood.

3.1.2 Thawing and freezing of cells

Cells were thawed in a water bath at 37 °C and immediately transferred to a centrifuge tube containing 50 ml fresh medium without antibiotics. Thereafter, cells were harvested at 1200 rpm for 10 min at RT and resuspended in an appropriate volume of fresh medium.

For freezing, 10^7 cells were pelleted by centrifugation (1200 rpm, 10 min, 4 °C), the supernatant was discarded and the remaining pellet resuspended in 1 ml freezing medium. Subsequently, cells were transferred to a cryo tube and frozen at -80 °C for 2-3 days prior to transfer to a liquid nitrogen tank for long term storage.

3.1.3 Determination of cell density

Before determination of the density, the cells were first diluted 1:5 in PBS. After this, equal volume of 0.4 % trypan blue in PBS was added to distinguish living and dead cells. Cells were counted in a Neubauer chamber slide respecting previous 1:10 dilution of the cells.

3.1.4 Subcloning to select single positive cell clones

To reveal single clones after transfection, cells were plated on 96 well plates in three different densities and cultured until cell growth could be observed by microscopy. Before plating, cell density was determined by a hemocytometer. Then, per cell type, three 96 well plates with three different dilutions were prepared:

- 0.1 cell/well
- 1 cell/well
- 10 cells/well (used as backup plate)

Hereby, all 96 well of the plate were filled whereas one well of a 96 well plate contained 200 µl medium. Importantly, to avoid cell death due to growth factor deprivation, culture medium consisted of 50 % fresh medium and 50 % conditioned medium which was obtained by sterile filtration from other cultures. Cells were grown at RT and were checked for contamination twice per week. In case of detection of cell growth respective wells were marked and cells were splitted to a bigger culture vessel to expand single clones. During culture the fraction of growing cells follows the Poisson distribution (Waldmann & Lefkovits 1984). If one well statistically contains one clone, 37 % of all wells demonstrate no growth. However, to ensure that each well contains only one single clone, subcloning must be repeated at least once. In case of 37 % of wells with no growth in the first round, less than 32 % of wells should display no growth in the second round to achieve an overall probability of 95 % of clonality (Coller & Coller 1983).

3.2 Cell biological methods

3.2.1 Stable transfection of Schneider S2 cells

3.2.1.1 Generation of stably overexpressing Schneider S2 cells

S2 cells were transfected using calcium phosphate. The target gene was cloned into the pAc5.1/V5-His A plasmid (Life Technologies) before transfection. Therefore, *vdup1* gene was amplified by PCR (see 3.3.11) using the RE65531 cDNA clone (DGRC) as template. During PCR, forward primer was modified to introduce an *EcoRV* restriction site whereas the reverse primer harbored an *XhoI* restriction site which overrides the stop codon in the PCR product. Next, the PCR product and the pAc5.1/V5-His A plasmid were double-digested with *EcoRV* and *XhoI* (New England Biolabs) and ligated to generate the pAc5.1/V5-His A-*vdup1* plasmid (see 3.3.12). In order to ensure stable overexpression of the target gene, the pCoHygro plasmid was cotransfected to allow selection of positive clones by hygromycin B. The day prior to transfection, 3 x 10^6 cells per reaction were seeded and grown overnight. For the transfection, 19 µg pAc5.1/V5-His A plasmid harboring the target gene were mixed with 1 µg pCo-Hygro plasmid and 36 µl of 2 M $CaCl_2$ in a 1.5 ml reaction tube (solution A).The reaction was filled up to 300 µl with ddH_2O. Then, 300 µl 2 x HBS were prepared in a fresh 1.5 ml reaction tube (solution B). To induce complex formation solution A was pipetted dropwise to solution B. After 30 min of incubation, the mixed transfection solution was pipetted dropwise to the cells. The next day, cells were washed twice with medium and cultured for 2 days in medium without antibiotics. To select positive clones hygromycin B (400 µg/ml) was added to the cell culture medium and the medium was replaced every 4-5 days until resistant colonies were visible.

3.2.1.2 Generation of stable vdup1 knockout Schneider S2 cells

S2 cells were seeded and transfected by calcium phosphate according to the procedure depicted in chapter 3.2.1. For transfection, 19 µg of the previously cloned pAc-sgRNA-Cas9-Puro vector (see 3.3.13) was transfected. Cotransfection of an additional resistance plasmid was not necessary as the pAc-sgRNA-Cas9-Puro already harbored a puromycin resistance gene. After transfection, cells were cultured for 24 h and then washed twice with medium. Cells were regenerated for 2 days in medium without antibiotics until supplementation with puromycin (5 µg/ml) to induce selection of transfection-positive clones. The medium was replaced every 4-5 days until resistant colonies were visible.

3.2.2 Cell lysis

5 x 10^6 cells were harvested by centrifugation and the supernatant was removed. After washing of the cell pellet with 1 ml PBS cells were lysed for 20 min on ice in an appropriate volume of S2 lysis buffer. To clear the protein lysates from cellular debris, the lysates were centrifuged for 20 min at 13000 rpm and 4 °C. Supernatants were used to determine protein concentration by BCA assay (Pierce) according to manufacturer's instructions. For SDS gel electrophoresis, 30 µg of protein was mixed with 5 x reducing SDS sample buffer and heated to 95 °C for 5 min (Laemmli 1970)

3.2.3 Generation of protein lysates from fly heads

Flies were transferred to a precooled 50 ml centrifuge tube and then shock frozen in liquid nitrogen. To separate fly heads from the remaining flies, shock frozen reaction tubes were inverted several times and fly heads were collected by tweezers (Neolab). Subsequently, 15 fly heads were transferred to a 1.5 ml reaction tube and homogenized in 60 µl 1 x SDS extraction buffer using a micro pestle (Roth). Extraction of proteins was performed for 10 min at RT. Next, to clear the protein lysates from debris, the lysates were centrifuged for 10 min at 13000 rpm. Supernatants were stored at -20 °C until further use. For SDS gel electrophoresis, 60

µl of protein was mixed with 15 µl 5 x reducing SDS sample buffer and heated to 95 °C for 10 min.

3.2.4 Cell death analysis

Cell viability was determined by flow cytometry. Upon dying, cells finally lose their cellular integrity and the plasma membrane becomes porous which enables entry of the otherwise cell impermeable dye propidium iodide (PI). As an intercalating agent PI stains all nucleic acids which allowed discrimination between dead cells (PI^+) and viable cells (PI^-) by measuring emission at 617 nm. 1 x 10^6 cells were seeded in 1 ml medium and subsequently treated with 20 mM H_2O_2. Then, after treatment, cells were washed with 1 ml PBS. To stain the cells 1 ml PI (25 µg/ml) was added and the cells were incubated for 5 min at RT before analysis. Quantification of specific cell death was calculated according to the following formula:

$$\text{Specific Cell Death [\%]} = \left[\frac{\text{dead cells [\%]-dead cells [\%]}_{\text{untreated control}}}{\text{100-dead cells [\%]}_{\text{untreated control}}}\right] \text{x } 100$$

3.2.5 Determination of ROS levels

Intracellular levels of ROS were determined by using the cell permeable dye H_2DCFDA. After entering the cell H_2DCFDA is cleaved by cellular esterases to DCF which is able to emit fluorescence after oxidation.

1 x 10^5 cells per well were collected and washed once with PBS. After this, cells were stained with 5 µM H_2DCFDA and incubated for 30 min at RT. Mean Fluorescence Intensity (MFI) was analyzed in living cells (high forward-scattered/sideward-scattered values, FSC/SSC values) using flow cytometry (ex 504 nm / em 529 nm). Results were calculated as **%** increase in MFI according to the following formula (Devadas *et al.* 2002; Kaminski *et al.* 2007):

$$\text{Increase in MFI [\%]} = \left[\frac{\text{MFI}_{\text{treated}}\text{-MFI}_{\text{control}}}{\text{MFI}_{\text{control}}}\right] \text{x } 100$$

3.2.6 CellROX staining for detection of ROS by confocal microscopy

3.2.6.1 Preparation of mounting solution

9.6 g Mowiol 4-88 (Sigma-Aldrich) was added to 24 g glycerol and mixed on a magnetic stirrer (Neolab). Subsequently, 24 ml ddH_2O was added and the preparation was incubated for 2 hrs at RT under constant stirring. Then, 48 ml 0.2M Tris-HCl (pH 8.5) was used to fill up the preparation to a total volume of 200 ml. Mounting solution was heated up to 50 °C and stirred for 4 hrs until Mowiol is almost completely resuspended. To separate undissolved Mowiol mounting solution was centrifuged at 5000 g for 15 min and RT. Supernatants were aliquoted and stored at -20 °C until further use.

3.2.6.2 Staining and imaging of the cells

Cells were stained with 5 µM CellROX® Green Reagent and incubated for 30 min at RT. Afterwards, staining solution was discarded and cells were washed three times with PBS. For fixation, cells were incubated with 2 % paraformaldehyde for 15 min at RT. Next, cells were centrifuged (1500 rpm, RT) and permeabilzed in PBS^{T++}. For visualization of nuclei, cells were stained with Hoechst 33342 (1:1000) for 5 min. After another centrifugation step (1500 rpm, RT), supernatant was removed and cells were mounted with 40 µl Mowiol. Analysis was performed by the LSM710 confocal microscope (Zeiss, Jena).

3.2.7 Thioredoxin activity assay

Besides glutathione the Trx system describes a second important regulator of the cellular redox balance. Hereby, the system comprises two major components Trx and TrxR which are both ubiquitously expressed. Harboring two reactive thiol groups in its active center, Trx is not only able to reduce oxidized proteins but it is also able to

scavenge free ROS. While executing its function Trx itself becomes oxidized and therefore inactive. Recovery of functionality was achieved by intrinsic TrxR activity.

To analyze Trx activity the fluorescence-based Trx activity assay FkTRX-02 (BIOZOL Diagnostica) was performed according to manufacturer's instructions. In brief, 5 x 10^6 cells were lysed in Trx activity assay lysis buffer and the protein concentration was determined by BCA assay (Pierce) according to manufacturer's instructions. For the assay 20 µg total protein per sample was used. Measurement was conducted in triplicates in a 96-well format (black plates) and fluorescence was recorded using GloMax®-Multi+ Detection System (Promega). Trx activity was calculated in the linear range by measuring the increase of fluorescence within a time period of 5 min. Activity was displayed as % activity compared to control transfected cells whose activity was set to 100 %.

3.2.8 Cell cycle analysis

PI-based cycle analysis was first described by Krishan (1975) which makes use of the variable amounts of cellular DNA during cell cycle progression. After permeabilization the cells were stained with the DNA-intercalating dye propidium iodide and visualized by flow cytometry. Hereby, each cell cycle phase gave rise to a characteristic peak in the analysis. Whereas in G_1 phase cells harbor a diploid chromosome set, cells in the G_2 phase have a tetraploid chromosome set before cytokinesis induction. Upon apoptosis, the genome is fragmented which is characteristic of the sub G_1 phase. To analyze cell cycle, 5 x 10^5 cells were permeabilized and stained overnight at 4 °C in the dark with 250 µl lysis buffer containing 50 µg/ml propidium iodide. The next day living cells (high FSC/SSC values) were analyzed by flow cytometry (FACS Canto II) by measuring emission at 617 nm. Furthermore, to quantify the percentage of the cells in a certain cell cycle phase, the polynomial method of Dean and Jett (Dean & Jett 1974) was used. This algorithm was embedded in the Flow Jo software.

3.2.9 Sodiumdodecylsulfate Polyacrylamide Gel Electrophoresis (SDS-PAGE)

The separation of proteins was conducted by discontinuous SDS-PAGE under reducing conditions (Laemmli 1970). Hereby, the anionic detergent SDS was used to cover intrinsic charge of the proteins with a constant negative charge. This allows separation of the analyzed proteins by molecular weight. If not otherwise stated, 10 % resolving gels and 5 % stacking gels were used for electrophoresis. In both cases, polymerization of acrylamide was initiated by addition of ammoniumpersulfate (APS) and tetramethylethylenediamine (TEMED). After preparation, the resolving gel was covered by isopropanol until the gel was completely polymerized. Subsequently, isopropanol was removed by rinsing with water and the gel surface was dried out before preparing the stacking gel. Separation was carried out in a gel chamber at 80 V constant voltage until protein samples passed the transition of the stacking gel to the resolving gel. Eventually, the voltage was increased to 130 V and separation of the proteins was continued until dye front reached the lower edge of the gel chamber. In order to assess the molecular weight of the analyzed proteins a molecular weight marker (New England Biolabs) was added in the first lane of the gel.

3.2.10 Purification of monoclonal antibodies from hybridoma cell lines

The generation of a hybridoma cell line secreting a *Drosophila*-specific α-Vdup1 monoclonal antibody was conducted by the DKFZ Monoclonal Antibody Facility (Heidelberg) In brief, a partial sequence derived from VDUP1 cDNA (Figure 6) was used for cloning and recombinant protein expression in bacteria. Proteins were purified and injected to BALB/c mice. B cells from reactive mice were isolated and fused to myeloma cells to obtain hybridoma cells. Antibody-secretion of hybridoma cells was tested by enzyme-linked immunosorbent assay (ELISA) and Western blot. Then, positive cells were subcloned.

>vdup1_sequence_for_immunization
CGCGCAAGTTGCTTAAATTCCTTATCATCTTCGACAACACTTCCCTCCTGTACTTCCCGGGC
CAGTTTCTCTCCGGACGGGTTCTAATCGAATTGCAGGATGAGACGCCTGCTTTGGGACTTCA
TTTCCATGTGGTAGGCGAAGGGGTCGTGCGCAACGGGCGGCGACAGGAGCGGACATACGATA
AGGAGAACTATATCGACTTTCGGATGCGACTTCTGGGGGACGTAGACCAAGGAGGTCCAGCT
ATACTCTCGCCAGGAATTCACAGCTTCCCCTTCAAACTCGGCTTGCCACTGGGTCTTCCATC
TACATTTCTCGGTCGGTACGGCTGGATTCAGTTCTACTGCAAGGCGGCGCTCCGCGAGAACA
ATGGCATTATCCATAAGAACCACCAGGTCTTCATTGTGATGAATCCCATCGACCTAAACCTT
GAAAAGCCCATCTTAGCACAACCGTTCACCTGCGAAGTTGAGCACAAGCTAGGCGTCGTCTG
TGTTAGTGGAGGTCAGATAAAGTGCAGAGTGTCC

Figure 6: DNA sequence of partial *vdup1* protein used for immunization.
Partial *vdup1* DNA sequence was cloned and transfected to bacteria for recombinant protein expression.

To collect antibody-containing cell supernatants, hybridoma cells were expanded and cultivated in RPMI 1640 medium at 37 °C and 70 % rH in a Heracell™ 240i CO_2 incubator (Thermo Fisher Scientific). Cells were grown until the color of the medium changed to yellow which indicated a low pH due to a high cell number. Cell supernatant was collected and conserved with sodium azide to final concentration of 0.02 % (w/v). Supernatant was stored at 4 °C until further use. Collection of cell supernatants was repeated until 5 l were collected in total. The supernatants were pooled and the dissolved antibodies precipitated by ammonium sulfate. Precipitation was conducted at 4 °C and constant stirring of the pooled supernatant until a saturation level of 50 % was reached. Amount of ammonium sulfate was calculated by the online tool Ammonium Sulfate Calculator (EnCor Biotechnology http://encorbio.com/protocols/AM-SO4.htm). Addition of 277 g/l ammonium sulfate was performed slowly to avoid heating of the supernatant solution due to enthalpy change of solution and, thereby, denaturation of antibodies. After complete solution of ammonium sulfate, the preparation was further incubated for 90 min at 4 °C. Next, preparation was centrifuged at 6000 g for 10 min and 4 °C in a Sorvall Evolution RC centrifuge (Thermo Fisher Scientific). Supernatants were removed and stored at 4 °C. The remaining protein pellet was resuspended in 100 ml ddH_2O. To remove remaining ammonium sulfate dissolved protein pellets were dialyzed against 5 l PBS at 4 °C. After 3 h of incubation PBS was removed and replaced by 5 l of fresh PBS.

Thereafter, antibody solution was further incubated overnight at 4 °C. The next day, dialysate was centrifuged for 10 min and 13000 rpm. Supernatants were carefully removed and sterile-filtrated (0.8 µm pore size, polyvinylidene fluoride (PVDF) low protein-binding filter, Merck Millipore). Antibodies were purified from the protein solution by affinity chromatography using a protein G sepharose column. A constant flow was generated by using the peristaltic pump P-1 (GE Healthcare). For packing, 5 ml protein G sepharose (Sigma-Aldrich) was loaded into a glass column (Biorad). Next, column was rinsed with 200 ml PBS at RT. Subsequently, protein solution was loaded to the column and the flow-through was stored at 4 °C in case of a second round of loading. To clean the bound antibodies, the column was washed by 150 ml 0.1 M Tris pH 8.0 and the flow-through was stored at 4 °C. Elution of the antibodies was conducted by applying 0.1 M glycine pH 3.0. Hereby, different fractions of the eluate were collected in 1.5 ml reaction tubes. During elution process the protein concentration of each fraction was immediately determined by spectrophotometry at 280 nm (OD_{280}). Fractions exhibiting OD_{280} > 0.4 were collected and pooled. Altogether, two distinct fractions were pooled. After pooling, pH was determined and the solution was neutralized by dropwise addition of 3 M Tris pH 8.8 until pH 7.0. Following neutralization, collected fractions were again dialyzed against 5 l PBS overnight at 4 °C and the protein concentration was measured by spectrophotometry whereas an OD_{280} value of 1.3 corresponds to a protein concentration of 1 mg/ml. Fraction A had a protein concentration of 0.787 mg/ml. Protein concentration of fraction B was adjusted to 1 mg/ml. Antibody solutions were filtrated by applying a 0.22 µm PVDF low protein-binding filter (Merck Millipore). For long-term storage antibody solutions were aliquoted and frozen at -20 °C. To assess purity, the antibody solutions were separated on by SDS PAGE (see 3.2.9). For this purpose, 10 µl of protein was mixed with either 5 µl reducing or non-reducing sample buffer and then incubated for 10 min at 95 °C. Next, the samples were loaded on a gel and separated as described in chapter 3.2.9. To visualize separated proteins gel was stained for 15 min with a coomassie solution. Subsequently, gel was destained for 1 h with coomassie destain solution. Both purified fractions were clean as there was only a band visible at 150 kDa (Figure 7). Under reducing conditions heavy and light chain were separated which was evident by two distinct bands at 50 kDa (heavy chain) and 25 kDa (light chain) (Figure 7).

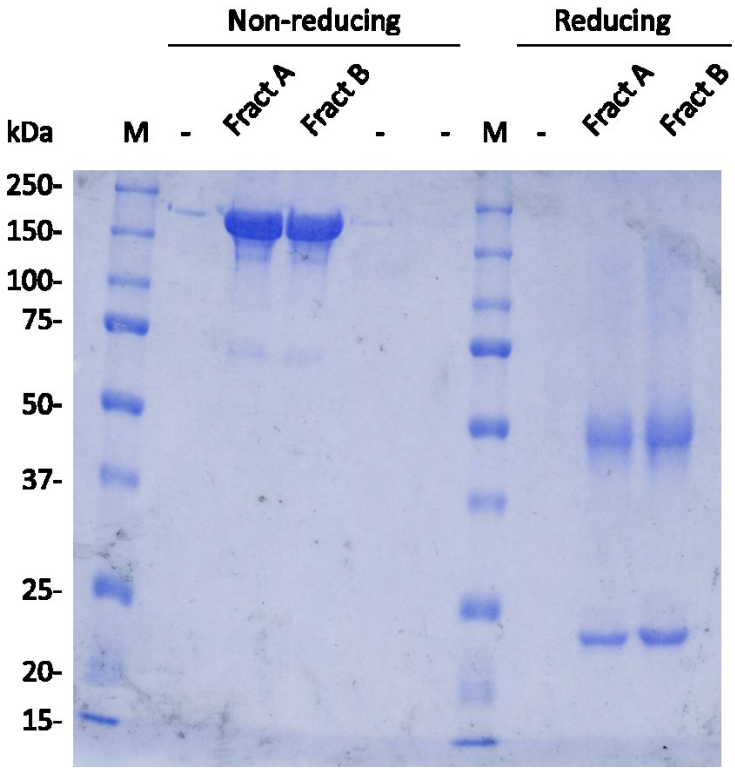

Figure 7: Coomassie-stained SDS gel confirming purity of antibody preparation.
Fraction A and B were applied on a non-reducing and reducing gel. Whereas in the non-reducing gel the antibody complex stayed intact, reducing conditions lead to separation of heavy and light chain.

3.2.11 Western blot (wet blot)

To facilitate identification and quantification of the proteins by application of antibodies, the SDS gel containing separated proteins was electrophoretically transferred to a nitrocellulose membrane (GE Healthcare) by using the wetblot procedure. Hereby, the blot sandwich was constructed in a holder cassette as follows:

- Sponge
- 2 sheets of filter paper
- SDS gel
- Nitrocellulose membrane
- 2 sheets of filter paper
- Sponge

Blotting was performed at a constant voltage of 90 V for 2 h in a cold room (4 °C). After blotting, transfer efficiency was checked by incubation of the membrane with Ponceau S solution for 5 min at RT. Hence, Ponceau S solution was removed and

the membrane was washed with water to remove unbound stain. To avoid unspecific binding of antibodies, the membrane was incubated with a blocking solution composed of 5 % skim milk powder (w/v) dissolved in PBS-T for 1 h at RT. The blocking solution was removed and then a protein-specific primary antibody was applied for 2 h at RT or at 4 °C overnight on a shaker. After three washing steps with PBS-T (3 x 5 min) the membrane was incubated with a HRP-conjugated secondary antibody for 1 h at RT on a shaker. Hereafter, the membrane was again washed three times with PBS-T for 5 min and treated with Western Lightning Plus-ECL (Perkin Elmer) or Amersham ECL Select Western Blotting Detection Reagent (GE Healthcare) to detect bound HRP by enhanced chemiluminescence (ECL) according to manufacturer's instructions. HRP-derived chemiluminescence was determined by the Vilber Lourmat acquisition system and analyzed by the Chemi Capt software. Band intensities were quantified by using ImageJ software by comparing intensities from the protein of interest with a reference gene (*e.g.* β- tubulin). In case of detection of further proteins, the membrane was either washed with PBS-T or the bound antibody complexes were displaced by incubation in stripping buffer at 56 °C for 30 min. After stripping, the membrane was washed five times and once again blocked with blocking solution.

3.2.12 Western blot (Semi-dry)

Separated proteins on an SDS gel were transferred to a nitrocellulose membrane (GE Healthcare) using the semi-dry procedure. For this purpose, PerfectBlue™ 'Semi-Dry' Electro Blotter was assembled according to manufacturer's instructions and blotting was performed at constant conduction current of 1 mA/cm^2 for 1 h. After blotting, protein detection was continued as described in chapter 3.2.11.

3.3 Molecular biological methods

3.3.1 Cultivation of bacteria

Bacteria were cultivated under aerobic conditions at 37 °C and 180 rpm in a Multitron Standard rotary shaker (Infors). In general, LB-Medium was supplemented with ampicillin (100 µg/ml) and inoculated with a single bacterial colony which was picked from an agar plate.

3.3.2 Generation of chemical competent bacteria by rubidium chloride method

To generate transformation-competent *E. coli* DH5α bacteria 1 ml overnight culture was used to inoculate 200 ml LB medium without antibiotics. Bacteria were cultivated at 37 °C on a shaker until an OD_{600} of 0.3-0.6 was reached. Then, the culture was incubated for 15 min on ice and pelleted at 1000 g for 15 min and 4 °C. After discarding the supernatant bacterial pellet was resuspended in 65 ml RF1 solution and incubated for 1 h on ice. Bacteria were again centrifuged (1000 g, 15 min, 4 °C), the pellet resuspended in 16 ml RF2 solution and incubated for 15 min on ice. Competent bacteria were frozen in liquid nitrogen and aliquots of 100 µl were stored at -80 °C until further use.

3.3.3 Bacterial transformation by heat shock

For transformation, 100 µl competent bacteria were thawed on ice. Then, 100-1000 ng plasmid DNA was added, carefully mixed, and incubated for 10 min on ice. To induce uptake of plasmid DNA by heat shock the bacteria were incubated at 42 °C for 30 s in a water bath. Next, the bacteria were incubated on ice for 2 min and mixed in 750 µl LB medium without antibiotics. For regeneration, bacteria were incubated on a shaker at 37 °C for 30-60 min. Finally, the bacteria were centrifuged at 2000 rpm and the supernatant was discarded except for 100 µl remaining LB medium, which was used for resuspending the bacterial pellet. Resuspended bacteria were

spread on agar plates containing ampicillin (100 µg/ ml) for the selection of positive clones and cultivated at 37 °C overnight.

3.3.4 Plasmid preparation on analytical scale (Miniprep)

Analytical preparation of bacterial plasmids was carried out by inoculation of 2 ml LB medium, supplemented with ampicillin (100 µg/ ml), with a single bacterial colony. Culture was grown at 37 °C overnight on a shaker and isolation of plasmid DNA was performed by using QIAGEN® Plasmid Mini kit according to manufacturer's instructions.

3.3.5 Plasmid preparation on preparative scale (Maxiprep)

In order to yield higher amounts of plasmid DNA preparation of bacterial plasmids was conducted by inoculation of 250 ml ampicillin-supplemented LB medium. Culture was grown overnight at 37 °C on a shaker and isolation of plasmid DNA was conducted by using QIAGEN® Plasmid Maxi kit according to manufacturer's instructions.

3.3.6 Determination of DNA and RNA concentrations

DNA and RNA concentrations were analyzed spectrophotometrically by measuring absorption at 260 nm on the NanoDrop Spectrophotometer (Thermo Scientific). Hereby, a DNA preparation was considered as pure if the 260/280 ratio was not lower than 1.8 or 2.0 for RNA preparations respectively.

3.3.7 Isolation of total RNA from cell culture (RNeasy Mini Kit)

Total RNA was isolated from S2 cells applying the RNeasy Mini Kit (QIAGEN) according to manufacturer's instructions. In brief, 5 x 10^6 cells were pelleted by

centrifugation (1200 rpm, 10 min, RT), the supernatant was discarded, and cells were resuspendend in 350 µl RLT buffer. Thereafter, 350 µl of 70 % absolute ethanol was added to the lysed cells, mixed and loaded on a silica column. To bind RNA, columns were centrifuged in a tabletop centrifuge at 13000 rpm for 1 min and the flow-through was discarded. In order to clean bound RNA from unwanted contaminants columns were washed twice by sequentially applying 700 µl of RW1 wash buffer and discarding the flow-through. Subsequently, columns were washed twice in the same manner with 500 µl of RPE buffer. To avoid impurity of eluted RNA by residual ethanol the columns were centrifuged again at 13000 rpm for 2 min. Then, the silica column was transferred to a clean RNAse-free elution tube and 15 µl of DEPC-supplemented peqGOLD RNase free water (Peqlab) was added directly on the dried out membrane. The water was incubated for 1 min before centrifugation at 13000 rpm for 1 min. The elution step was repeated once again to yield 30 µl of RNA in total. Eluted RNA was stored at -80 °C until further use.

3.3.8 Isolation of total RNA from whole flies (TRIzol)

In order to isolate total RNA from whole flies by phenol chloroform extraction, TRIzol reagent (Life Technologies) was used. For this purpose, 6-8 flies were transferred to a precooled empty *Drosophila* culture vial and immediately killed in liquid nitrogen. Subsequently, flies were homogenized in 1 ml TRIzol reagent and stored at -20 °C overnight to increase the yield of RNA. On the next day, the lysates were thawed at RT and 200 µl chloroform was added. After mixing, the lysates were incubated for 10 min at RT and afterwards centrifuged at 13000 rpm for 15 min and 4 °C to induce phase separation. Here, the RNA is located in the upper aqueous phase which was carefully transferred to a fresh reaction tube. To precipitate the RNA from the aqueous phase, 550 µl isopropanol was added and the sample was vortexed. After 15 min incubation at RT samples were centrifuged (13000 rpm, 25 min, 4 °C), the supernatant was discarded and the pellet was dried for 10 min at RT. Next, pellets were washed with 1 ml 70 % absolute ethanol and again centrifuged (13000 rpm, 25 min, 4 °C). Finally, supernatant was discarded, the pellet dried and resuspended in 30 µl RNAse-free water. RNA concentration was determined by analyzing the samples with the NanoDrop system.

3.3.9 Generation of cDNA by reverse transcription

cDNA was synthesized from previously isolated total RNA by RT-PCR using mRNA-specific oligo dT primers. RT-PCR reaction composition for one sample is listed below:

Reagent	Volume
25 mM $MgCl_2$	4 µl
10 x PCR buffer	2 µl
10 mM dNTPs mix	2 µl
20 U/µl RNase inhibitor	1 µl
50 U/µl MuLV reverse transcriptase	1 µl
100 pmol/µl oligo dT primer	1 µl
RNA	1 µg in 9 µl ddH_2O
Total	**20 µl**

The RT-PCR reaction was conducted in the C1000 Thermal cycler (Biorad) using the below conditions. For further use, synthesized cDNA was stored at -20 °C before using in a qRT-PCR reaction

Time	Temperature	Step
10 min	25 °C	Annealing
45 min	42 °C	Elongation
5 min	95 °C	Reverse transcriptase inactivation
Forever	4 °C	Hold

3.3.10 Quantitative real time PCR (qRT-PCR)

To analyze specific gene expression, cDNA was subjected to quantitative real time PCR (qRT-PCR) by using gene-specific primers. Addition of fluorescent reporter dyes to the qRT-PCR reaction allows detection of gene amplification during synthesis. This enables either relative or absolute quantification of the amplified DNA. Here, the Power SYBR™ Green Master Mix (Life Technologies) was used. SYBR Green is able to intercalate into double-stranded DNA where it fluoresces upon light excitation. With each cycle during the PCR reaction the amount of amplified DNA increases and this correlates with higher fluorescence signal. Relative quantification was analyzed by determining cycle threshold (Ct) values and normalization to gene expression of ribosomal protein L32 (Rpl32/rp49) which serves as a reference gene. Fold expression was calculated according to the ΔΔCt method (Pfaffl 2001). Gene expression was analyzed by 7500 real time PCR system including corresponding 7500 software version 2.0.1 (Life Technologies). qRT-PCR was carried out according to manufacturer's instructions in 96-well format and in triplicates.

The composition of the prepared master mixes is depicted in the following table:

Reagent	Volume
Template cDNA	2 µl
2x Power SYBR™ Green Master Mix	12.5 µl
25 µM forward primer	1 µl
25 µM reverse primer	1 µl
ddH_2O	8.5 µl
Total	**25 µl**

3.3.11 Amplification of cDNA by polymerase chain reaction

Amplification of cDNA was carried out by polymerase chain reaction (PCR) using gene-specific primers. Furthermore, Phusion® High-Fidelity DNA Polymerase (New England Biolabs) was used to ensure proper amplification with a minimum of mismatches due to its proof reading activity. The PCR protocol was optimized to high GC content templates. The composition of the prepared master mixes is depicted in the following table:

Reagent	Volume
5 x Phusion GC buffer	10 µl
10 mM dNTPs mix	1 µl
10 µM forward primer	2.5 µl
10 µM reverse primer	2.5 µl
cDNA template	10 ng
2 U/µl Phusion DNA polymerase	0.5 µl
Nuclease-free water	Ad 50 µl
Total	**50 µl**

PCR was conducted in the GeneAmp PCR system 9700 (Life Technologies) using the following program:

Time	Temperature	Step	
3 min	98 °C	Initial denaturation	
20 s	98 °C	Denaturation	
20 s	55 °C	Annealing	**x 30**
1 min	72 °C	Elongation	
3 min	72 °C	Final elongation	
forever	4 °C	Hold	

In order to purify the PCR product after amplification, the QIAquick PCR Purification Kit (QIAGEN) was performed conforming to manufacturer's instructions. Subsequently, DNA concentration was determined photospectrometrically by the NanoDrop system.

3.3.12 Manipulation of DNA

3.3.12.1 Restriction digest

Sequence-specific cleavage of DNA was achieved by using restriction endonucleases. An appropriate digest reaction was dependent on the amount of enzyme, choice of the buffer, duration and the temperature. Restriction endonucleases were obtained from New England Biolabs. All different parameters were adjusted according to manufacturer's instructions. A typical restriction digest reaction had a total volume of 20 µl. However, on preparative scale, total reaction volume was increased to 40 µl whereas 4-5 µg DNA were used for the digest.

3.3.12.2 Dephosphorylation of vector DNA

To prevent religation of linearized vector DNA, CIP (New England Biolabs) was used for dephosphorylation of the 5' termini. Reaction was adapted to conditions given in the manufacturer's instructions.

3.3.12.3 Ligation

For the ligation of DNA fragments with linearized vectors, the T4 DNA ligase (New England Biolabs) was used. T4 DNA ligase catalyzes the phosphodiester bond formation between 3'-OH and 5'-P ends between vector and insert. Therefore, insert DNA is stably integrated in the vector. Ligation of cohesive ends was conducted using a molecular ratio between 1:3 and 1:5 (vector to insert DNA).

3.3.13 Cloning of custom oligonucleotides to pAc-sgRNA-Cas9-Puro

The E-CRISP software tool (Heigwer *et al.* 2014) was used to design *vdup1*-specific NGG nucleotides for cloning into the pAc-sgRNA-Cas9-Puro vector. The three best hits, scored by specificity, annotation and efficiency (SAE score), were selected for cloning according to Bassett *et al.* 2013. In brief, gene sequences were modified to allow later transcription from the U6 promoter. Then forward and reverse oligos were obtained by Sigma-Aldrich (Munich). To anneal both oligos 5 µl of each forward and reverse oligo (100 µM) were mixed with 10 µl 2 x annealing buffer and incubated using to following temperature protocol on the GeneAmp PCR system 9700 (Life Technologies):

Time	Temperature	Cycles
1 min	98 °C	
5 s	98-88 °C (decrease 0.1 °C per cycle)	x 99
10 s	88-78 °C (decrease 0.1 °C per cycle)	x 99
10 s	78-68 °C (decrease 0.1 °C per cycle)	x 99
10 s	68-58 °C (decrease 0.1 °C per cycle)	x 99
10 s	58-48 °C (decrease 0.1 °C per cycle)	x 99
10 s	48-38 °C (decrease 0.1 °C per cycle)	x 99
1 s	38-18 °C (decrease 0.2 °C per cycle)	x 99
forever	18 °C	

Subsequently, oligos were phosphorylated for 30 min at 37 °C using T4 polynucleotide kinase (PNK, Life Technologies) according to the following pipetting scheme:

Reagent	Volume
Annealed oligo	1 µl
10 x T4 DNA Ligase Buffer	1 µl
10 U/µl T4 PNK	1 µl
Nuclease-free water	7 µl
Total	**10 µl**

In parallel, 2 µg of pAc-sgRNA-Cas9-Puro vector was digested with *BspQI* (New England Biolabs) in the following reaction:

Reagent	Volume
pAc-sgRNA-Cas9-Puro	2 µg
10 x NEBuffer 4	5 µl
BspQI (10 U/µl)	2 µl
Nuclease-free water	X µl
Total	**50 µl**

Restriction digest was performed for 1 h at 37 °C.

In addition, to avoid vector relegation, 1 µl CIP (New England Biolabs) was added to the reaction and incubated for 10 min at 37 °C. Dephosphorylated vector DNA was purified by MinElute Reaction Cleanup Kit (QIAGEN) according to manufacturer's instructions and eluted in 30 µl ddH_2O.

Then, phosphorylated oligo was diluted tenfold in ddH_2O and ligated with the dephosphorylated vector for 2 h at RT:

Reagent	Volume
Dephosphorylated pAc-sgRNA-Cas9-Puro	1 µl
10 x diluted oligo	2 µl
10 x T4 DNA Ligase Buffer	1 µl
400 U/µl T4 DNA ligase	1 µl
Nuclease-free water	5 µl
Total	**10 µl**

After this, 2 µl of the ligation preparation were used to transform chemically competent *DH5α* bacteria by heat shock (see 3.3.3). Transformed bacteria were spread on LB plates containing ampicillin (100 µg/ml) and incubated at 37 °C overnight. Single colonies were picked and used for inoculation of 2 ml LB medium supplemented with ampicillin (100 µg/ml). Cultures were incubated overnight at 37 °C on a shaker. The next day, plasmids were prepared using QIAGEN® Plasmid Mini kit according to manufacturer's instructions. Correct ligation of the designed oligo to the pAc-sgRNA-Cas9-Puro vector was confirmed by sequencing (see 3.3.17)

3.3.13.1 Identification of CRISPR-Cas9-mediated genomic cleavage

CRISPR-Cas9 technique was used to introduce *vdup1*-specific insertions or deletions (indels) which were created by cellular repair mechanisms after induction of double-strand breaks (Ran *et al.* 2013). To identify CRISPR-Cas9-mediated cleavage of genomic DNA, the GeneArt® Genomic Cleavage Detection Kit (Life Technologies) was used according to manufacturer's instructions. The kit is based on PCR amplification of the genomic region of putative cleavage site and later evidence of genomic cleavage using a specific detection enzyme. Cleavage efficiency can be determined by calculating band intensities after separation of PCR products by agarose gel electrophoresis. Before using the kit, *vdup1*-specific primers were designed to allow amplification of a 400-500 bp PCR product covering the putative cleavage site. As the detection reaction generated two distinct PCR product bands,

primers were designed with the Primer-BLAST tool (National Center for Biotechnology Information, NCBI) so that the cleavage site was not located at the center of the PCR product. First, 2 x 10^6 cells were harvested and the supernatant discarded. Next, cells were lysed and DNA was extracted according to manufacturer's instructions. Then, the cell lysate was subjected to PCR according to manufacturer's instructions using previously designed *Vdup1*-cl_det-fw and *Vdup1*-cl_det-rv primers. As an internal control, provided control DNA including primers was also subjected to PCR. This control DNA should lead to two distinct bands in the later agarose gel (225 and 291 bp fragments) and to a cleavage efficiency of 50 %. PCR was conducted in the GeneAmp PCR system 9700 (Life Technologies). Subsequently, PCR products were used for cleavage assay which was performed according to manufacturer's instructions. In brief, PCR products were denaturated and stepwise cooled down to 4 °C in the GeneAmp PCR system 9700 (Life Technologies). Hereby, DNA single-strands harboring indels can base-pair randomly with WT single-strands. This subsequently leads to formation of mismatches which can be cleaved by the detection enzyme. Detection enzyme was added to the reaction and samples were incubated for 1 h at 37 °C. To allow cleavage detection, samples were separated on a 2 % agarose gel. As an additional control, PCR products without treatment with detection enzyme were loaded on the agarose gel. Stained DNA fragments were visualized by Gel Doc™ XR+ System (Biorad) and band intensities were calculated using ImageJ software (National Institutes of Health). Cleavage efficiency was calculated according to the following formula:

$$\text{Cleavage efficiency} = 1-\sqrt{1-\text{fraction cleaved}}$$

$$\text{Fraction cleaved} = \frac{\text{sum of cleaved band intensities}}{\text{sum of cleaved and parental band intensities}}$$

3.3.14 Site-directed mutagenesis by inverse PCR

Drosophila VDUP1 protein contains five cysteine residues which could mediate the proposed interaction with TRX-2 by forming disulfide bridges. In order to abolish the interaction, all five cysteine residues were individually and sequentially mutated on genetic level. For site-directed mutagenesis a KOD polymerase-based inverse PCR approach was chosen as KOD polymerase is characterized by high sequence accuracy due to its proof-reading activity. Hereby, the pAc5.1/V5-His A-*vdup1* plasmid was used as template and the triplet code of the corresponding cysteine residue in the resulting PCR product was changed by using mutated primers during the inverse PCR to give rise to alanine instead of cysteine in the translated protein. Primers were designed using the PrimerX online tool applying standard settings (http://www.bioinformatics.org/primerx/cgi-bin/DNA_1.cgi). Forward and reverse primers were chosen to harbor the triplet-changing point mutation in the middle of the sequence. Furthermore, forward and reverse primers had a significant overlap to generate a circular PCR product which can be directly transformed to bacteria without any additional ligation step. Primers were synthesized by Sigma-Aldrich and inverse PCR was conducted in the GeneAmp PCR system 9700 (Life Technologies) thermocycler using the following reaction composition and temperature protocol.

Reagent	Volume
10 x KOD buffer	5 µl
10 ng/µl pAc5.1/V5-His A-*vdup1* plasmid	2 µl
10 µM forward primer	1 µl
10 µM reverse primer	1 µl
10 mM dNTPs mix	5 µl
25 mM $MgSO_4$	3 µl
DMSO	2.5 µl
1 U/µl KOD polymerase	1.5 µl
Nuclease-free water	29 µl
Total	**50 µl**

Time	Temperature	Step	
2 min	95 °C	Initial denaturation	
20 s	95 °C	Denaturation	
30 s	Primer T_m -15 °C	Annealing	**x20**
6.5 min	72 °C	Elongation	
7 min	72 °C	Final elongation	
forever	4 °C	Hold	

Successful amplification was checked by agarose gel electrophoresis (see 3.3.15). As the pAc5.1/V5-His A-*vdup1* plasmid was replicated in *E. coli DH5α* and, therefore, is methylated 1 µl *DpnI* (10 U/µl, New England Biolabs) was added to the PCR-positive reactions and incubated for 2 h at 37 °C. Due to its specificity for methylated DNA, *DpnI* cuts only pAc5.1/V5-His A-*vdup1* template plasmid but not the PCR products containing mutated cysteine sites. Next, 20 µl of the digested PCR products were transformed to *DH5α* by heat shock (see 3.3.3) After heat shock transformation bacteria were spread on LB agar plates supplemented with 100 µg/µl ampicillin and grown overnight at 37 °C. Positive clones were picked and used for inoculation of 2 ml LB medium containing 100 µg/µl ampicillin. Cultures were grown overnight at 37 °C on a shaker. The next day plasmids were prepared by using QIAGEN® Plasmid Mini kit according to manufacturer's instructions. To verify proper mutagenesis the plasmids were sequenced by Seqlab (Göttingen, see 3.3.17).

3.3.15 Agarose gel electrophoresis

Separation of DNA samples was performed by agarose gel electrophoresis. For gel preparation 1 % agarose (w/v) was dissolved in 1 x TAE buffer by boiling in a microwave oven. To allow visualization of DNA agarose gel was supplemented with 6 µl of the DNA-intercalating agent ethidiumbromide per 100 ml gel solution. Before loading the DNA samples were mixed with 5 x DNA loading buffer (Bioline). Besides the samples 5 µl of the DNA molecular weight standard HyperLadder™ 1kb (Bioline)

was loaded onto the gel. Separation of the gel was conducted in a horizontal electrophoresis chamber filled with 1 x TAE buffer. The voltage was set to 5 V per cm electrode distance. Stained DNA fragments were visualized by excitation at 312 nm (fluorescence at 590 nm) using the Gel Doc™ XR+ System (Biorad).

3.3.16 Cleanup of modified DNA by MinElute Reaction Cleanup Kit

Restriction digest and dephosphorylation of DNA are catalyzed by enzymatic reactions which contain diverse components that may perturb subsequent reactions as DNA ligation. Therefore, the removal of these components was conducted by applying the MinElute Reaction Cleanup Kit (QIAGEN) according to manufacturer's instructions. To assess cleanup quality DNA concentration was measured using the NanoDrop system.

3.3.17 DNA sequencing

Sequencing of DNA plasmids was carried out by Seqlab Sequence Laboratories, Göttingen, Germany corresponding to the didesoxy method (Sanger *et al.* 1977).

3.4 *Drosophila* methods

3.4.1 Backcrossing and balancing

To ensure isogenicity of the genetic background *UAS-Vdup1-RNAi* and *UAS-Vdup1* flies were backcrossed at least four times to a w^- strain (provided by A. Teleman, DKFZ) using standard *Drosophila* genetics (Greenspan 1996). Tub-GAL4 driver and all balancer strains already harbor w^- background, and therefore, backcrossing is not necessary. In order to generate a stable stock flies in F5 generation possessing either *UAS-Vdup1-RNAi* or *UAS-Vdup1* transgene heterozygously were crossed to a corresponding chromosome-specific balancer strain to avoid loss of the transgene over time. Flies were reared at 25 °C and 70 % rH in a 12 h:12 h light and dark cycle.

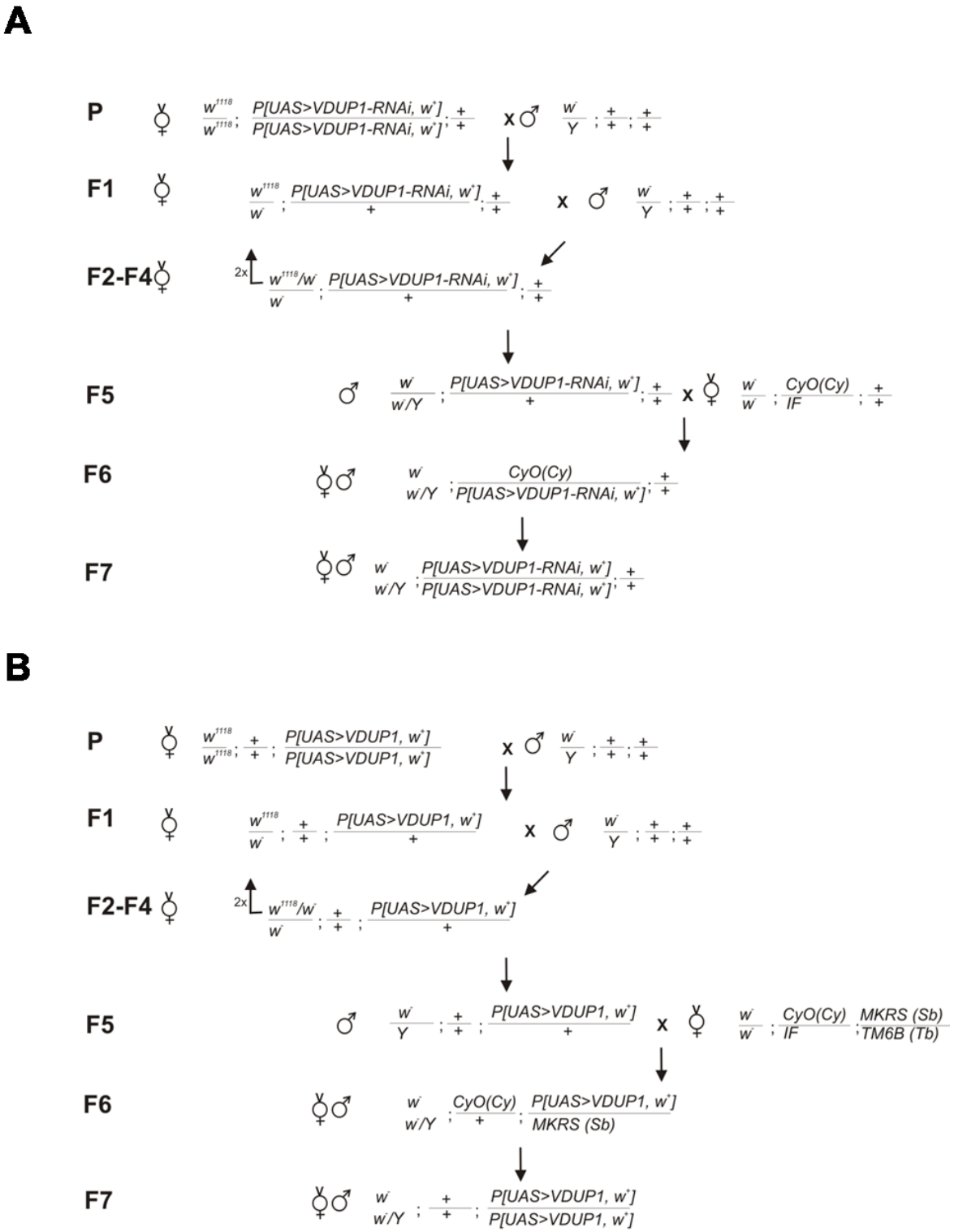

Figure 8: Backcrossing and balancing.
Flies expressing *UAS-Vdup1-RNAi* (A) or *UAS-Vdup1* (B) were backcrossed to a w^- strain to ensure isogenecity of the progeny. In addition, to generate stable stocks for future set up of crosses, F5 generation progeny were crosses to a corresponding balancer strain.

3.4.2 Setup of crosses and collection of age-matched flies

In order to generate functional knockdown or overexpression of a target gene in the progeny, male flies from the tub-GAL4 driver fly line were crossed to female virgins from a corresponding isogenic responder line (Vienna Drosophila Research Center, VDRC). If not otherwise stated, the tub-GAL4 diver line (provided by A. Teleman, DKFZ) was crossed to either a *UAS-Vdup1-RNAi* (VDUP1 knockdown in all tissues, Figure 9A), a *UAS-Vdup1* (VDUP1 overexpression in all tissues, Figure 9B) or to a w^- control strain (Figure 9C). Setup of crosses and collection of age-matched flies was performed according to Linford *et al.* (2013). For this purpose, 30 female *UAS-Vdup1* or *UAS-Vdup1-RNAi* virgin flies per vial were collected and mated with 15 tub-GAL4 male flies for two days in an embryo collection cage. The embryo cages were closed by a grape agar plate which was coated with yeast paste. After 24 h, the grape agar plate was changed and after another 24 h eggs were washed with PBS to remove residual yeast paste. Next, 32 µl of the washed eggs were then seeded in new vials and incubated at 25 °C and 70 % rH until the first progeny eclosed. The progeny were collected and transferred to new vials. After two days of mating, female and male flies were separated. The resulting flies can be further used in subsequent experiments.

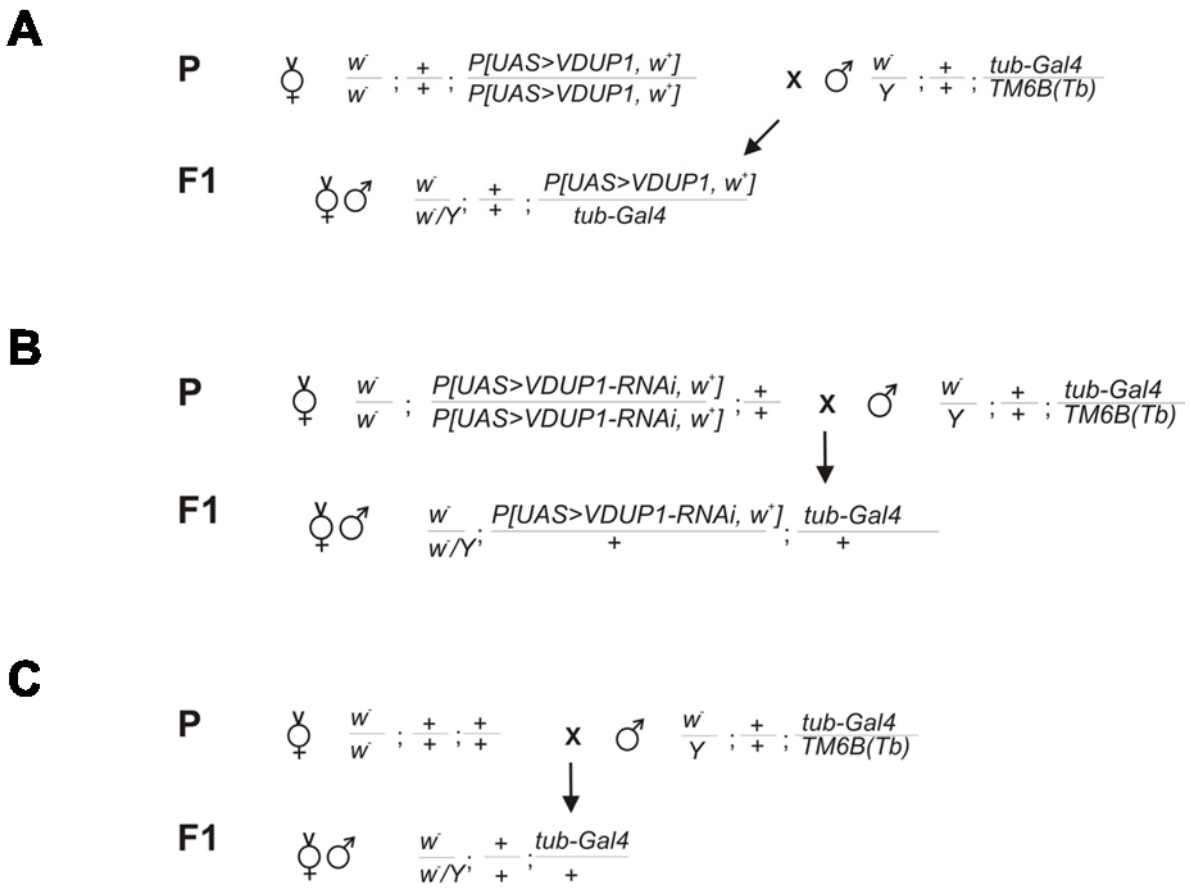

Figure 9: Setup of experimental crosses.
Functional overexpression (A) or knockdown (B) was established by crossing previously isogenized flies to a tub-GAL4 driver strain. As a control w- flies were crossed to tub-GAL4 driver flies (C).

3.4.3 Lifespan experiments

3 x 235 flies of each group and gender were distributed to small vials containing standard cornmeal food (30 flies per vial). Flies were reared at 25 °C and 70 % rH in a 12 h:12 h light and dark cycle. After 2-3 days, flies were transferred into new vials and dead flies were recorded.

3.4.4 Weight

From each group and gender, 100 flies (10 x 10) were anesthetized by diethyl ether and weighted by a high precision scale (Sartorius). The resulting weight was divided by 100 to get the mean weight per fly.

3.4.5 Starvation

To evaluate starvation resistance, 150 flies from each group and gender were distributed to small vials containing a 1.5 cm x 1.5 cm filter paper soaked with 150 µl ddH_2O to assure a proper supply of water. Per vial, 10 flies were reared and dead flies were recorded every 6 h or 12 h overnight. Evaporated water was refilled once the filter paper was dried out.

3.4.6 Determination of oxidative stress resistance by paraquat treatment

Paraquat is a quaternary ammonium bipyridyl compound which is widely used as an herbicide. However, in biology paraquat is also used as a redox-cycling agent which induces oxidative stress by generation of superoxide anions upon metabolizing. Prior paraquat treatment 200 flies from each group and gender were starved for 3-4 h to exclude influence of the remaining food in the gut on the experimental outcome. To analyze oxidative stress resistance, flies were subsequently distributed to small vials (10 flies per vial) containing a 1.5 cm x 1.5 cm filter paper soaked with either 150 µl 5 % sucrose (Control) or 15 mM paraquat in 5 % sucrose (PQ). Dead flies were recorded every 6 h or 12 h overnight and evaporated liquid was refilled when the filter paper was dried out.

4 RESULTS

Previous studies in our lab identified TXNIP, a crucial negative regulator of the cellular redox state, as a novel factor involved in regulation of T cell receptor (TCR)-induced oxidative signaling. Furthermore, TXNIP mRNA and protein expression was increased in T cells and various other tissues from aged human donors (Sass unpublished data). Increased TXNIP expression correlates with decreased stress resistance and impaired cellular anti-oxidative capacity (Ikarashi *et al.* 2002; Yang *et al.* 1998; Sass 2010). Thus, TXNIP is a novel regulator of resistance towards oxidative stress during aging. Since up-regulation of TXNIP expression is age-dependent, it is important to know whether this is part of a general mechanism affecting healthy aging. For this purpose, a suitable *in vivo* model has to be established. A rodent model was not considered due to long lifespan of mice and rats (2-4 years). It is not possible to use *C. elegans* as a model because *C. elegans* does not express a TXNIP homologue. *Drosophila* is an established aging model with a relatively short lifespan (70-100 days). In addition, genetic tools are readily available to manipulate TXNIP expression in flies as well as in cell lines. Furthermore, it expresses the homologue of TXNIP, VDUP1, and, therefore, *Drosophila* was used as an *in vitro* and *in vivo* model system.

4.1 Generation of VDUP1-overexpressing Schneider S2 *Drosophila* cells

To study the effect of VDUP1 in *Drosophila* stably VDUP1-overexpressing Schneider S2 cells were generated. Therefore, VDUP1 cDNA (clone PFLC1/RE65532, *Drosophila* Genomics Resource Center) was cloned into the *Drosophila* expression plasmid pAc5.1/V5-His A (Life Technologies). Then, the resulting pAc5.1/V5-His A-*vdup1* plasmid, in combination with a plasmid carrying a hygromycin B resistance gene, was transfected into S2 cells. pAc5.1/V5-His A without transgene served as empty vector (EV) control. After 3 weeks of selection by hygromycin B, appropriate overexpression of VDUP1 was analyzed by qRT-PCR and Western blot. To check

VDUP1 expression on transcriptional level, total RNA from pAc5.1/V5-His A- *vdup1*-(OE-VDUP1) and pAc5.1/V5-His A (EV)-transfected S2 cells was isolated. RNA was used for reverse transcription reaction and the resulting cDNA was subjected to qRT-PCR using *vdup1*-specific primers. Gene expression was normalized to the *Drosophila* housekeeping gene *rp49.* As indicated in Figure 10A, S2 cells transfected with pAc5.1/V5-His A-*vdup1* showed a pronounced overexpression of VDUP1 on mRNA level which was 29000-fold increased compared to empty vector control-transfected cells. To confirm overexpression of VDUP1 on protein level, OE-VDUP1- and EV-transfected cells were lysed and protein lysates were analyzed by immunoblotting using monoclonal antibody that was generated in cooperation with the DKFZ antibody facility (see chapter 3.2.10). Figure 10B shows a representative Western blot image displaying high expression in VDUP1-overexpressing cells. In contrast, VDUP1 was not detected in EV-transfected cells. As control, expression of the transgene was confirmed by detection of the V5-epitope-tag in the VDUP1-overexpressing S2 cells which was not present in EV-transfected cells. Furthermore, despite the high VDUP1 overexpression, expression of the putative interaction partner thioredoxin-2 (TRX-2) was not changed. Upon increase of the amount of loaded protein, VDUP1 expression was detected in EV-transfected cells (Figure 10C) indicating a low basal expression level. Quantification of three independent transfection reactions revealed massive VDUP1 overexpression in VDUP1-overexpressing S2 cells (Figure 10D). In conclusion, an *in vitro* overexpression system was established that can be used for functional analysis of VDUP1.

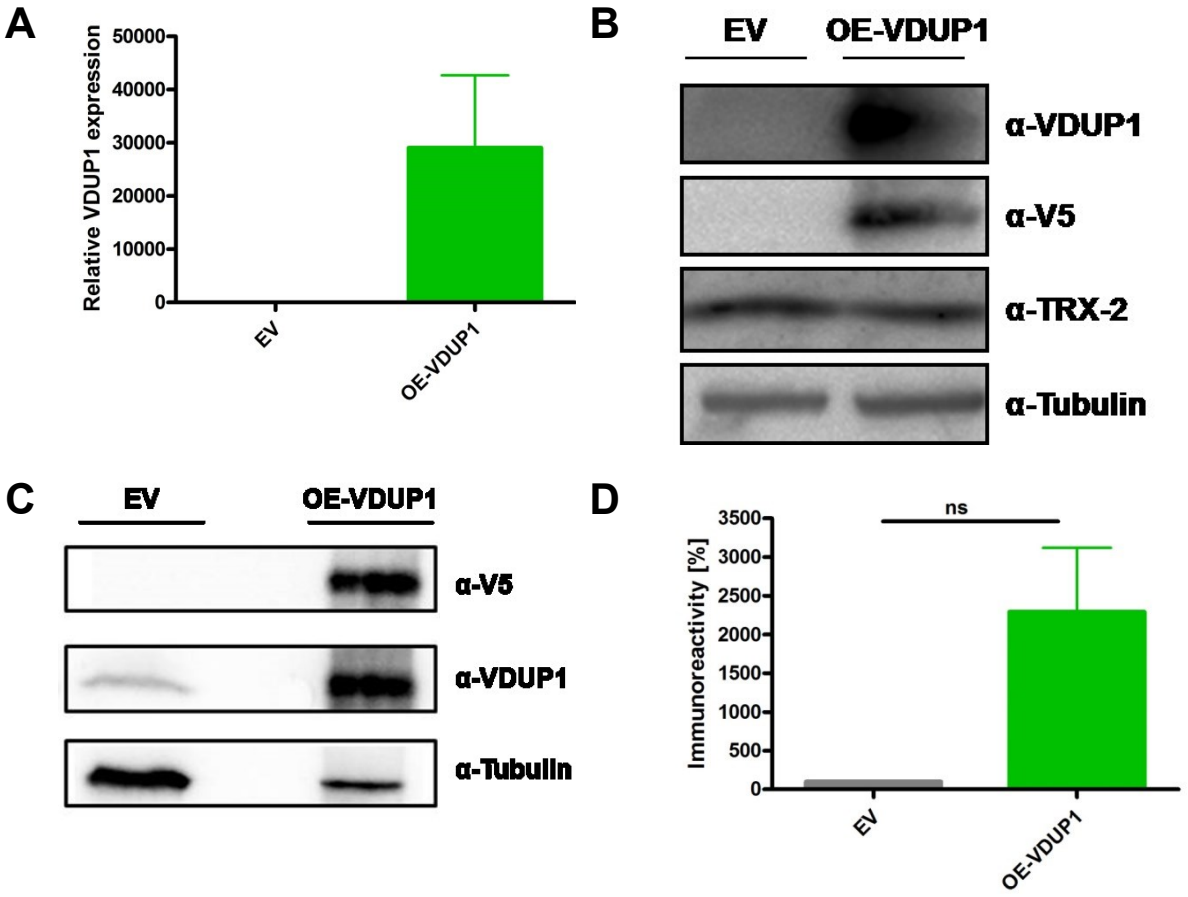

Figure 10: Validation of VDUP1 overexpression in S2 cells.
S2 cells were transfected with empty vector control (EV,pAc5.1/V5-His A) or VDUP1 overexpression vector (OE-VDUP1, pAc5.1/V5-His A- *vdup1*). **(A)** After selection, total RNA was isolated and reverse transcribed. Gene expression was determined by qRT-PCR. Results are displayed as relative gene expression compared to EV-transfected cells and were normalized to *rp49* expression. **(B)** S2 cells were lysed and 30 µg of protein was subjected to SDS-PAGE and Western blot analysis. The panel shows a representative blot of EV- and VDUP1-transfected S2 cells indicating a massive overexpression of VDUP1 **(C)** S2 cell lysates were subjected to SDS-PAGE and Western blot analysis. To verify expression of endogenous VDUP1, the amount of loaded protein in EV-transfected S2 cells was increased to 80 µg. For VDUP1-transfected S2 cells 30 µg of protein was used. **(D)** Quantification of Western blot results. VDUP1 signals were divided by the values of the respective tubulin signals. The value of EV was set to 100 %.The p-value was determined by an unpaired welch's t-test (mean +/- SEM, n=3) and showed no significance ($p>0.05$).

4.2 Cell cycle progression in S2 cells is not influenced by VDUP1 overexpression

In humans, TXNIP functions as a potential tumor suppressor gene which is downregulated in several tumors such as gastrointestinal, breast, and liver cancer (Ikarashi *et al.* 2002; Yang *et al.* 1998; Sheth *et al.* 2006). In this context, TXNIP inhibits COPS5 which is described as a crucial inducer of nuclear export of $p27^{kip1}$ and its subsequent proteasomal degradation. However, due to COPS5 inhibition, $p27^{kip1}$ is translocated into the nucleus and, thereby, leads to cell cycle arrest in G_1 phase (Jeon *et al.* 2005). In *Drosophila,* an effect of VDUP1 on cell cycle had, so far, not been analyzed. Hence, the impact of VDUP1 overexpression in S2 cells on cell cycle progression was investigated by flow cytometry. Cell cycle progression was measured by staining of nuclear DNA. Resulting peaks were evaluated and the percentage of cells in a respective cell cycle phase was calculated using the polynomial method of Dean and Jett (Dean and Jett, 1974). A representative image of cell cycle analysis for control-transfected cells and VDUP1-overexpressing cells is depicted in Figure 11A and B, respectively. Control-transfected (EV) cells were detected to be mostly in G_2 phase (56 %), whereas a minor portion of the cells was in G_1 (28 %) and S phases (4 %) (Figure 11C). Compared to the EV-transfected cells, VDUP1-overexpressing cells exhibited only minor changes regarding cell cycle phase distribution. 46 % of the cells were in G_2 phase while 24 % were in G_1 and 5 % in S phase. Moreover, a G_1 arrest could not be observed (Figure 11C). Thus, overexpression of VDUP1 in S2 cells had no relevant influence on cell cycle.

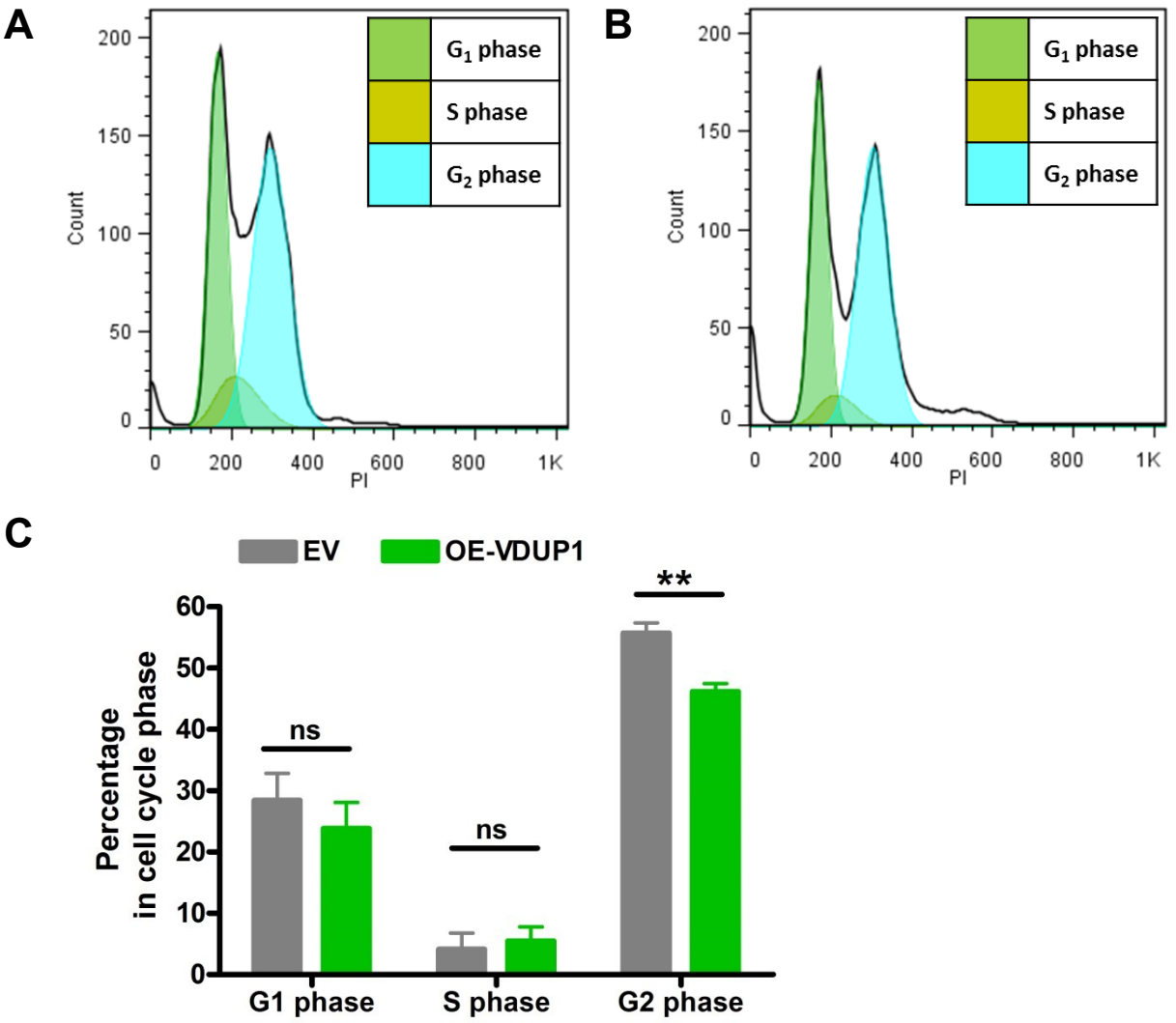

Figure 11: VDUP1 overexpression has no effect on cell cycle progression.
EV-transfected and VDUP1-overexpressing S2 cells were lysed overnight in PI-containing Triton X100 lysis buffer . The next day, cells were analyzed by flow cytometry. Representative image of cell cycle analysis from EV-transfected **(A**) and VDUP1-overexpressing **(B)** S2 cells showing percentage of cells in respective cell cycle phase. **(C)** Quantification of three independent experiments. p-value was determined by an unpaired student's t-test (mean +/- SEM, n=3, ns: not significant, **: p<0.01).

4.3 mRNA expression of Thioredoxin-2 and redox-related genes is not influenced by VDUP1 overexpression in S2 cells

Based on its role as a critical regulator in the cellular redox equilibrium, human TXNIP is able to shift cells into a pro-oxidative status, which is deteriorative for diverse cellular processes (Sass 2010; Nishiyama *et al.* 1999; Junn *et al.* 2000; Wang *et al.* 2002). To balance the cellular redox state, cells upregulate enzymes and intracellular ROS scavengers, which are known to have an anti-oxidative function (Balaban *et al.* 2005; Valko *et al.* 2007). To investigate a possible counter-regulation mechanism, the expression of key anti-oxidative proteins, including the three known *Drosophila* thioredoxins, was analyzed by qRT-PCR:

- Thioredoxin-2 transcript variant A (*Trx-2A*)
- Thioredoxin-2 transcript variant B (*Trx-2B*)
- Thioredoxin T (*TrxT/ DmTrx-1*)
- Deadhead (*dhd*)
- Catalase (*Cat*)
- Superoxide dismutase (*Sod/ Sod1/ CuZnSOD*)
- Superoxide dismutase 2 (*Sod2/ MnSOD*)
- Superoxide dismutase 3 (*Sod3*)

VDUP1 overexpression in S2 cells did not influence gene expression of redox-related genes (Figure 12). In addition, unchanged expression of the two TRX-2 transcript variants confirms the results obtained for TRX-2 on protein level (Figure 10A). Taken together, VDUP1 overexpression in S2 cells had no significant influence on mRNA expression of anti-oxidative key proteins.

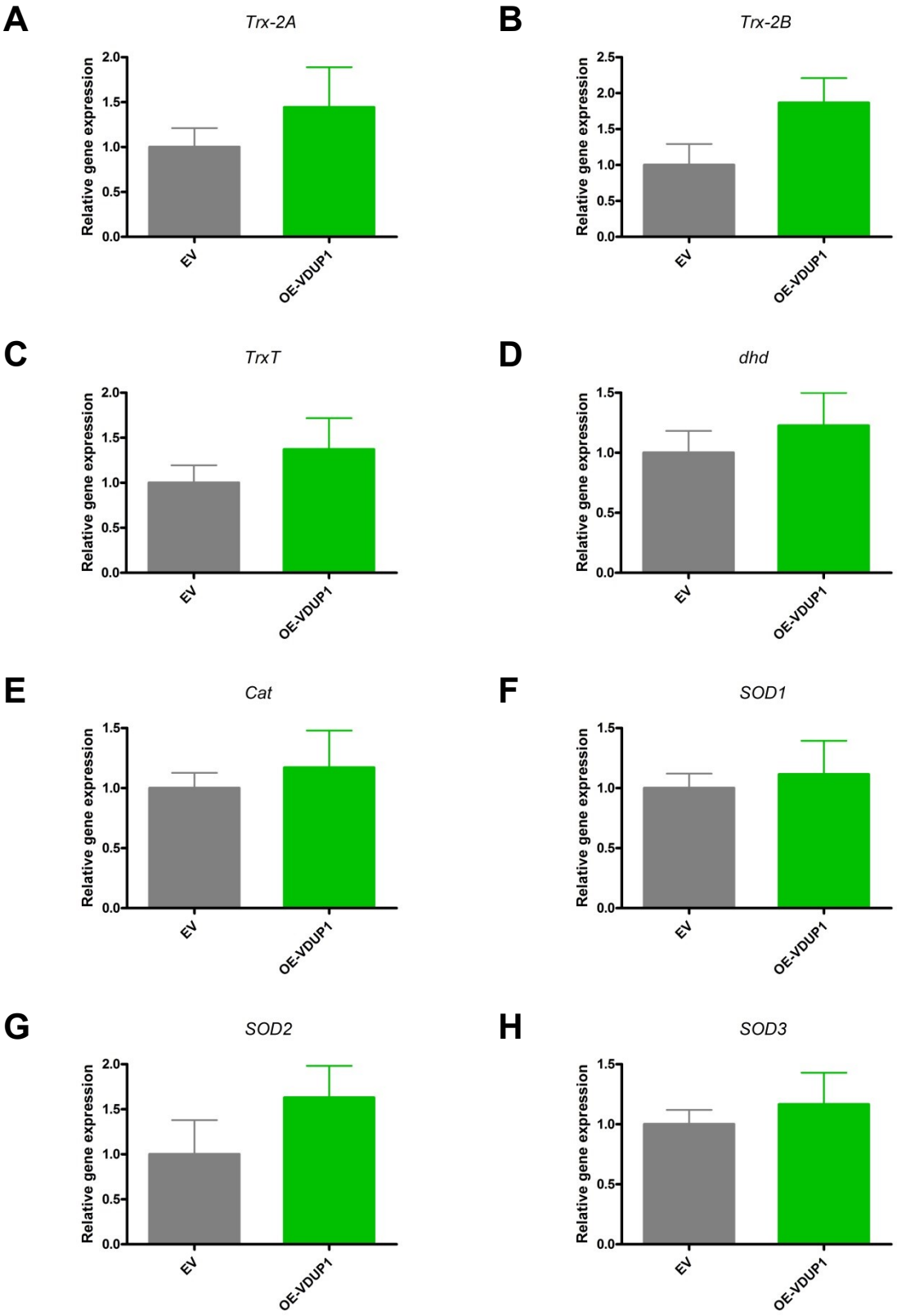

Figure 12: Gene expression of redox-related genes is unchanged upon VDUP1 overexpression in S2 cells.
Total RNA from EV-or VDUP1-transfected S2 cells was isolated and cDNA synthesized. Gene expression was determined by qRT-PCR. Results are displayed as relative gene expression compared to EV-transfected cells and were normalized to *rp49* expression.

4.4 VDUP1-overexpression leads to a higher basal ROS production in S2 cells

In humans, increased TXNIP expression is linked to a shift towards a pro-oxididative celluar status (higher basal ROS levels). It has been shown that the interaction of TXNIP with Trx is causative for this correlation as it leads to reduced Trx activity (Junn *et al.* 2000). To elucidate a potential role of *Drosophila* VDUP1 in influencing the oxidative balance in insect cells, basal ROS levels in S2 cells were measured. Consequently, VDUP1-overexpressing cells, as well as EV-transfected S2 cells were stained with the redox-sensitive dye H_2DCFDA and were then subjected to flow cytometry analysis. VDUP1-overexpressing cells showed about 20 % increase in basal ROS levels compared to EV-transfected cells (Figure 13A). To confirm the results obtained by flow cytometry analysis cells were stained with the redox-sensitive dye CellROX® Green and subjected to confocal microscopy. Hereby, VDUP1-overexpressing S2 cells showed a 32 % increase in ROS compared to EV-transfected cells indicating higher basal ROS levels (Figure 13B and C). Hence, VDUP1 overexpression in S2 cells leads to a shift towards a pro-oxidative cellular status.

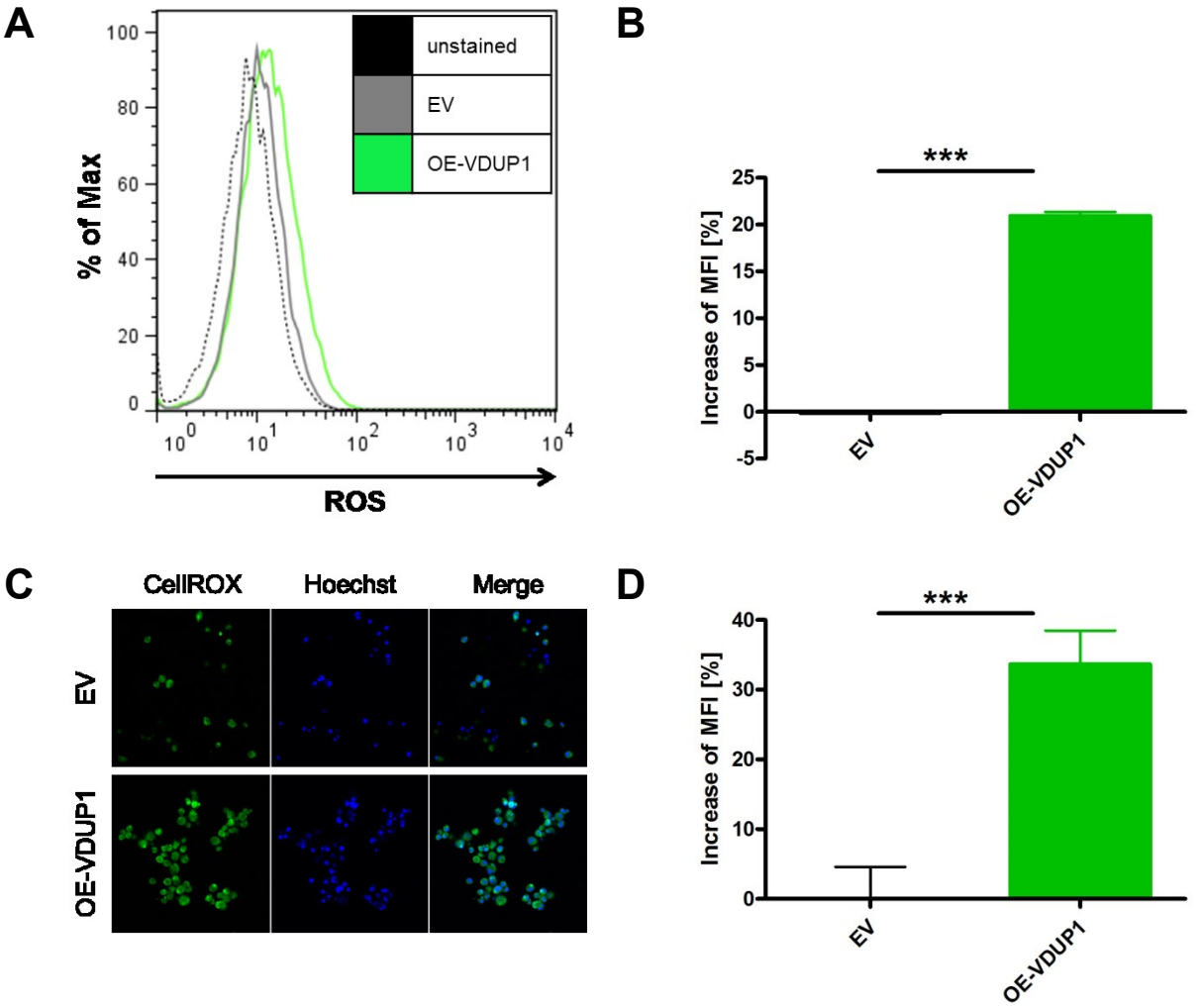

Figure 13: VDUP1-overexpressing cells exhibit enhanced basal ROS levels.
EV-transfected and VDUP1-overexpressing S2 cells were stained with H_2DCFDA before flow cytometry analysis was conducted **(A)** Representative histogram for DCF oxidation **(B)** Quantification of three independent experiments. Data are expressed as % increase in mean fluorescence intensity (MFI) and were normalized to EV-transfected cells. p-value was determined by an unpaired student's t-test (mean +/- SEM, n=3, ***: p<0.001) **(C)** EV-transfected and VDUP1-overexpressing S2 cells were stained with CellROX (green) or Hoechst (blue) to visualize nuclei. Afterwards, stained cells were analyzed by confocal microscopy. **(D)** Quantification of CellROX staining from panel (C). Data are expressed as % increase in mean fluorescence intensity (MFI) and were normalized to EV-transfected cells. p-value was determined by an unpaired student's t-test (mean +/- SEM, n=3, ***: p<0.001).

4.5 Enhanced VDUP1 expression leads to reduced thioredoxin activity in S2 cells

As reported, TXNIP is able to interact with Trx *via* disulfide bridge formation. This interaction prevents proper function of Trx as an antioxidative protein (Patwari *et al.* 2006; Junn *et al.* 2000; Wang *et al.* 2002). So far, the interaction of VDUP1 with Trx has not been described in *Drosophila*. However, due to its specific function in humans and its impact on basal ROS production a similar mechanism in *Drosophila* is implicated. Therefore, Trx activity in S2 cells was analyzed using the FkTRX-02 Trx activity assay. Hereby, cells were lysed and the resulting lysates were utilized for the fluorescence-based assay. In case of VDUP1 overexpression, Trx activity was decreased by 13 % (Figure 14). This further substantiates the role of VDUP1 in modulating the cellular redox balance by influencing central processes in the cell leading to shift towards a pro-oxidative environment.

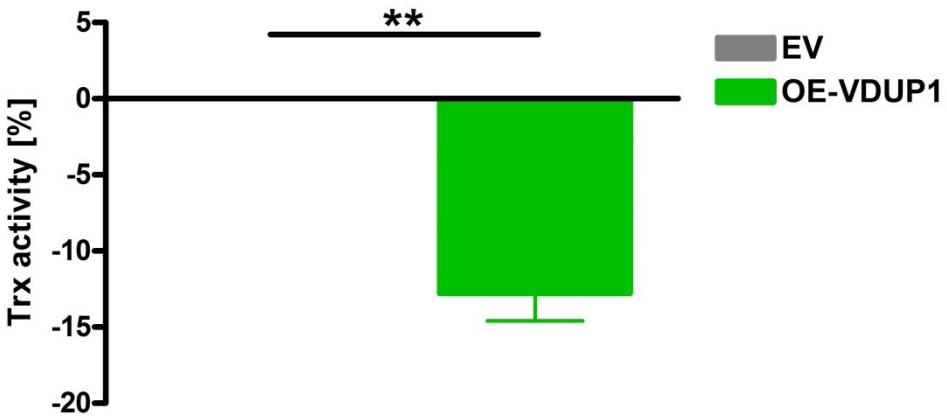

Figure 14: VDUP1 overexpression leads to reduced thioredoxin activty in S2 cells.
S2 cells were lysed and FkTRX-02 Trx activity assay was conducted according to manufacturer's instructions. Trx activity was displayed as % Trx activity and normalized to EV-transfected cells. p-value was determined by an unpaired student's t-test (mean +/- SEM, n=3) and showed statistical significance ($p<0.01$).

4.6 Increased VDUP1 expression sensitizes S2 cells towards oxidative stress

Previous experiments showed that VDUP1 overexpression in S2 cells resulted in higher basal ROS levels indicating a permanent pro-oxidative cellular environment (Figure 13). Thus, the next step was to investigate whether a permanent pro-oxidative state in the cell leads to deterioration of cellular function. As postulated by Harman, impairment of the cellular redox balance renders the cells more susceptible to oxidative stress (Harman 1956). Therefore, it was tested whether VDUP1 overexpression led to increased cellular oxidative stress. For this purpose, S2 cells were treated with hydrogen peroxide (H_2O_2) to induce oxidative damage. Afterwards, viability was determined by PI staining and subsequent flow cytometry analysis. As depicted, VDUP1-overexpressing S2 cells, which were treated for 24 hrs (Figure 15A, right panel), show increased cell death compared to EV control S2 cells (Figure 15A, left panel). Furthermore, analysis revealed no differences in cell viability upon short-term exposure to H_2O_2 (0-2 hrs). However, longer treatment with H_2O_2 (4-24 hrs) demonstrated a pronounced effect on specific cell death. 21 % of VDUP1-overexpressing cells showed cell death whereas at the same time point only 8 % of EV-transfected cells showed cell death. The observed difference in specific cell death became more prominent at later time points. At 8 hrs of treatment the difference was 25 %, at 12 hrs 30 % and at 24 hrs 36 % (Figure 15B). In conclusion, VDUP1 overexpression sensitized S2 cells to oxidative stress. This was expressed in higher levels of specific cell death upon H_2O_2 treatment especially at later time points.

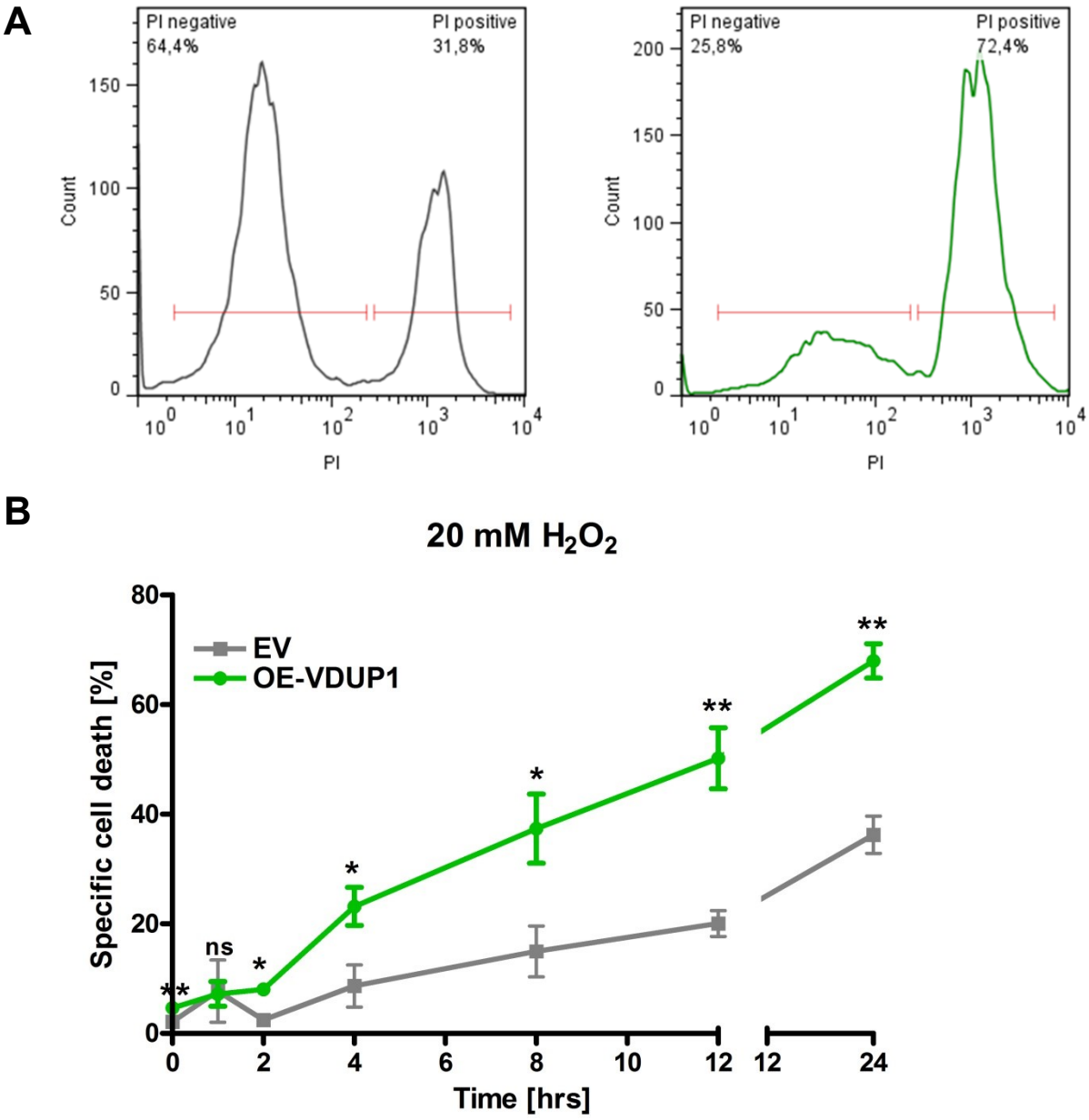

Figure 15: Overexpression of VDUP1 reduces resistance towards oxidative stress in S2 cells. S2 cells were treated with H_2O_2 and stained with PI. Analysis was performed by flow cytometry. **(A)** Representative histograms after 24 hrs of H_2O_2 treatment and PI staining for S2-EV (left panel) and VDUP1-overexpressing cells (right panel). Red bars indicate gating for PI-negative and PI-positive cells. **(B)** Kinetics of specific cell death upon H_2O_2 treatment for indicated time points. Data are presented as % specific cell death and normalized to EV-transfected cells without H_2O_2 treatment (0 hrs). p-value was determined by an unpaired student's t-test (mean +/- SEM, n=3, ns: not significant, *: $p<0.05$, ** : $p<0.01$).

4.7 Generation of VDUP1 loss-of-function models by site-directed mutagenesis and CRISPR-Cas9-mediated deletion

Overexpression of VDUP1 in S2 cells revealed a potential role of VDUP1 in regulation of the cellular redox equilibrium. To investigate whether it is possible to rescue the effect of VDUP1 overexpression on the cellular redox balance, two loss-of-function models were developed. The first model is based on site-directed mutagenesis of functional cysteine residues in the VDUP1 protein. TXNIP exerts its function to inhibit Trx by forming a disulfide bond between cysteine 247 and cysteine 32 in the active center of the Trx protein (Patwari *et al.* 2006). Mutation of the involved cysteine residues led to abrogation of Trx-TXNIP interaction. Moreover, the abolishment of the interaction rescued the effects of TXNIP-induced deterioration of oxidative balance (Patwari *et al.* 2006). However, in *Drosophila* an interaction between the TXNIP homologue VDUP1 and TRX-2 has not been described yet. In order to examine whether replacing cysteine residues in VDUP1 protein with alanine residues would rescue VDUP1-induced pro-oxidative effects in S2 cells, site-directed mutagenesis was carried out. *Drosophila* VDUP1 harbors five cysteine residues which could potentially mediate the interaction with TRX-2. Hence, mutagenesis was performed for all five constructs (mutant C1-C5). Proper nucleotide exchange was confirmed by sequencing. Corresponding mutant plasmids for all five original cysteine residues could be generated by site-directed mutagenesis (Figure 16). S2 cells were transfected with all five VDUP1 cysteine mutant plasmids.

A **Mutant C1**

WT: ATT CAG TTC TAC **TGC** AAG GCG GCG CTC
Mut: ATT CAG TTC TAC **GCA** AAG GCG GCG CTC

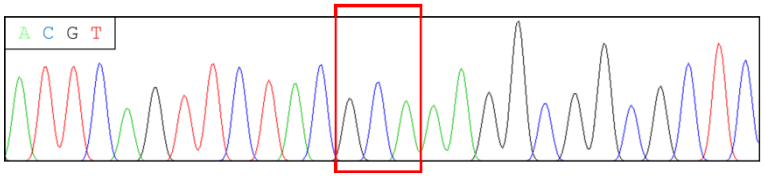

B **Mutant C2**

WT: CAA CCG TTC ACC **TGC** GAA GTT GAG CAC
Mut: CAA CCG TTC ACC **GCC** GAA GTT GAG CAC

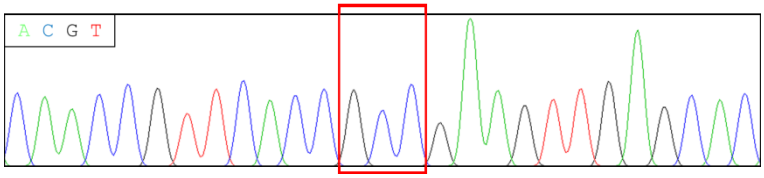

C **Mutant C3**

WT: CTA GGC GTC GTC **TGT** GTT AGT GGA GGT
Mut: CTA GGC GTC GTC **GCT** GTT AGT GGA GGT

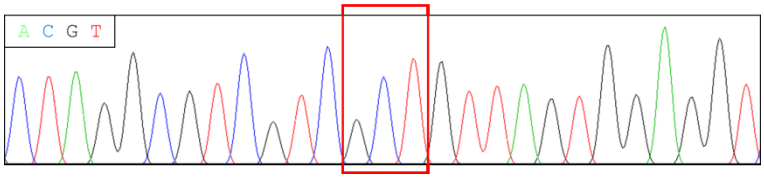

D **Mutant C4**

WT: GGT CAG ATA AAG **TGC** AGA GTG TCC CTT
Mut: GGT CAG ATA AAG **GCC** AGA GTG TCC CTT

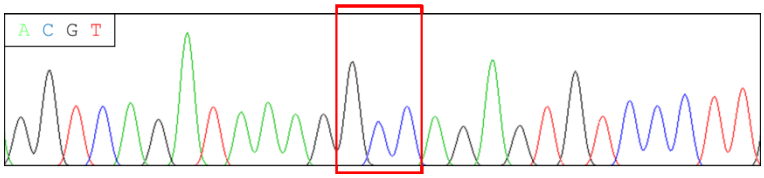

E **Mutant C5**

WT: AAT CTT CAT GGC **TGC** CGC CTG ATC AAA
Mut: AAT CTT CAT GGC **GCC** CGC CTG ATC AAA

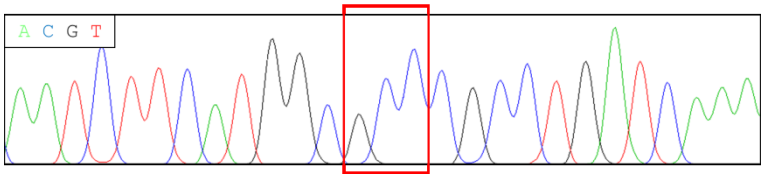

Figure 16: Generation of cysteine mutant plasmids.
pAc5.1/V5-His A-*vdup1* was used to generate mutations in cysteine-coding codons by site-directed mutagenesis. For each of the 5 cysteine codons the WT sequence is displayed in comparison to the mutated sequence (upper part). In addition, resulting plasmids were sequenced. Basecalling of the mutated region is displayed for each cysteine construct (lower part). The red box indicates mutated codon. Sequences and sequencing results are presented as follows: **(A)** cysteine residue 1, **(B)** cysteine residue 2**, (C)** cysteine residue 3**, (D)** cysteine residue 4 and cysteine residue 5 **(E)**.

Next, an *in vitro* system was established which lacked VDUP1 expression. To do so, transfectable vectors were generated to induce CRISPR-Cas9- mediated specific knockout of *vdup1* in S2 cells. First, three different *vdup1*-specific NGG nucleotides were selected by the E-CRISPR tool (Heigwer *et al.* 2014) and cloned into the pAc-sgRNA-Cas9-Puro vector according to Bassett *et al.* (2013). Hereby, three plasmids could be generated which express different sgRNAs and, therefore, target three different genomic regions of *vdup1*. Sequencing revealed two positive clones for sgRNA1 (K1A and K1B) and one positive clone for sgRNA2 (K2D). For sgRNA3 no positive clone could be obtained. To evaluate efficiency of genomic cleavage, the GeneArt® Genomic Cleavage Detection Kit was utilized. Resulting PCR products were separated by agarose gel electrophoresis (Figure 17). As shown in Figure 17A (right panel), the genomic region harboring the putative cleavage site could be amplified in all three different CRISPR constructs (K1A, K1B and K2D) as well as for untransfected (UT) S2 cells. After applying detection enzyme, the PCR products from CRISPR constructs displayed cleavage whereas UT control cells showed no cleavage. In addition, control DNA was also shown to be cleaved by the detection enzyme (Figure 17A left panel). Cleavage efficiency of K1A and K1B was over 80 % whereas for K2D only a lower efficiency of 50 % could be achieved. However, control DNA was cleaved by 45 %. UT S2 cells do not express a CRISPR construct and, therefore, did not show cleavage of DNA (Figure 17B). Thus, cleavage efficiency for all three CRISPR constructs was high. K1A, K1B and K2D constructs were transfected into S2 cells by calcium phosphate. In addition, pAc-sgRNA-Cas9-Puro was transfected as empty vector control (CRISPR-EV). To verify VDUP1 knockout on protein level, cells transfected with K1A construct were subjected to immunoblot analysis. Indeed, K1A-transfected cells did not show expression of VDUP1 (Figure 17C). Taken together, the course to establish two independent loss-of-function systems could be set. Nonetheless, after transfection of respective plasmids and selection, the cells in both systems generated a pool of different clones exhibiting different VDUP1 expression levels or *vdup1* cleavage efficiencies. Notably, knockout cells harbor a pool of different indels which led to frameshifts in most cases and, therefore, non-functional proteins. However, if indels affect three base pairs (or a multiple of three base pairs), the resulting proteins may still be functional due to an unchanged reading frame. Thus, cells overexpressing mutant VDUP1 as well as cells transfected with CRISPR-Cas9 must be subcloned before using the cells for

functional experiments. Subcloning of S2 cells was performed as described previously (see chapter 3.1.4). Due to the long generation time (67 h) subcloning is still ongoing and could not be completed yet.

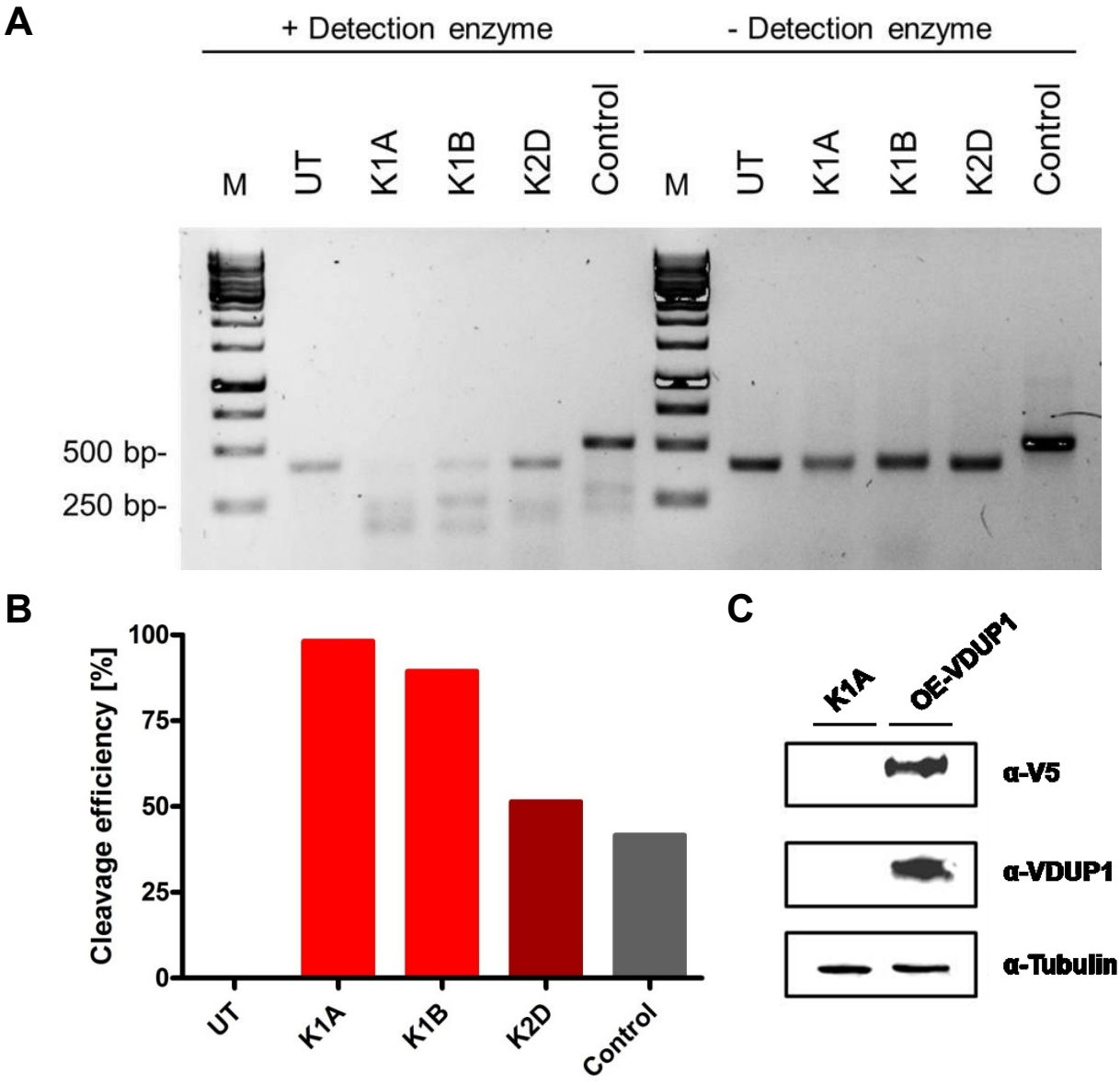

Figure 17: Validation of CRISPR-Cas9-mediated genomic cleavage.
(A) Cells were lysed and genomic region of expected cleavage was amplified using PCR. After denaturation and reannealing, samples were incubated with detection enzyme (left) or left untreated (right). Resulting DNA was separated by agarose gel electrophoresis. **(B)** Band intensities of DNA samples were determined and cleavage efficiency was calculated. Histogram shows quantification of the agarose gel **(C)** S2 cells were lysed and 30 µg of protein was subjected to SDS-PAGE and Western blot analysis. The panel shows a representative blot of K1A- and VDUP1-transfected S2 cells indicating a high VDUP1 knockout efficiency.

4.8 Generation of a *Drosophila in vivo* model system

In previous experiments Schneider S2 cells were used to study the effect of VDUP1 overexpression *in vitro*. VDUP1 overexpression led to higher levels of basal ROS which ultimately rendered S2 cells more sensitive towards oxidative stress. According to Harman's free radical theory a pro-oxidative shift is causative for aging (Harman 1956). In addition, the v*dup1* homologue TXNIP is expressed in an age-dependent manner in humans. Whereas young individuals show relatively low TXNIP expression in T cells, levels increase in older individuals (Sass 2010). To underpin the results generated in the *in vitro* system and to investigate the effect of VDUP1 manipulation on healthy aging, a *Drosophila in vivo* model was generated. Altogether, the fly model consists of three different fly strains: (1) A VDUP1 knockdown strain (VDUP1-RNAi) which harbors a shRNA gene leading to RNA interference-mediated knockdown of endogenous *vdup1* mRNA. Thereby, the VDUP1 knockdown strain represents young human individuals demonstrating low TXNIP expression. (2) A VDUP1-overexpressing strain (VDUP1) which overexpresses ectopic VDUP1. Having high levels of VDUP1, the overexpression strain represents aged human individuals and (3) a control strain (WT) with unmodified endogenous VDUP1 expression. Functional knockdown or overexpression was ensured by the GAL4-UAS system which enables gene expression in the progeny by crossing tub-GAL4 male driver flies to a corresponding responder line (UAS-*Vdup1*-RNAi or UAS-*Vdup1*). To minimize effects attributable to variability in genetic background all fly strains were backcrossed at least four times to a w^- strain before the experimental crosses. Furthermore, to establish synchronized eclosion of the progeny, collection of age-matched eggs was conducted as previously described (Linford *et al.* 2013)

4.8.1 Analysis of VDUP1 on transcript level in *Drosophila*

To test VDUP1 expression, total RNA was isolated from whole flies and the resulting mRNA was subsequently reverse transcribed to cDNA. Next, cDNA was subjected to qRT-PCR to analyze VDUP1 expression during aging in young (12 days of age), medium old (32 days of age) and old flies (52 days of age).

Knockdown efficiency in male flies was relatively poor for young flies (20 % knockdown efficiency). Nevertheless, knockdown efficiency increased during aging and was more than 50 % for medium old and old flies (Figure 18A). In female knockdown flies VDUP1 gene expression was reduced over 50 % in young (12 days) and old flies (52 days). However, medium-aged flies (32 days) did not show any knockdown on mRNA level compared to the corresponding WT flies (Figure 18B). Ectopic overexpression of VDUP1 displayed a 60- to 160-fold overexpression in male flies (Figure 18A) whereas expression in female flies ranges from 100-fold in 12 day old flies to 160-fold in 32 day old flies (Figure 18B). Altogether, whereas knockdown efficiency in the proposed fly model showed variability, sustained overexpression was achieved during the whole lifespan of flies.

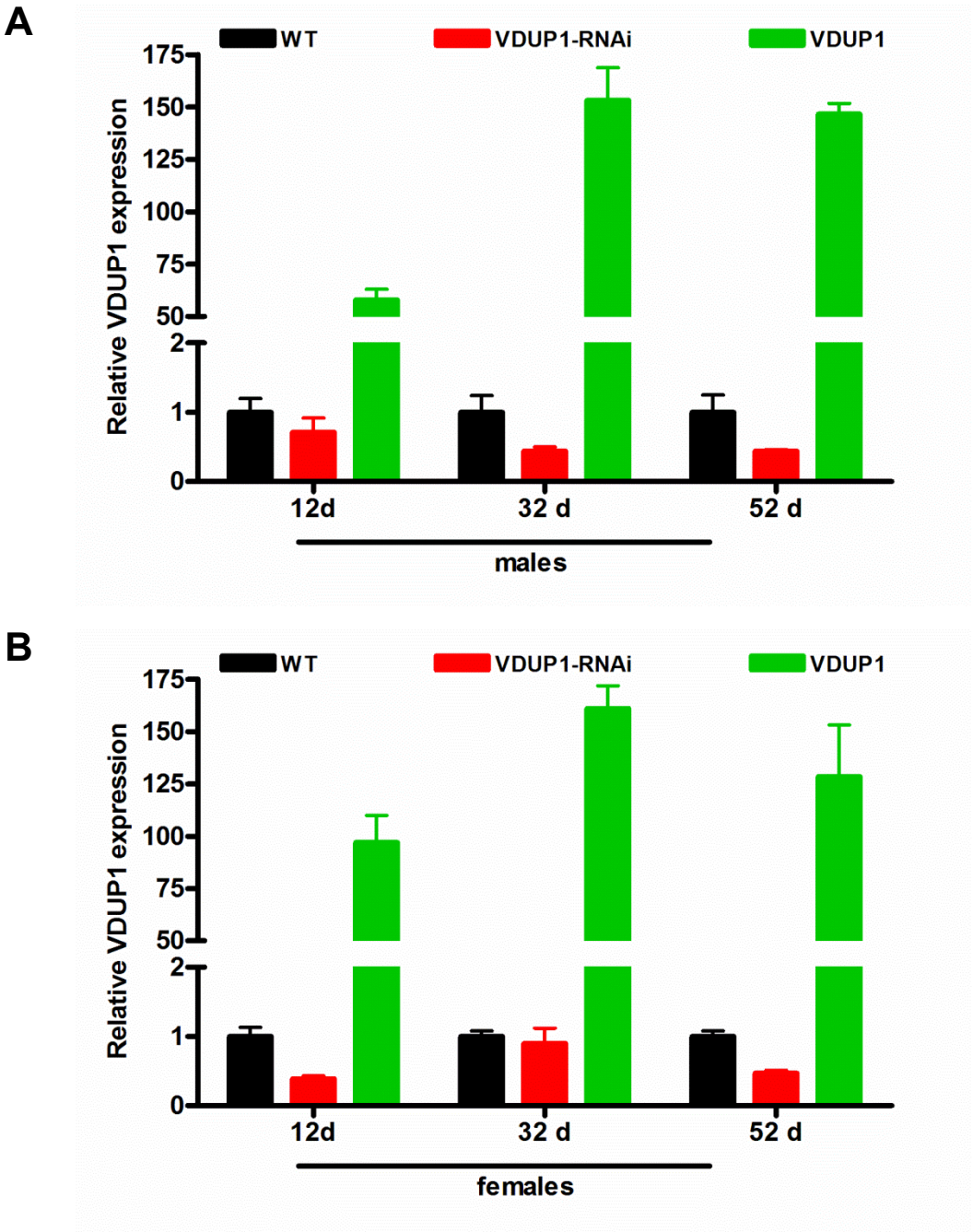

Figure 18: Characterization of fly model on mRNA level.
Total RNA of the flies of different ages (12, 32 or 52 days) was isolated by TRIzol. cDNA was generated from mRNA and relative VDUP1 expression of male **(A)** and female **(B)** flies was determined by qRT-PCR. Results are displayed as relative gene expression compared to WT flies and were normalized to *rp49* expression.

4.8.2 Analysis of VDUP1 on protein level in *Drosophila*

To verify the functionality of the *Drosophila* model also on protein level, lysates were generated from fly heads at the indicated time points as VDUP1 is highly expressed in the brain (Mandalaywala *et al.* 2008). Figure 19 shows VDUP1 protein expression in the different genders and genotypes and VDUP1 expression changes over time. Flies displayed potent VDUP1 knockdown although showing minimal expression in young (12 days) and old flies (52 days) (Figure 19A and B). Next, functional VDUP1 overexpression was verified (Figure 19C and D). Although overexpression was relatively low compared to the corresponding wild type strain in male as well as in female flies, VDUP1 expression increased constantly upon aging with old flies (52 days) showing the highest VDUP1 expression (Figure 19C and D). Importantly, in contrast to human cells, age-dependent upregulation of VDUP1 in WT animals was not observed in *Drosophila* at this particular age as VDUP1 expression in the WT strain remains constant.

Taken together, in contrast to the previous mRNA data, knockdown efficiency was high on protein level in both genders and could be maintained over time. However, in principle, VDUP1 mRNA expression data determined by qPCR could be confirmed on protein level. Overexpression of VDUP1 was shown to be mild in young flies of both genders whereas overexpression efficiency increased with older age. Nevertheless, age-dependent upregulation of VDUP1 in WT flies at the analyzed time points could not be observed.

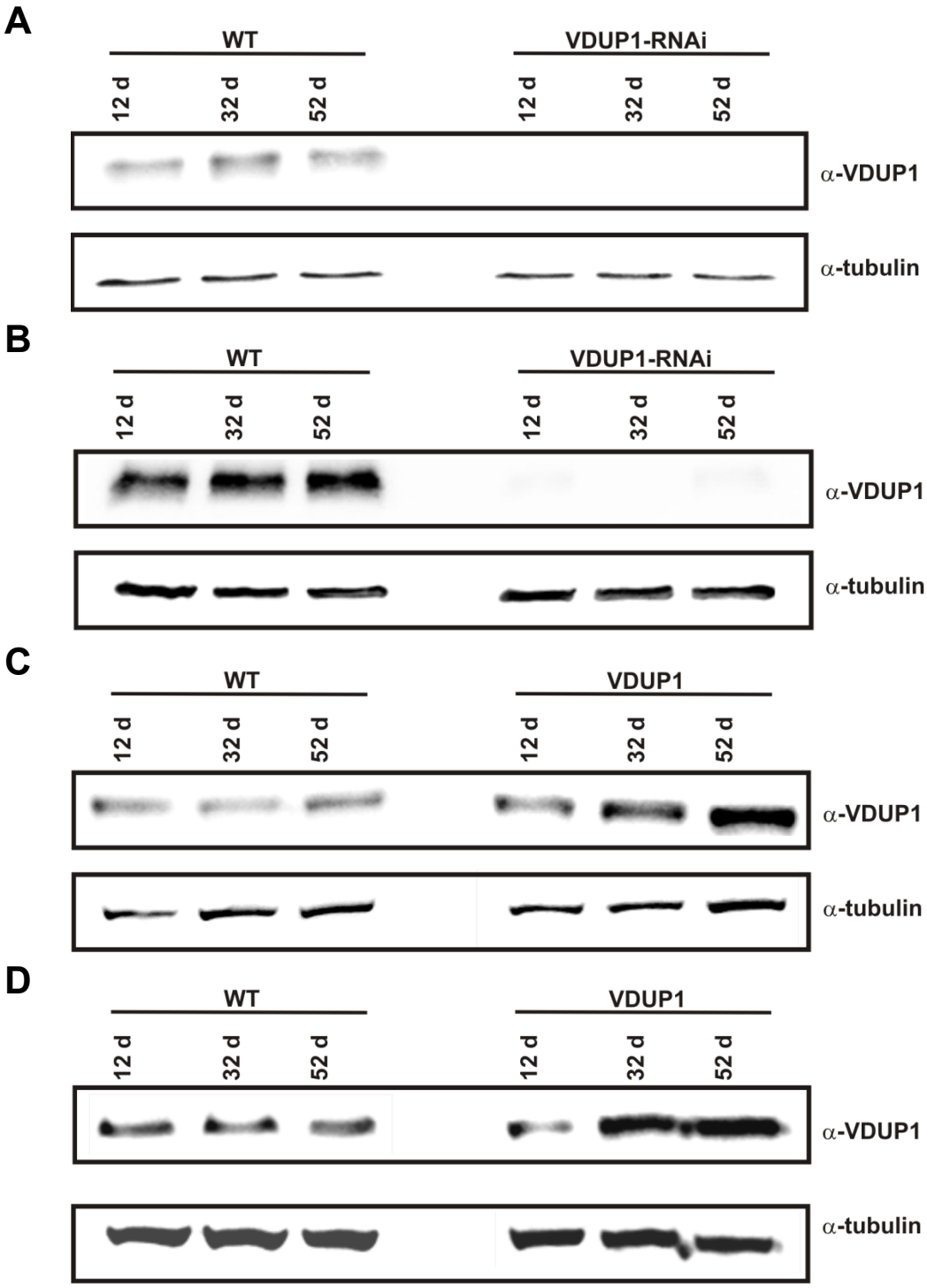

Figure 19: Characterization of the fly model on protein level.
Protein lysates from five fly heads were separated by SDS-PAGE and subjected to Western blot analysis. VDUP1 expression was analyzed for male **(A)** and female **(B)** VDUP1 knockdown flies as well as for male **(C)** and female **(D)** VDUP1 overexpression flies confirming functionality of the fly model. Blots were probed with antibodies directed against VDUP1 (upper panel) and β-tubulin (lower panels). d: days.

4.9 VDUP1 manipulation sensitizes flies to oxidative stress

After successful establishment of an in vivo fly model, different experiments were performed to analyze VDUP1 function on an organismal level. Fly lifespan correlates with body weight (Speakman 2005). A higher weight is beneficial for lifespan due to an improved supply of nutrients for a longer time periods. Furthermore, differences in weight can lead to metabolic changes and, therefore, to differences in the redox equilibrium (Speakman 2005). Due to the importance on lifespan, alterations in body weight after VDUP1 manipulation were analyzed. Hence, weight of the flies after VDUP1 manipulation was determined. Female flies showed 40 % increased body weight in comparison to their male counterparts (Figure 20A), which is mainly due to their bigger body size (Figure 20B). However, within a gender group fly weight was not altered with changing VDUP1 expression (Figure 20A). Thus, weight, as a possible factor influencing subsequent experiments, can be excluded.

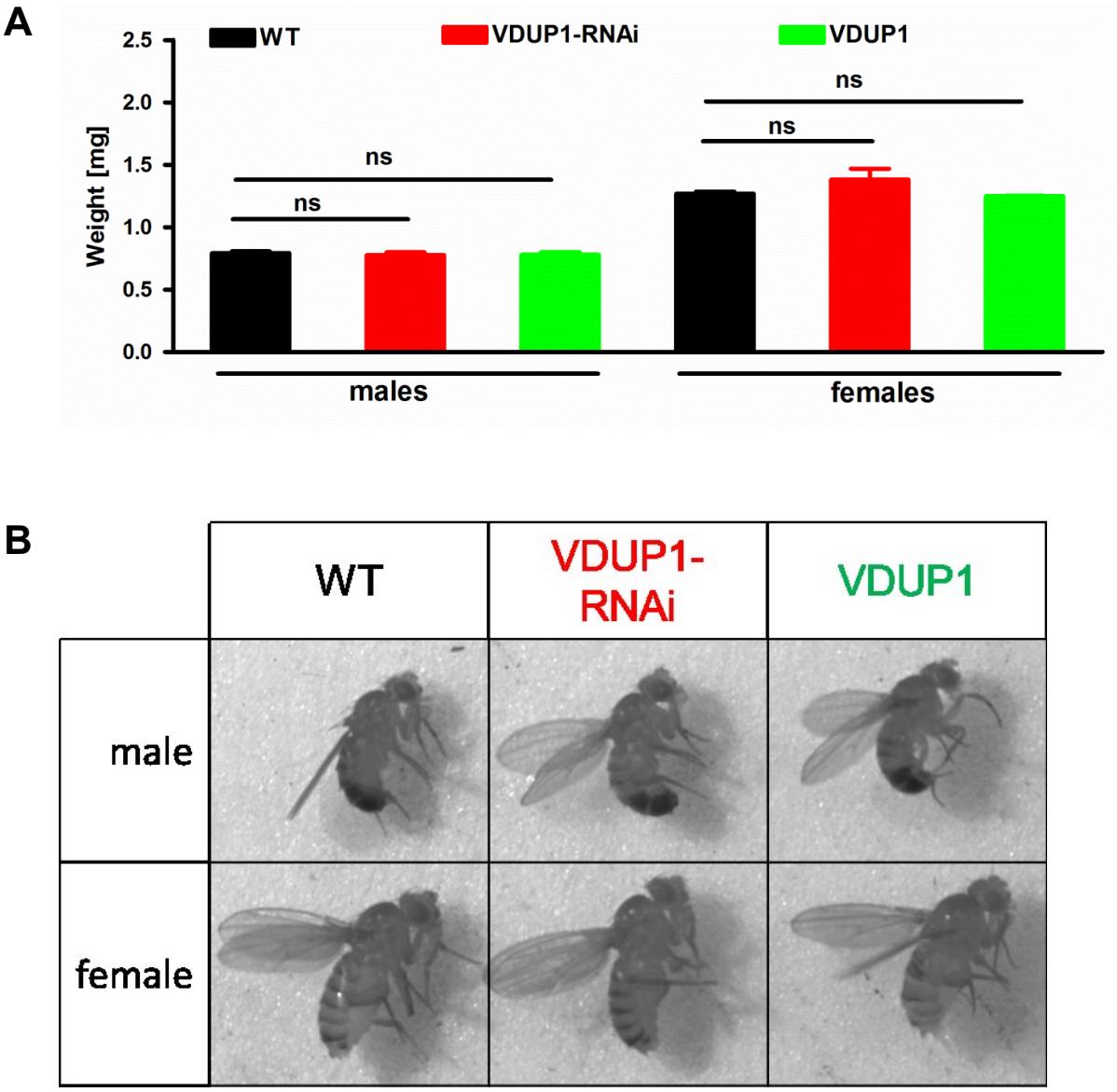

Figure 20: Weight of the flies is not influenced by VDUP1 manipulation.
(A) 10 x 10 flies were anesthetized and the weight was determined. The resulting weight was divided by 10 to get the weight of a single fly. p-value was determined by an unpaired student's t-test (mean +/- SEM, n=3) and showed no statistical significance ($p>0.05$).**(B)** Representative image of flies showing equal body sizes for males and females**.**

TXNIP is known to be a cellular stress regulator (Nishiyama *et al.* 1999; Junn *et al.* 2000; Wang *et al.* 2002). Moreover, previous experiments in *Drosophila* S2 cells indicated a role in cellular stress. Hence, the role of VDUP1 on different stress sources in vivo was investigated. First, the effect of VDUP1 manipulation on starvation stress was investigated in flies. During starvation dead flies were recorded every 6-12 hrs until all flies were dead. In general, female flies showed a higher resistance towards starvation stress compared to male flies (Figure 21) which might

be again attributed to their bigger body size and weight (Figure 20). Altogether, VDUP1 expression had no influence on starvation resistance.

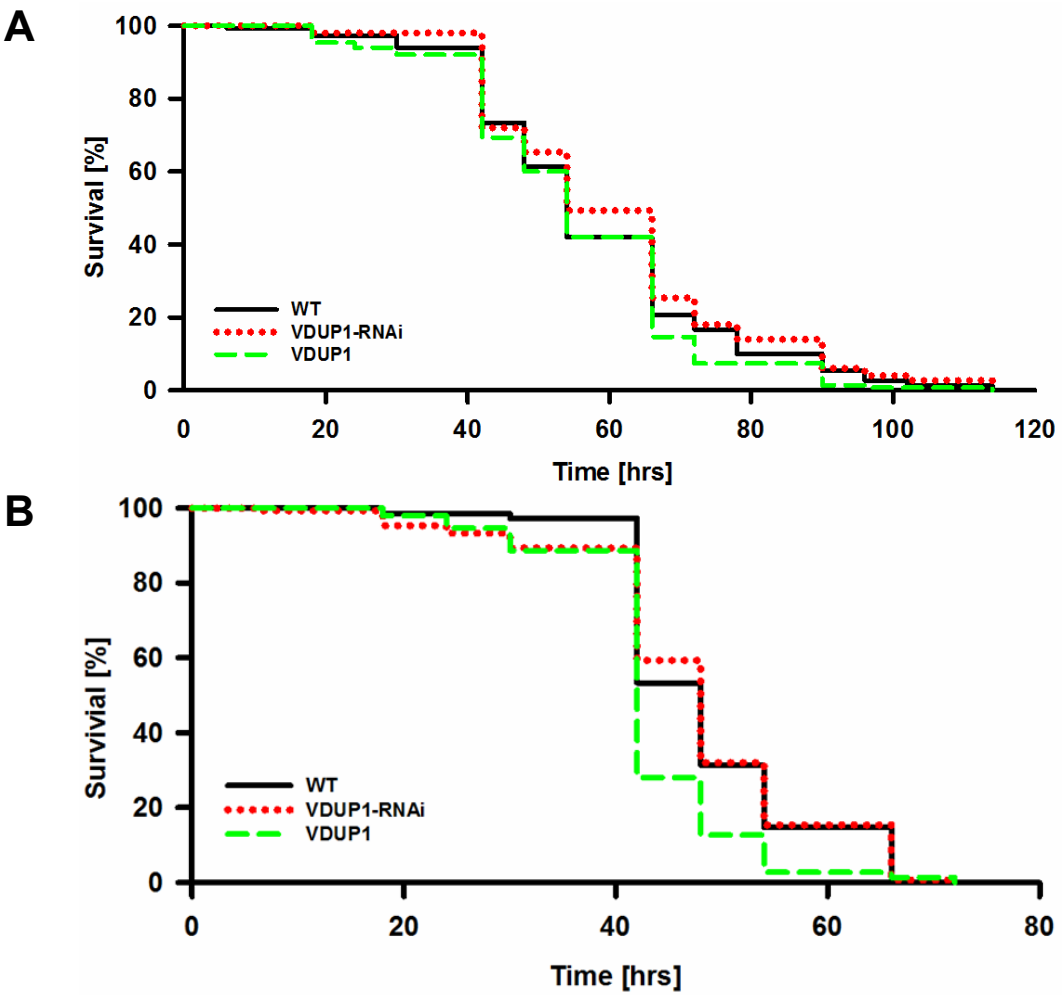

Figure 21: VDUP1 manipulation has no influence on starvation stress.
150 male **(A)** or female flies **(B)** per genotype were starved for the indicated time period. Water supply was ensured by a water-soaked filter paper. Dead flies were recorded every 6-12 hrs until all flies were dead.

Upon VDUP1 overexpression, Schneider S2 cells exhibited higher basal ROS levels (Figure 13). These can be, in part, attributed to a lower Trx activity (Figure 14). After treatment of S2 cells with H_2O_2, VDUP1-overexpressing cells show a lower resistance towards oxidative stress (Figure 15). To reveal whether VDUP1 manipulation also affects oxidative stress resistance *in vivo* flies were treated with the redox-cycling agent paraquat (PQ) which induced oxidative stress upon metabolization (Liou *et al.* 1997; McCarthy *et al.* 2004). A 5 % sucrose solution served as a control. As seen in Figure 22, PQ treatment substantially reduced survival (Figure 22A and B) whereas control treatment only led to sporadic death of

single flies (Supplementary Figure 1). Moreover, upon VDUP1 knockdown, flies showed no change in the survival curve and, therefore, in oxidative resistance (Figure 22A, male flies: 57.3 hrs compared to 67.5 hrs and Figure 22B, female flies 78.0 hrs compared to 72.6 hrs). Furthermore, VDUP1 overexpression had a strong effect on fly survival. VDUP1-overexpressing flies showed profoundly increased mortality upon PQ treatment compared to the corresponding WT strain. PQ treatment of male VDUP1 overexpression flies displayed a 39 % reduced survival (41.3 hrs compared to 67.5 hrs). The corresponding female flies exhibited a 43 % reduction of survival (41.6 hrs compared to 72.6 hrs). Moreover, survival curves were characterized by an initially high mortality during the first 20 hrs in both genders. This primary difference was perpetuated until the end of the experiment after 160 hrs. In conclusion, VDUP1 manipulation in *Drosophila* had no effect on weight of the flies and this was also reflected by an unchanged tolerance towards starvation stress. However, differential resistance towards oxidative stress between the single genotypes could be demonstrated. Whereas VDUP1 knockdown had no effect on oxidative stress resistance, overexpression of VDUP1 led to a reduced oxidative resistance. Therefore, the effect of VDUP1 manipulation is attributed to specific changes in cellular redox balance.

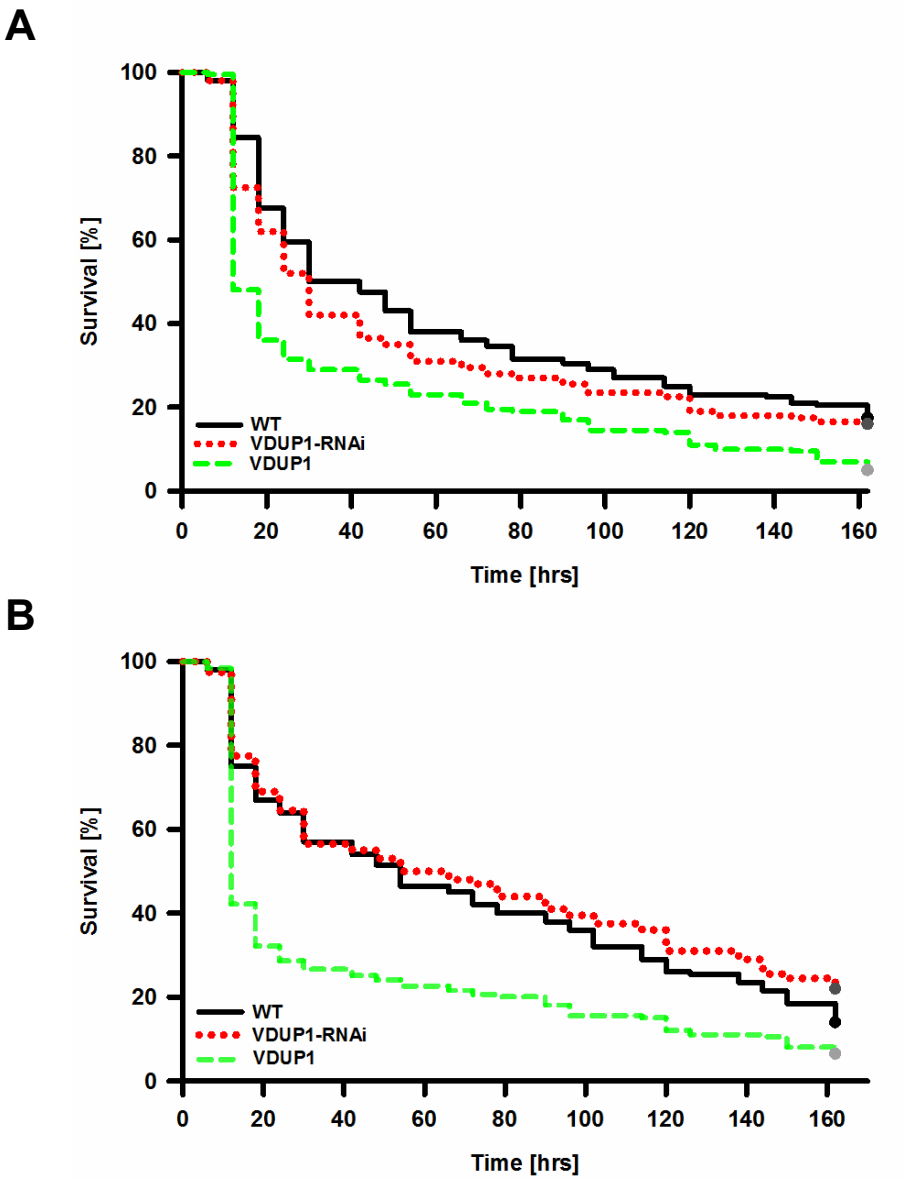

Figure 22: VDUP1 overexpression sensitizes flies towards oxidative stress.
Male **(A)** or female **(B)** flies were transferred to vials containing PQ. Flies were monitored for 160 hrs and dead flies were recorded every 6-12 hrs. Survival differences between groups were tested in each sex using log-rank test ($p<0.001$).

Table 2 gives a summary of mean survival rates determined upon PQ treatment.

Table 2: Overview of mean survival after PQ treatment in hrs.

males			females		
WT	VDUP1-RNAi	VDUP1	WT	VDUP1-RNAi	VDUP1
67.5	57.3	41.3	72.6	78.0	41.6

4.10 Paraquat treatment downregulates VDUP1 expression in flies

Having seen that VDUP1 knockdown had only mild effects on oxidative stress resistance in flies, changes in VDUP1 expression after PQ treatment were analyzed. For this purpose, age-matched eggs were seeded and hatched flies were mated for two days. After mating, flies were starved for three hrs before being transferred to new vials containing either 5 % sucrose without PQ (-PQ) or 5 % sucrose supplemented with PQ (+PQ). Flies were reared for 13- 17 hrs and afterwards lysed to extract total RNA. Next, cDNA was synthesized which was used for subsequent qRT-PCR. In WT flies, PQ treatment led to a pronounced downregulation of VDUP1 expression (male: 66 %, female: 80 %). VDUP1 knockdown flies, which were treated with PQ, exhibit similar VDUP1 expression as WT flies without PQ treatment (male: 76 %, female: 62 %) (Figure 23). Thus, PQ treatment alone led to marked downregulation of VDUP1 expression in the flies. PQ treatment could mimic genetically induced VDUP1 knockdown. Nevertheless, PQ treatment could not decrease VDUP1 expression further in VDUP1 knockdown flies.

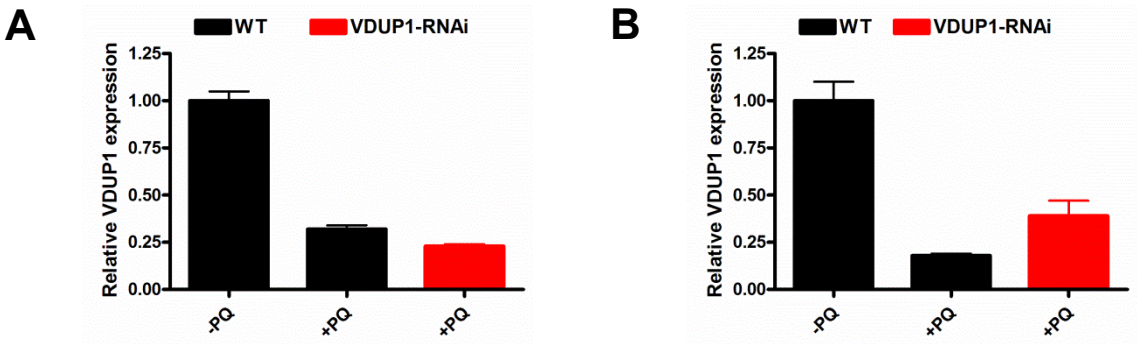

Figure 23: VDUP1 expression in flies is downregulated upon PQ treatment.
Aged-matched flies were starved and afterwards treated with either sucrose alone (-PQ) or sucrose supplemented with PQ (+PQ). Subsequently, total RNA was isolated and cDNA synthesized. Resulting cDNA was used for qRT-PCR using gene-specific primers. VDUP1 expression of male **(A)** or female flies **(B)** of the indicated genotypes. Results are displayed as relative gene expression compared to WT flies without PQ treatment and were normalized to *rp49* expression.

4.11 Mean lifespan of *Drosophila* is significantly shortened after VDUP1 overexpression

According to Harman's free radical theory aging is caused by the cytotoxic effects of ROS in cells (Harman 1956). Previous experiments in flies and S2 cells demonstrated elevated ROS levels and increased sensitivity towards oxidative stress upon VDUP1 overexpression. Therefore, the permanent state of a pro-oxidative environment and hence the accumulation of oxidative damage over time may impair diverse cellular processes. The latter eventually leads to aging of the cell. To analyze whether VDUP1 manipulation has an effect on overall lifespan, 705 flies per gender and genotype were reared in vials containing standard food without any additional supplementation. Functional knockdown of VDUP1 displayed only minor effects on healthy lifespan (Figure 24). Whereas VDUP1 knockdown in male flies showed no effect on lifespan compared to a corresponding WT strain (Figure 24A, 64.2 days to 68.1 days), female flies exhibited a marginal but significant prolongation in mean lifespan (Figure 24B, 73.3 days compared to 68.3 days). Nevertheless, maximum lifespan of the flies was not changed.

VDUP1 overexpression led to striking effects irrespective of the fly gender. Both male and female flies demonstrated a significantly shortened lifespan upon VDUP1 overexpression. Reduction of mean lifespan in male flies was 22 % (53.1 days compared to 68.1 days) whereas for female flies a reduction of mean lifespan of 19 % (55.5 days compared to 68.3 days) was observed. Despite the effect on mean lifespan, the maximum lifespan was not altered (Figure 24). To conclude, VDUP1 overexpression in flies caused a significant reduction of mean lifespan. This shortened lifespan was attributed to enhanced sensitivity towards oxidative stress (Figure 22). Hence, the effects of VDUP1 overexpression could be applied to the human situation where higher TXNIP expression upon aging correlated with increased ROS levels (Sass 2010). Moreover, female VDUP1 knockdown flies showed a prolonged lifespan which was associated with a mildly increased resistance towards oxidative stress (Figure 22). In turn, male VDUP1 knockdown flies display no change in lifespan compared to WT flies, which has to be further investigated. Yet, regardless of the genotype of the flies maximum lifespan was not changed.

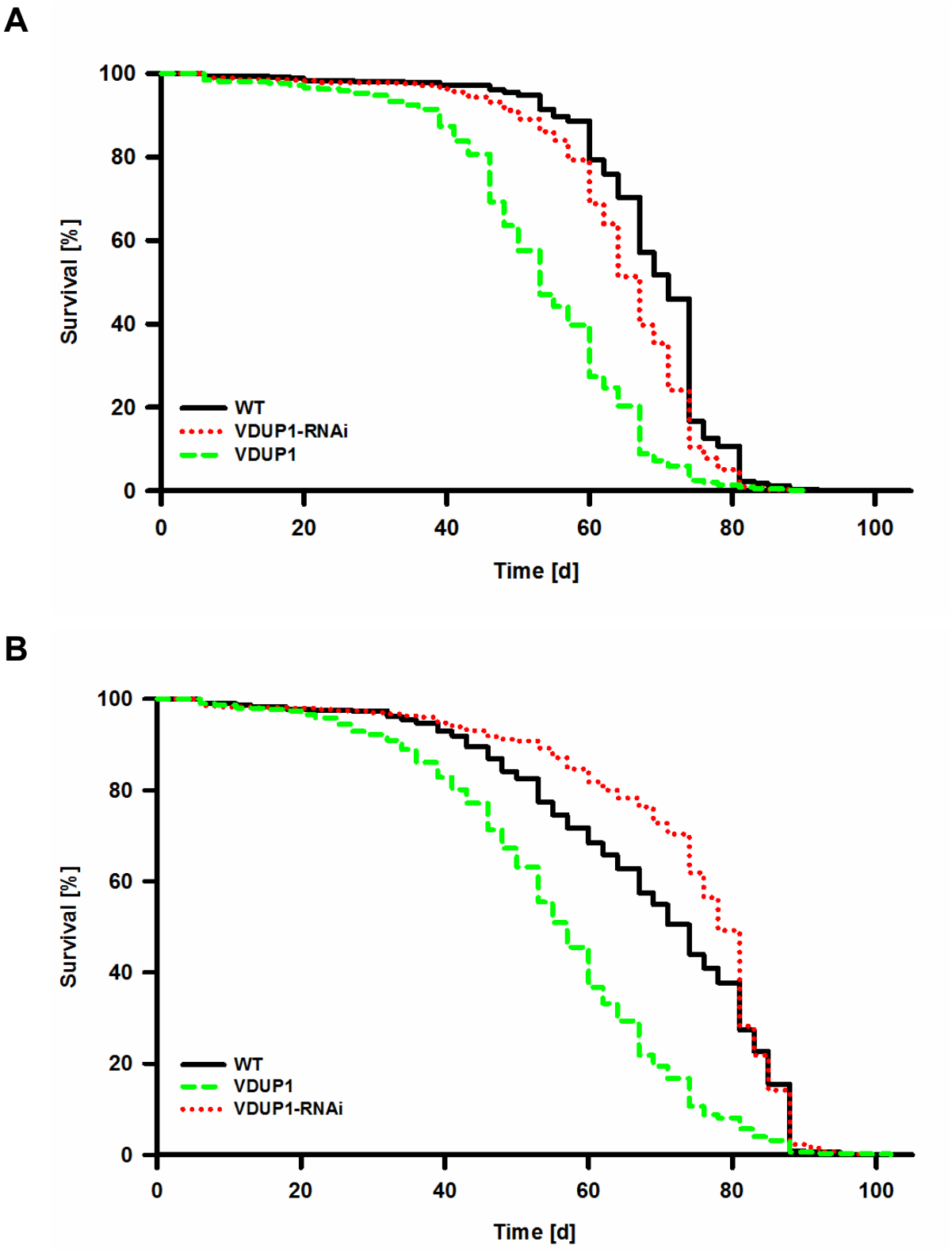

Figure 24: VDUP1 overexpression shortens mean lifespan of flies.
705 male **(A)** and female **(B)** flies per genotype were reared in vials containing standard food. Every 2-3 days flies were transferred into new vials and dead flies were recorded until all flies were dead. Survival differences between groups were tested in each sex using log-rank test ($p<0.001$). d= days.

In Table 3, mean lifespan rates determined during the experiment are summarized, again pointing to enhanced sensitivity towards oxidative stress as a cause of reduced survival in VDUP1-overexpressing flies.

Table 3: Overview of mean lifespan in days.

males			females		
WT	**VDUP1-RNAi**	**VDUP1**	**WT**	**VDUP1-RNAi**	**VDUP1**
68.1	64.2	53.3	68.3	73.3	55.5

5 DISCUSSION

Aging is a complex process marked by the accumulation of molecular, cellular, and organ damage eventually leading to impaired cellular function and an increased vulnerability to disease and death (Fontana *et al.* 2010). Biologically, there are several mechanisms which are causative for aging including telomere erosion, premature senescence, defective stem cell regeneration and enhanced oxidative stress (Harman 1956; Hayflick & Moorhead 1961; Harman 1972; Harley *et al.* 1990; Lansdorp *et al.* 1994). Addressing the last point, in 1956, Denham Harman developed the “free radical theory of aging” which correlated accumulation of cellular damage in macromolecules to aging. He stated that ROS were produced during metabolic processes which cause damage of cellular components like proteins, lipids and DNA. Over time this damage accumulates in cells and eventually leads to malfunction of diverse cellular processes (Harman 1956) Later, Harman specified his theory by the so called mitochondrial theory of aging which defined mitochondria as primary source of ROS (Harman 1972). In later years, the original theory was constantly modified and extended (Gruber *et al.* 2008). For example, in the oxidative stress theory of aging it was defined that oxidative stress and aging resulted from physiological processes in the cell. In particular, ROS are generated during ATP synthesis in the mitochondrial ETC. This is accompanied by an impaired anti-oxidative defense and a non-efficient repair of ROS-induced damage (Sohal & Weindruch 1996).

Moreover, it is known that upon aging the immune system becomes senescent, which is marked by accumulation of molecular defects in innate and adaptive immunity. In addition, aging is reported to promote a shift of naïve T cells to a memory phenotype, which is correlated to a higher risk of mortality in the elderly (Miller 1996; Linton & Dorshkind 2004). In previous studies, involvement of an oxidative signal after T cell receptor activation was described (Devadas *et al.* 2002; Gulow *et al.* 2005). TCR-triggering led to a proximal activation of PKCθ which mediated H_2O_2 release from complex I of the mitochondrial transport chain (Kaminski *et al.* 2007; Kaminski *et al.* 2010; Kamiński *et al.* 2012; Kamiński *et al.* 2013; Röth *et al.* 2014).

As cellular oxidative damage increased upon aging, the question was addressed whether the TCR-induced H_2O_2 signal was influenced during aging. It could be shown that elevated ROS levels in the elderly could impair T cell signaling and, thereby, led to malfunction of the immune system. On this account, possible factors regulating the TCR-induced ROS signal were investigated. TXNIP was identified as a critical regulator (Sass 2010). Furthermore, expression of TXNIP in T cells revealed to be age-dependent showing elevated expression in older individuals. Interestingly, enhanced age-dependent TXNIP expression was not restricted to T cells but could also be seen in other cell types like macrophages, hepatocytes, and hematopoietic stem cells (Sass, unpublished work). In addition, higher TXNIP expression is correlated with lower stress resistance raising the question whether TXNIP functions as a general regulator of aging processes.

This study was focused on generation of an appropriate *in vivo* and *in vitro* model to clarify the mechanism of TXNIP in age-related changes of cellular redox equilibrium as well as in the aging process itself.

5.1 Generation of a *Drosophila* model to study TXNIP (VDUP1) as a general regulator of aging

TXNIP is implicated in various metabolic processes such as lipid metabolism and the pathogenesis of age-related diseases such as diabetes (Donnelly *et al.* 2004; Oka *et al.* 2006; J. Chen *et al.* 2008). In diabetes, it could be demonstrated that elevated glucose levels resulted in enhanced TXNIP expression in β-cells. Furthermore, high levels of TXNIP induced activation of NLRP3, which led to induction of β-cell apoptosis (R Zhou *et al.* 2010; Schroder *et al.* 2010). Defective autophagy is a common sign of aging which is linked to ER stress. TXNIP was shown to be induced by ER stress through activation of protein kinase RNA-like endoplasmic reticulum kinase (PERK) and inositol-requiring enzyme 1α (IRE1α) pathways inducing NLRP3-mediated β-cell death (Oslowski *et al.* 2012; Lerner *et al.* 2012). In contrast, higher TXNIP expression induced peptide disulfide isomerases (PDI) activity leading to decreased ER stress (Lee *et al.* 2014). This provided a feedback loop of unfolded

protein response (UPR) signaling. Conclusively, age-dependent upregulation of TXNIP might exert a protective function in reducing ER stress which results from age-dependent loss of autophagy. Maintenance of a stem cell pool is essential to provide tissue regeneration. However, a reduced replicated potential of stem cells is deteriorative and often connected to an aged phenotype (Sharpless & DePinho 2007). It was reported that TXNIP played a role in the maintenance of the HSC pool upon oxidative stress. Thereby, TXNIP interfered with the interaction of mouse double minute 2 (MDM2) and p53 enhancing p53 stability. Otherwise, p53 reduced intracellular levels of ROS by induction of genes involved in anti-oxidative defense (Jung *et al.* 2013). Loss of TXNIP reduces p53-mediated induction of ant-oxidative genes and, thereby, contributes to higher cellular oxidative stress and defects in the hematopoietic system. Together with an age-dependent upregulation of TXNIP in HSC (Sass unpublished data), this suggests a conservative function upon aging. However, the studies described above are only assumptions of a potential function of TXNIP in the aging process and do not clarify the question whether TXNIP is a general regulator of aging.

To address this question, several animal models were considered. Mice as well as a *C. elegans* model were excluded due to long lifespan and the lack of a TXNIP homologue respectively. *Drosophila* is a widely-accepted aging model as it has several advantages compared to other *in vivo* models such as a relatively short lifespan, convenient husbandry, and facile genetics (Linford *et al.* 2013). Furthermore, it is possible to study many animals at the same time, which enables a meaningful statistical analysis.

Knowledge about the function of the *Drosophila* TXNIP homologue VDUP1 is limited. VDUP1 was reported to be expressed in the brain in a glucose-dependent manner (Levendusky *et al.* 2009). Glucose-dependent upregulation is, therefore, a common feature compared to humans (Schulze *et al.* 2004; Minn *et al.* 2005). Like in humans, this indicates a potential role in glucose homeostasis or various metabolic processes (Parikh *et al.* 2007; Wu *et al.* 2013).

In addition, *vdup1* was reported to harbor a binding site for the hedgehog (Hh)-dependent transcription factor Ci implying Hh-dependent regulation of VDUP1 expression in neurogenesis (Chang *et al.* 2010). Sustained VDUP1 expression after Hh knockout in the brain affected neurogenesis and cell proliferation (Mandalaywala

et al. 2008; Levendusky *et al.* 2009; Chang *et al.* 2010). It is conceivable that higher TXNIP levels in old flies are involved in neuro-degeneration due to induction of cell cycle arrest and senescence in brain cells. However, in comparison to humans, a direct influence of VDUP1 on fly aging has not been described.

To elucidate the importance of VDUP1 for aging in *Drosophila,* an *in vitro* system in the early embryo *Drosophila* cell line Schneider S2, which stably overexpressed VDUP1, was generated. Thereby, enhanced VDUP1 overexpression could be shown on mRNA as well as on protein level (Figure 10). To study the effect of VDUP1 manipulation in a whole organism, *Drosophila* was used an *in vivo* model. The *in vivo* model consists of three different fly strains ranging from a VDUP1-RNAi strain, possessing low VDUP1 expression, over a WT, which served as an internal control, to a strain exhibiting VDUP1 overexpression. Modulation of VDUP1 expression was realized by the GAL4-UAS system. Moreover, flies from different ages (12, 32 and 52 days after eclosion) were examined. While knockdown efficiency in the flies was less pronounced on mRNA level, overexpression was maintained during the entire lifespan (Figure 18). Nevertheless, on protein level, a proper knockdown efficiency was established. In contrast, VDUP1 overexpression in flies on protein level could be detected only in medium- and old-aged flies (Figure 19). This could be attributed to augmented proteasomal degradation which was described for human TXNIP by Zhang *et al.* (2010) and Sass (2010). However, an age-dependent upregulation of VDUP1 expression in *Drosophila* was not observed until 52 days of life (Figure 19). We presently test whether VDUP1 is detected after 52 days of life. However, the results suggest a different regulation of VDUP1 in *Drosophila* compared to humans. Despite the lack of an age-dependent upregulation, it is possible to phenocopy the human system as both, human TXNIP as well as *Drosophila* VDUP1, disturb cellular redox balance.

5.2 VDUP1 leads to a pro-oxidative shift in cellular redox balance

Reduction of proliferative capacity is a common sign of aged tissue. For instance, reduced proliferation was demonstrated for vascular smooth muscle cells and hepatocytes (Guntani *et al.* 2011; Iakova *et al.* 2003). In humans, TXNIP is an important regulator of differentiation, proliferation, and involved in the pathogenesis of different diseases such as cancer (Kim *et al.* 2007). For instance, in various cancer types TXNIP expression was shown to be low assuming that TXNIP acts as a tumor suppressor by downregulation of proliferation (Butler *et al.* 2002; Ikarashi *et al.* 2002; Sheth *et al.* 2006; Morrison *et al.* 2014). TXNIP exerts its anti-proliferative function by induction of a G_0/G_1 cell cycle arrest (Han *et al.* 2003). More precisely, G_0/G_1 arrest is induced by COPS5 interaction and, thereby, a stabilization of $p27^{kip1}$ in the nucleus (Jeon *et al.* 2005). The anti-proliferative function of TXNIP could, therefore, also have direct implications on cellular senescence. Cellular senescence due to a stable cell cycle arrest is an explicit sign of aging which is mainly caused by telomere shortening or increased expression of $p16^{INK4a}$ (Bodnar *et al.* 1998; Collado *et al.* 2007; Campisi & d'Adda di Fagagna 2007). Consequently, senescence results in impaired wound healing and tissue regeneration (Gosain & DiPietro 2004; Sousounis *et al.* 2014). Beyond the anti-proliferative role of TXNIP in humans, an inhibitory function of *Drosophila* VDUP1 on lamina precursor cell proliferation in the brain was demonstrated (Chang *et al.* 2010). Cell cycle progression was investigated in S2 cells. Of note, S2 cells were described as being spontaneously immortalized (Schneider 1972). For this reason, S2 cells could overcome the Hayflick limit and evade cellular senescence. Upon VDUP1 overexpression, S2 cells showed only a minor influence on cell cycle as the distribution of cells in the different cell cycle phases was unchanged (Figure 11). Due to the fact that S2 cells are an early embryonic cell line with characteristics of macrophages this may point to a cell type-specific mechanism in *Drosophila* rather than a general mechanism as proposed in the humans (Schneider 1972; Rämet *et al.* 2002). For this reason, cell cycle of other cell types needs to be investigated upon VDUP1 overexpression. Of particular interest are stem cells in which cell cycle arrest represents a crucial mechanism of aging (Sharpless & DePinho 2007).

Besides the function of cell cycle inhibition, human TXNIP is a regulator of the cellular redox equilibrium. This function is attributed to the specific formation of a mixed disulfide between TXNIP and the active center of Trx, which eventually inhibits the activity of Trx (Patwari *et al.* 2006; Patwari *et al.* 2009). Due to the specific inhibition of Trx, increased TXNIP expression led to higher basal ROS levels in human cells (Nishiyama *et al.* 1999; Junn *et al.* 2000; Wang *et al.* 2002). According to Harman's theory, oxidative stress is strongly correlated with aging. So far no direct involvement of *Drosophila* VDUP1 in oxidative stress regulation or aging is known. Therefore, basal ROS levels in S2 cells upon VDUP1 overexpression were determined by two distinct methods. Both DCF staining as well as confocal microscopy proved enhanced ROS generation under basal conditions. This indicated a similar function of VDUP1 in *Drosophila* and humans. Furthermore, overexpression of TXNIP was reported to lead to reduction of Trx expression as well as a reduced activity (Nishiyama *et al.* 1999; Wang *et al.* 2002). The *Drosophila* Trx system consists of three Trx homologues TRX-2, TrxT and DHD. Whereas Trx-2 is expressed in both genders, expression of DHD and TrxT is restricted to females and males respectively (Salz *et al.* 1994; Pellicena-Pallé *et al.* 1997; Bauer *et al.* 2002; Svensson *et al.* 2003). Expression of TRX-2, the fly homologue of human Trx1, as well as the two other known *Drosophila* thioredoxins TrxT and DHD were analyzed by qRT-PCR. Upon VDUP1 overexpression, no change in gene expression of the three different Trx could be detected in S2 cells on mRNA level (Figure 12). For TRX-2, unchanged expression was also confirmed on protein level (Figure 10B). Thus, an inhibitory effect on gene expression counteracting VDUP1 overexpression could be excluded for *Drosophila* VDUP1. However, gene expression of the three Trx is not necessarily connected to their anti-oxidative function. Therefore, Trx activity was checked by a fluorescence-based assay confirming decreased Trx activity after VDUP1 overexpression (Figure 14). The Trx activity assay served as an indirect proof of reduced overall Trx activity. Whether the activity levels of the single Trx were influcenced by VDUP1 manipulation needs to be subject of further investigations. A recent report linked age-associated degeneration of the central auditory system in rats to decreased expression of mitochondrial Trx2 in the brain. Likewise, an age-dependent upregulation of TXNIP expression could be observed which led to disruption of Trx2-ASK1 complex and ASK1-induced apoptosis (Sun *et al.* 2015). Although the results generated during this study did not show a reduced expression

of TRX-2, it is conceivable that increased VDUP1 expression could disrupt the potential interaction of *Drosophila* ASK1 and TRX-2 promoting apoptosis and ultimately neurodegeneration. Nonetheless, to date an interaction between VDUP1 and ASK1 in *Drosophila* is not reported.

In addition to the Trx system, the cell possesses several other redox systems, including SODs, catalase and non-enzymatic scavengers like glutathione (Droge 2002). The interplay of these redox systems orchestrates and maintains the cellular redox equilibrium. Therefore, expression levels of anti-oxidative enzymes such as SOD1, SOD2, SOD3 and catalase were determined in VDUP1-overexpressing cells by qRT-PCR. No changes in gene expression on mRNA level were observed (Figure 12). Loss of TRX-2 expression in *Drosophila* was correlated with upregulation of gene expression of anti-oxidative enzymes such as catalase, SOD and glutathione synthetase (M. Tsuda *et al.* 2010). However, a TRX-2 downregulation upon VDUP1 overexpression was not seen. Therefore, downregulation of anti-oxidative enzymes is unlikely. The results pointed to a Trx-specific mechanism whereas VDUP1 was not affecting other redox systems. In addition, VDUP1 exerted its function not by regulation of gene expression but *via* inhibition of Trx activity. Whether VDUP1 overexpression impairs intracellular glutathione levels as well as the ratio of reduced to oxidized glutathione needs to be further elucidated.

5.3 VDUP1 overexpression reduces resistance towards oxidative stress

In humans, TXNIP is described as an essential regulator in cellular glucose uptake by mediating internalization of the endogenous glucose transporter Glut1 (Wu *et al.* 2013). Permanently high levels of TXNIP impair cellular glucose homeostasis as a proper import of glucose will be disturbed. This eventually results in undersupply of the cell with glucose. Otherwise, malnutrition leads to a smaller body size and reduced starvation resistance. Thus, flies were starved from nutrients and survival was monitored. No differences between the fly strains could be observed, which

excluded an influence of VDUP1 on starvation stress (Figure 21). Furthermore, fly weight was not changed after VDUP1 manipulation (Figure 20).

Previous reports in human cells show sensitization of cells to oxidative stress upon TXNIP overexpression (Schulze *et al.* 2004). The study was focused on revealing *Drosophila* VDUP1s function in oxidative stress resistance. In *Drosophila*, no such function was described for VDUP1 so far. However, TRX-2 knockout was shown to sensitize flies to PQ-induced death (M. Tsuda *et al.* 2010). To analyze the effect of VDUP1 manipulation on resistance towards oxidative stress, VDUP1-overexpressing S2 cells were treated with H_2O_2. It could be shown that the shift towards a pro-oxidative cellular environment induced by VDUP1 overexpression led to enhanced oxidative stress sensitivity indicated by increased cell death (Figure 15). In line with the human data, the results confirmed a central role of VDUP1 in regulating sensitivity towards oxidative stress in *Drosophila*.

Next, to confirm the role of VDUP1 in sensitization to oxidative stress in an *in vivo* experiment, flies were treated with PQ and survival was monitored. VDUP1 knockdown had no effect on resistance towards oxidative stress in flies. However, VDUP1 overexpression led to reduced survival of the flies (Figure 22). These results are in line with the literature describing TXNIP overexpression as a cause for enhanced cellular oxidative stress and β –cell death (Schulze *et al.* 2004; Masutani *et al.* 2012). Yet, it was not clear why VDUP1 knockdown had no effect on oxidative stress resistance. From previous experiments performed in human T cells it could be shown that the TCR-mediated generation of ROS was sufficient to downregulate TXNIP expression (Sass 2010). PQ is a potent inducer of oxidative stress in the cell. Therefore, a comparable mechanism of VDUP1 downregulation upon PQ treatment might also be implicated in flies. In order to test whether a similar effect of VDUP1 downregulation existed in *Drosophila*, flies were treated with PQ and VDUP1 expression was determined by qRT-PCR. Here, a profound downregulation of VDUP1 after PQ treatment could be demonstrated which was able to mimic genetically-induced VDUP1 knockdown (Figure 23). Treating VDUP1 knockdown flies with PQ could not further reduce VDUP1 expression on the mRNA level. Hence, PQ treatment led to a similar VDUP1 expression level in WT flies compared to genetic VDUP1 knockdown. Referring back to the oxidative stress experiment, PQ-induced knockdown of VDUP1 was causative for an equal expression level of

VDUP1 of WT and VDUP1 knockdown flies resulting in a similar resistance towards oxidative stress (Figure 22).

Taken together, VDUP1 overexpression in S2 cells and in flies led to a higher sensitivity towards oxidative stress (Figure 15) which was attributed to a reduced Trx activity (Figure 14) together with higher levels of basal ROS (Figure 13). Furthermore, *in vivo*, an influence on weight and starvation stress could be excluded. This pointed to a unique function of VDUP1 in *Drosophila* by influencing resistance towards oxidative stress. Thereby, both, human TXNIP as well as the *Drosophila* homologue VDUP1, exert their function as a central regulator of oxidative stress resistance.

5.4 VDUP1 overexpression in *Drosophila* shortens lifespan

Drosophila is a common model in aging research. Much of the fundamental research about aging and the underlying processes was performed in flies. For example, the phenomenon of CR was observed more than 40 years ago when David *et al.* (1971) revealed that the food composition plays an important role in lifespan. However, the molecular processes behind CR are still a subject of debate. One possible mechanism involved the mTOR pathway since genetic as well as pharmacological inhibition of mTOR by rapamycin prolonged *Drosophila* lifespan up to 50 % (Kapahi *et al.* 2004; Bjedov *et al.* 2010). Furthermore, reduced IIS signaling was shown to extend *Drosophila* lifespan. For instance, mutation of the insulin receptor as well as of the corresponding insulin receptor substrate CHICO led to lifespan prolongation up to 50 % (Tatar *et al.* 2001; Clancy *et al.* 2001). Aside from metabolic interventions, there are also reports showing involvement redox-related aging processes in *Drosophila*. For example, overexpression of SOD in *Drosophila* was shown to extend lifespan (Landis & Tower 2005). In addition, an age-dependent decline of function for cytochrome c oxidase (complex IV) in flies could be shown by Schwarze *et al.* (1998). This functional decline led to enhanced ROS production in aged mitochondria. Most importantly, as discussed before, reduced TRX-2 expression is correlated to a decreased lifespan (Svensson & Larsson 2007; A. Tsuda *et al.* 2010).

To test the influence of VDUP1 manipulation on lifespan, flies were reared under standard conditions and survival was monitored until all flies were dead. Only mild effects on lifespan were observed upon VDUP1 knockdown. Male flies exhibit no effect on lifespan in contrast to female VDUP1 knockdown flies which showed a 12 % prolongation of mean lifespan (Figure 24). As the knockout efficiency in both genders was maintained throughout the experiment, only gender-specific reasons can be taken into account (Figure 19). In aging research gender-specific differences are common phenomena. For example, Magwere *et al.* (2004) demonstrated gender-dependent differences in CR. Lifespan of male flies peaked at 40 % standard food concentration whereas female flies exhibit maximal lifespan when the food concentration was reduced to 60 %. During the lifespan experiment the food concentration was standardized excluding potential nutritional effects. As a consequence, this indicated a gender-specific regulation of metabolism, which is subject of further studies. Interestingly, in the lifespan experiments VDUP1 manipulation had no impact on maximum lifespan. This can be explained by a heterogeneous fly population which also has single flies with an exceptionally long lifespan compared to the bulk of flies in one genotype.

In contrast to the mild effects seen after VDUP1 knockdown, VDUP1 overexpression in flies led to a marked reduction of mean lifespan of about 20 %. This implies that a permanent disturbance of the cellular redox equilibrium by VDUP1 overexpression is potentially harmful to cellular processes and, therefore, to the whole organism. This deterioration was expressed as a reduced mean lifespan of the fly. Increased expression of the human VDUP1 homologue TXNIP was also shown to be linked to a higher sensitivity towards oxidative stress (Schulze *et al.* 2004). Furthermore, enhanced expression of the VDUP1 human homologue TXNIP upon aging could be identified in various tissues (Sass, unpublished work). Assuming a similar function in both organisms and together with the observation of an age-dependent upregulation in humans, VDUP1 might be a general regulator of aging. Hence, by VDUP1 overexpression, flies can be a suitable model to mimic the cellular conditions in old human individuals. This suggests that age-dependent upregulation of TXNIP in humans correlates with sustained alteration of the cellular redox equilibrium which potentially causes symptoms of old age and eventually death. Thus, it could be clearly shown that regulation of the cellular redox equilibrium by VDUP1 is a novel mechanism during aging in *Drosophila*.

Altogether this study provides new insight into the molecular mechanism of VDUP1 activity. In humans, the VDUP1 homologue, TXNIP, was characterized as a crucial regulator of the cellular redox balance. Moreover, TXNIP expression was shown to be age-dependent displaying an elevated TXNIP expression upon aging. To analyze TXNIP function in aging processes, a *Drosophila* model was used as lifespan analyses are more practical to realize. The results obtained from *Drosophila* pointed to a similar function as observed in humans. The study could show that VDUP1 is a specific regulator of the cellular redox equilibrium which exerts its function, in part, by inhibition of Trx. This inhibition, in return, led to higher basal ROS production in the cell rendering cells as well as whole flies more sensitive towards oxidative stress after overexpression. In addition to its role in oxidative stress, a profound effect on fly lifespan could be observed (Figure 25). This makes VDUP1 a pivotal regulator which limits lifespan in the *Drosophila* model. Furthermore, due to the analogy to the human system, TXNIP represents a central protein in controlling the redox-dependent aging process.

5.5 Outlook

Future studies should focus on the substantiation of VDUP1's function as a redox regulator. For example, to provide a missing link between a disturbed cellular redox balance and aging, signs of ROS-induced oxidative damage (*e.g.* lipid peroxidation) could be further investigated. Another important issue is to investigate the physical interaction between TRX-2 and VDUP1 in *Drosophila* since all redox-related functions of human TXNIP require an interaction between TXNIP and Trx. It has also to be taken into account that VDUP1 might be able to bind the other two known Trx, namely TrxT and DHD. Aside from a potential interaction between Trx and VDUP1 there could be other interacting partners which provides a link between VDUP1 expressing and aging. A recent report from Qiao *et al.* (2015) described a role for TXNIP in autophagy induction. Together with the intrinsic mTOR inhibitor REDD1, TXNIP forms a complex which induces ROS-mediated autophagy. A loss of REDD1 disrupts the interaction with TXNIP and leads to failed autophagy due to accumulation of dysfunctional mitochondria. Because autophagy is a common sign of aging, it is conceivable to investigate cellular autophagy after VDUP1 manipulation in

flies. Nevertheless, a potential deteriorative effect of VDUP1 knockdown in flies is unlikely as, so far, VDUP1 knockdown flies do not show any sign of reduced survival due to dysfunctional mitochondria. To gain further insight into the VDUP1 mechanism of action, the generation of a loss-of-function in flies would be important to investigate. For this purpose, two S2 cell-based *in vitro* models were generated. First, cysteine residues in the VDUP1 protein were mutated in order to abrogate the proposed interaction between VDUP1 and TRX-2. In the second model a complete genetic knockout of the *vdup1* gene by CRISPR-Cas9 technology was realized. Due to clonal effects, for both systems subcloning is necessary before starting physiological experiments. Besides the function in diverse redox processes, there are cumulative reports describing TXNIP as a regulator in metabolism. For instance, TXNIP was reported to be responsible for internalization of the glucose transporter Glut-1 and, thereby, regulating glucose homeostasis (Wu *et al.* 2013). Taken together, the investigation of the connection of TXNIP/VDUP1 and aging is a challenging task for future.

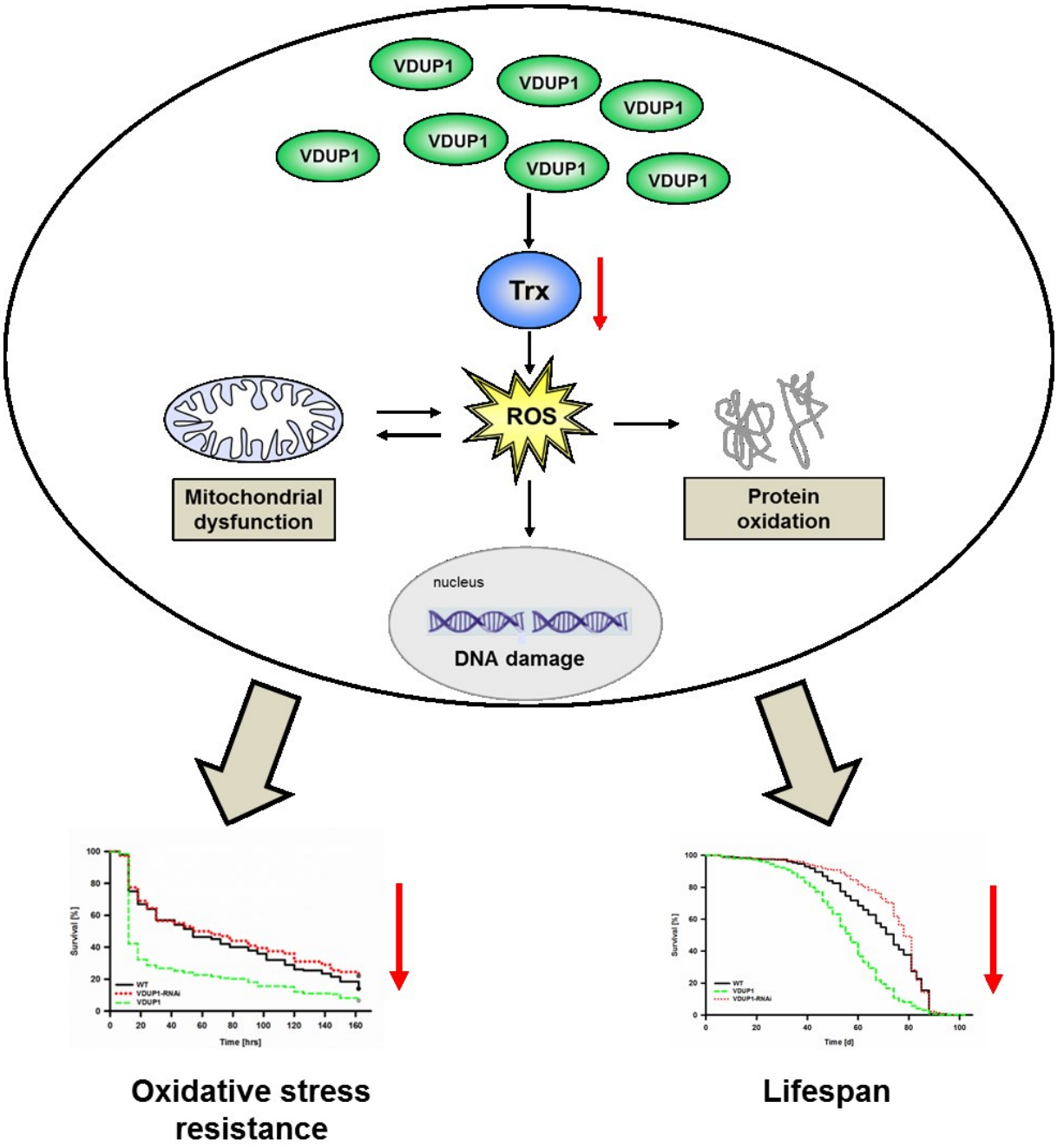

Figure 25: Higher VDUP1 expression sensitizes flies towards oxidative stress and shortens lifespan
Enhanced VDUP1 expression in *Drosophila* results in downregulation of Trx activity. In turn, levels of basal ROS increase leading to damage accumulation in DNA and proteins as well as an impairment of mitochondrial function. Permanent pro-oxidative redox balance leads to reduced oxidative resistance and lifespan shortening (adapted from Haigis & Yankner 2010).

REFERENCES

Adler, A.S. *et al.*, 2007. Motif module map reveals enforcement of aging by continual NF-kappaB activity. *Genes & development*, 21(24), pp.3244–57.

Agarwal, S. & Sohal, R.S., 1994. Aging and proteolysis of oxidized proteins. *Arch Biochem Biophys*, 309(1), pp.24–28.

Agarwal, S. & Sohal, R.S., 1996. Relationship between susceptibility to protein oxidation, aging, and maximum life span potential of different species. *Exp Gerontol*, 31(3), pp.365–372.

Aguirre, J. & Lambeth, J.D., 2010. Nox enzymes from fungus to fly to fish and what they tell us about Nox function in mammals. *Free radical biology & medicine*, 49(9), pp.1342–53.

Alcaín, F.J. & Villalba, J.M., 2009. Sirtuin activators. *Expert opinion on therapeutic patents*, 19(4), pp.403–14.

Alers, S. *et al.*, 2012. Role of AMPK-mTOR-Ulk1/2 in the regulation of autophagy: cross talk, shortcuts, and feedbacks. *Molecular and cellular biology*, 32(1), pp.2–11.

Allsopp, R.C. *et al.*, 1992. Telomere length predicts replicative capacity of human fibroblasts. *Proc Natl Acad Sci U S A*, 89(21), pp.10114–10118.

Alvarez, C.E., 2008. On the origins of arrestin and rhodopsin. *BMC Evol Biol*, 8, p.222.

Andrade, L.N. de S. *et al.*, 2012. Evidence for premature aging due to oxidative stress in iPSCs from Cockayne syndrome. *Human molecular genetics*, 21(17), pp.3825–34.

Anisimov, V.N. *et al.*, 2005. Metformin decelerates aging and development of mammary tumors in HER-2/neu transgenic mice. *Bulletin of experimental biology and medicine*, 139(6), pp.721–3.

Anisimov, V.N., 2010. Metformin for aging and cancer prevention. *Aging*, 2(11), pp.760–74.

Armanios, M. & Blackburn, E.H., 2012. The telomere syndromes. *Nature reviews. Genetics*, 13(10), pp.693–704.

Artandi, S.E. *et al.*, 2002. Constitutive telomerase expression promotes mammary carcinomas in aging mice. *Proc Natl Acad Sci U S A*, 99(12), pp.8191–8196.

Bahadorani, S. *et al.*, 2010. Perturbation of mitochondrial complex V alters the response to dietary restriction in Drosophila. *Aging cell*, 9(1), pp.100–3.

Balaban, R.S., Nemoto, S. & Finkel, T., 2005. Mitochondria, oxidants, and aging. *Cell*, 120(4), pp.483–495.

Bass, T.M. *et al.*, 2007. Effects of resveratrol on lifespan in Drosophila melanogaster and Caenorhabditis elegans. *Mech Ageing Dev*, 128(10), pp.546–552.

Bassett, A.R. *et al.*, 2013. Mutagenesis and homologous recombination in Drosophila cell lines using CRISPR/Cas9. *Biology Open*, 3(1), pp.42–49.

Bauer, H., Kanzok, S.M. & Schirmer, R.H., 2002. Thioredoxin-2 but not thioredoxin-1 is a substrate of thioredoxin peroxidase-1 from Drosophila melanogaster: isolation and characterization of a second thioredoxin in D. Melanogaster and evidence for distinct biological functions of Trx-1 and Trx-2. *The Journal of biological chemistry*, 277(20), pp.17457–63.

Baur, J.A. *et al.*, 2006. Resveratrol improves health and survival of mice on a high-calorie diet. *Nature*, 444(7117), pp.337–342.

Bayne, A.-C. V *et al.*, 2005. Enhanced catabolism of mitochondrial superoxide/hydrogen peroxide and aging in transgenic Drosophila. *The Biochemical journal*, 391(Pt 2), pp.277–84.

Beckman, K.B. & Ames, B.N., 1998. The free radical theory of aging matures. *Physiol Rev*, 78(2), pp.547–581.

Benzi, G. *et al.*, 1992. The mitochondrial electron transfer alteration as a factor involved in the brain aging. *Neurobiol Aging*, 13(3), pp.361–368.

Berggren, M. *et al.*, 1996. Thioredoxin and thioredoxin reductase gene expression in human tumors and cell lines, and the effects of serum stimulation and hypoxia. *Anticancer Res*, 16(6B), pp.3459–3466.

Bernardes de Jesus, B. *et al.*, 2012. Telomerase gene therapy in adult and old mice delays aging and increases longevity without increasing cancer. *EMBO molecular medicine*, 4(8), pp.691–704.

Bjedov, I. *et al.*, 2010. Mechanisms of life span extension by rapamycin in the fruit fly Drosophila melanogaster. *Cell Metab*, 11(1), pp.35–46.

Bjorksten, J., 1968. The crosslinkage theory of aging. *Journal of the American Geriatrics Society*, 16(4), pp.408–27.

Blackney, M.J. *et al.*, 2014. Cloning and expression analysis of Drosophila extracellular Cu Zn superoxide dismutase. *Bioscience reports*, 34(6), p.e00164.

Blasco, M.A., 2007. Telomere length, stem cells and aging. *Nature chemical biology*, 3(10), pp.640–9.

Bodnar, A.G. *et al.*, 1998. Extension of life-span by introduction of telomerase into normal human cells. *Science (New York, N.Y.)*, 279(5349), pp.349–52.

Bodnar, J.S. *et al.*, 2002. Positional cloning of the combined hyperlipidemia gene Hyplip1. *Nature genetics*, 30(1), pp.110–6.

Boily, G. *et al.*, 2008. SirT1 regulates energy metabolism and response to caloric restriction in mice. *PloS one*, 3(3), p.e1759.

Bonner, J.M. & Boulianne, G.L., 2011. Drosophila as a model to study age-related neurodegenerative disorders: Alzheimer's disease. *Experimental gerontology*, 46(5), pp.335–9.

Le Bourg, E., 2011. Using Drosophila melanogaster to study the positive effects of mild stress on aging. *Experimental gerontology*, 46(5), pp.345–8.

Bowling, A.C. *et al.*, 1993. Age-dependent impairment of mitochondrial function in primate brain. *J Neurochem*, 60(5), pp.1964–1967.

Brys, K., Vanfleteren, J.R. & Braeckman, B.P., 2007. Testing the rate-of-living/oxidative damage theory of aging in the nematode model Caenorhabditis elegans. *Experimental gerontology*, 42(9), pp.845–51.

Butler, L.M. *et al.*, 2002. The histone deacetylase inhibitor SAHA arrests cancer cell growth, up-regulates thioredoxin-binding protein-2, and down-regulates thioredoxin. *Proc Natl Acad Sci U S A*, 99(18), pp.11700–11705.

Cadenas, S. *et al.*, 1994. Caloric and carbohydrate restriction in the kidney: effects on free radical metabolism. *Experimental gerontology*, 29(1), pp.77–88.

Calamini, B. *et al.*, 2010. Pleiotropic mechanisms facilitated by resveratrol and its metabolites. *The Biochemical journal*, 429(2), pp.273–82.

Campisi, J., 2000. Cancer, aging and cellular senescence. *In Vivo*, 14(1), pp.183–188.

Campisi, J. & d'Adda di Fagagna, F., 2007. Cellular senescence: when bad things happen to good cells. *Nat Rev Mol Cell Biol*, 8(9), pp.729–740.

Cantó, C. *et al.*, 2009. AMPK regulates energy expenditure by modulating NAD+ metabolism and SIRT1 activity. *Nature*, 458(7241), pp.1056–60.

Canto, C. & Auwerx, J., 2009. Caloric restriction, SIRT1 and longevity. *Trends Endocrinol Metab*, 20(7), pp.325–331.

Cawthon, R.M. *et al.*, 2003. Association between telomere length in blood and mortality in people aged 60 years or older. *Lancet*, 361(9355), pp.393–395.

Chakkalakal, J. V *et al.*, 2012. The aged niche disrupts muscle stem cell quiescence. *Nature*, 490(7420), pp.355–60.

Chan, A.C. *et al.*, 1991. The zeta chain is associated with a tyrosine kinase and upon T-cell antigen receptor stimulation associates with ZAP-70, a 70-kDa tyrosine phosphoprotein. *Proceedings of the National Academy of Sciences*, 88(20), pp.9166–9170.

Chang, S. *et al.*, 2010. Hedgehog-dependent down-regulation of the tumor suppressor, vitamin D3 up-regulated protein 1 (VDUP1), precedes lamina development in Drosophila. *Brain Res*, 1324, pp.1–13.

Chen, D. *et al.*, 2008. Tissue-specific regulation of SIRT1 by calorie restriction. *Genes & development*, 22(13), pp.1753–7.

Chen, D. & Guarente, L., 2007. SIR2: a potential target for calorie restriction mimetics. *Trends Mol Med*, 13(2), pp.64–71.

Chen, J. *et al.*, 2008. Thioredoxin-interacting protein: a critical link between glucose toxicity and beta-cell apoptosis. *Diabetes*, 57(4), pp.938–944.

Chen, K.S. & DeLuca, H.F., 1994. Isolation and characterization of a novel cDNA from HL-60 cells treated with 1,25-dihydroxyvitamin D-3. *Biochim Biophys Acta*, 1219(1), pp.26–32.

Chutkow, W.A. *et al.*, 2008. Thioredoxin-interacting protein (Txnip) is a critical regulator of hepatic glucose production. *J Biol Chem*, 283(4), pp.2397–2406.

Claesson, M.J. *et al.*, 2012. Gut microbiota composition correlates with diet and health in the elderly. *Nature*, 488(7410), pp.178–84.

Clancy, D.J. *et al.*, 2001. Extension of life-span by loss of CHICO, a Drosophila insulin receptor substrate protein. *Science (New York, N.Y.)*, 292(5514), pp.104–6.

Collado, M., Blasco, M.A. & Serrano, M., 2007. Cellular Senescence in Cancer and Aging. *Cell*, 130(2), pp.223–233.

Coller, H.A. & Coller, B.S., 1983. Statistical analysis of repetitive subcloning by the limiting dilution technique with a view toward ensuring hybridoma monoclonality. *Hybridoma*, 2(1), pp.91–6.

Colman, R.J. *et al.*, 2009. Caloric restriction delays disease onset and mortality in rhesus monkeys. *Science*, 325(5937), pp.201–204.

Conboy, I.M. *et al.*, 2005. Rejuvenation of aged progenitor cells by exposure to a young systemic environment. *Nature*, 433(7027), pp.760–4.

Copeland, J.M. *et al.*, 2009. Extension of Drosophila life span by RNAi of the mitochondrial respiratory chain. *Current biology : CB*, 19(19), pp.1591–8.

Cornelius, E., 1972. Increased incidence of lymphomas in thymectomized mice--evidence for an immunological theory of aging. *Experientia*, 28(4), p.459.

David, J., Van Herrewege, J. & Fouillet, P., 1971. Quantitative under-feeding of drosophila: Effects on adult longevity and fecundity. *Experimental Gerontology*, 6(3), pp.249–257.

Davidovic, M. *et al.*, 2010. Old age as a privilege of the “selfish ones”. *Aging and disease*, 1(2), pp.139–46.

Davoli, T. & de Lange, T., 2011. The causes and consequences of polyploidy in normal development and cancer. *Annual review of cell and developmental biology*, 27, pp.585–610.

Dean, P.N. & Jett, J.H., 1974. Mathematical analysis of DNA distributions derived from flow microfluorometry. *The Journal of cell biology*, 60(2), pp.523–7.

Deeks, S.G., 2011. HIV infection, inflammation, immunosenescence, and aging. *Annual review of medicine*, 62, pp.141–55.

Devadas, S. *et al.*, 2002. Discrete generation of superoxide and hydrogen peroxide by T cell receptor stimulation: selective regulation of mitogen-activated protein kinase activation and fas ligand expression. *J Exp Med*, 195(1), pp.59–70.

Donnelly, K.L. *et al.*, 2004. Increased lipogenesis and fatty acid reesterification contribute to hepatic triacylglycerol stores in hyperlipidemic Txnip-/- mice. *J Nutr*, 134(6), pp.1475–1480.

Donnelly, K.L. *et al.*, 2004. Increased lipogenesis and fatty acid reesterification contribute to hepatic triacylglycerol stores in hyperlipidemic Txnip-/- mice. *The Journal of nutrition*, 134(6), pp.1475–80.

Droge, W., 2002. Free radicals in the physiological control of cell function. *Physiol Rev*, 82(1), pp.47–95.

Dröge, W. *et al.*, 1994. Functions of glutathione and glutathione disulfide in immunology and immunopathology. *FASEB journal : official publication of the Federation of American Societies for Experimental Biology*, 8(14), pp.1131–8.

El-Mir, M.-Y. *et al.*, 2000. Dimethylbiguanide Inhibits Cell Respiration via an Indirect Effect Targeted on the Respiratory Chain Complex I. *Journal of Biological Chemistry*, 275(1), pp.223–228.

Eriksson, M. *et al.*, 2003. Recurrent de novo point mutations in lamin A cause Hutchinson-Gilford progeria syndrome. *Nature*, 423(6937), pp.293–8.

Fenton, H.J.H., 1894. LXXIII.?Oxidation of tartaric acid in presence of iron. *Journal of the Chemical Society, Transactions*, 65, p.899.

Ferguson, M. *et al.*, 2005. Age-associated decline in mitochondrial respiration and electron transport in Drosophila melanogaster. *Biochemical Journal*, 390(2), pp.501–511.

Fernandes, A.P. & Holmgren, A., 2004. Glutaredoxins: glutathione-dependent redox enzymes with functions far beyond a simple thioredoxin backup system. *Antioxidants & redox signaling*, 6(1), pp.63–74.

Fernandez-Marcos, P.J. & Auwerx, J., 2011. Regulation of PGC-1 , a nodal regulator of mitochondrial biogenesis. *American Journal of Clinical Nutrition*, 93(4), p.884S–890S.

Ferreira, A.M.D.C. *et al.*, 1993. Copper(I) transfer into metallothionein mediated by glutathione. *Biochemical Journal*, 292(3), pp.673–676.

Filomeni, G., Rotilio, G. & Ciriolo, M.R., 2002. Cell signalling and the glutathione redox system. *Biochem Pharmacol*, 64(5-6), pp.1057–1064.

Finco, T.S. *et al.*, 1998. LAT is required for TCR-mediated activation of PLCgamma1 and the Ras pathway. *Immunity*, 9(5), pp.617–26.

Finkel, T. & Holbrook, N.J., 2000. Oxidants, oxidative stress and the biology of ageing. *Nature*, 408(6809), pp.239–247.

Flachsbart, F. *et al.*, 2009. Association of FOXO3A variation with human longevity confirmed in German centenarians. *Proc Natl Acad Sci U S A*, 106(8), pp.2700–2705.

Flores, I., Cayuela, M.L. & Blasco, M.A., 2005. Effects of telomerase and telomere length on epidermal stem cell behavior. *Science (New York, N.Y.)*, 309(5738), pp.1253–6.

Fontana, L. & Klein, S., 2007. Aging, adiposity, and calorie restriction. *JAMA*, 297(9), pp.986–994.

Fontana, L., Partridge, L. & Longo, V.D., 2010. Extending healthy life span--from yeast to humans. *Science*, 328(5976), pp.321–326.

Foukas, L.C. *et al.*, 2013. Long-term p110α PI3K inactivation exerts a beneficial effect on metabolism. *EMBO molecular medicine*, 5(4), pp.563–71.

Freitas, A.A. & de Magalhães, J.P., 2011. A review and appraisal of the DNA damage theory of ageing. *Mutation research*, 728(1-2), pp.12–22.

Fridovich, I., 1995. Superoxide radical and superoxide dismutases. *Annu Rev Biochem*, 64, pp.97–112.

Galimov, E.R. *et al.*, 2014. Prooxidant properties of p66shc are mediated by mitochondria in human cells. *PloS one*, 9(3), p.e86521.

Galimov, E.R., 2010. The Role of p66shc in Oxidative Stress and Apoptosis. *Acta naturae*, 2(4), pp.44–51.

Gardner, T.S., 1948. The use of Drosophila melanogaster as a screening agent for longevity factors; pantothenic acid as a longevity factor in royal jelly. *Journal of gerontology*, 3(1), pp.1–8.

Gasdaska, P.Y. *et al.*, 1994. The predicted amino acid sequence of human thioredoxin is identical to that of the autocrine growth factor human adult T-cell derived factor (ADF): thioredoxin mRNA is elevated in some human tumors. *Biochim Biophys Acta*, 1218(3), pp.292–296.

Gillum, M.P. *et al.*, 2011. SirT1 Regulates Adipose Tissue Inflammation. *Diabetes*, 60(12), pp.3235–3245.

Giorgio, M. *et al.*, 2005. Electron transfer between cytochrome c and p66Shc generates reactive oxygen species that trigger mitochondrial apoptosis. *Cell*, 122(2), pp.221–33.

Gosain, A. & DiPietro, L.A., 2004. Aging and wound healing. *World journal of surgery*, 28(3), pp.321–6.

Green, D.R., Galluzzi, L. & Kroemer, G., 2011. Mitochondria and the autophagy-inflammation-cell death axis in organismal aging. *Science (New York, N.Y.)*, 333(6046), pp.1109–12.

Greenspan, R.J., 1996. *Fly Pushing: The Theory & Practice of Drosophila Genetics*, Cold Spring Harbor Laboratory Press.

Greer, E.L. *et al.*, 2010. Members of the H3K4 trimethylation complex regulate lifespan in a germline-dependent manner in C. elegans. *Nature*, 466(7304), pp.383–7.

Greer, E.L. & Brunet, A., 2009. Different dietary restriction regimens extend lifespan by both independent and overlapping genetic pathways in C. elegans. *Aging cell*, 8(2), pp.113–27.

Gringhuis, S.I. *et al.*, 2000. Displacement of Linker for Activation of T Cells from the Plasma Membrane Due to Redox Balance Alterations Results in Hyporesponsiveness of Synovial Fluid T Lymphocytes in Rheumatoid Arthritis. *The Journal of Immunology*, 164(4), pp.2170–2179.

Gruber, J., Schaffer, S. & Halliwell, B., 2008. The mitochondrial free radical theory of ageing--where do we stand? *Front Biosci*, 13, pp.6554–6579.

Gulow, K. *et al.*, 2005. HIV-1 trans-activator of transcription substitutes for oxidative signaling in activation-induced T cell death. *J Immunol*, 174(9), pp.5249–5260.

Guntani, A. *et al.*, 2011. Reduced proliferation of aged human vascular smooth muscle cells--role of oxygen-derived free radicals and BubR1 expression. *The Journal of surgical research*, 170(1), pp.143–9.

Gupta, S., 1989. Membrane signal transduction in T cells in aging humans. *Ann N Y Acad Sci*, 568, pp.277–282.

Haendeler, J., 2006. Thioredoxin-1 and posttranslational modifications. *Antioxidants & redox signaling*, 8(9-10), pp.1723–8.

Haigis, M.C. & Yankner, B.A., 2010. The aging stress response. *Mol Cell*, 40(2), pp.333–344.

Hampton, M.B., Kettle, A.J. & Winterbourn, C.C., 1998. Inside the neutrophil phagosome: oxidants, myeloperoxidase, and bacterial killing. *Blood*, 92(9), pp.3007–17.

Han, S.H. *et al.*, 2003. VDUP1 upregulated by TGF-beta1 and 1,25-dihydorxyvitamin D3 inhibits tumor cell growth by blocking cell-cycle progression. *Oncogene*, 22(26), pp.4035–4046.

Hancock, C.R. *et al.*, 2011. Does calorie restriction induce mitochondrial biogenesis? A reevaluation. *FASEB journal : official publication of the Federation of American Societies for Experimental Biology*, 25(2), pp.785–91.

Harley, C.B., Futcher, A.B. & Greider, C.W., 1990. Telomeres shorten during ageing of human fibroblasts. *Nature*, 345(6274), pp.458–460.

Harman, D., 1956. Aging: a theory based on free radical and radiation chemistry. *J Gerontol*, 11(3), pp.298–300.

Harman, D., 1972a. Free radical theory of aging: dietary implications. *Am J Clin Nutr*, 25(8), pp.839–843.

Harman, D., 1972b. The biologic clock: the mitochondria? *Journal of the American Geriatrics Society*, 20(4), pp.145–7.

Harrison, D.E. *et al.*, 2009. Rapamycin fed late in life extends lifespan in genetically heterogeneous mice. *Nature*, 460(7253), pp.392–395.

Hartl, F.U., Bracher, A. & Hayer-Hartl, M., 2011. Molecular chaperones in protein folding and proteostasis. *Nature*, 475(7356), pp.324–32.

Hawkes, H.-J.K., Karlenius, T.C. & Tonissen, K.F., 2014. Regulation of the human thioredoxin gene promoter and its key substrates: a study of functional and putative regulatory elements. *Biochimica et biophysica acta*, 1840(1), pp.303–14.

Hayflick, L. & Moorhead, P.S., 1961. The serial cultivation of human diploid cell strains. *Exp Cell Res*, 25, pp.585–621.

Van Heemst, D., 2010. Insulin, IGF-1 and longevity. *Aging and disease*, 1(2), pp.147–57.

Heigwer, F., Kerr, G. & Boutros, M., 2014. E-CRISP: fast CRISPR target site identification. *Nature methods*, 11(2), pp.122–3.

Hekimi, S., Lapointe, J. & Wen, Y., 2011. Taking a “good” look at free radicals in the aging process. *Trends in cell biology*, 21(10), pp.569–76.

Herranz, D. *et al.*, 2010. Sirt1 improves healthy ageing and protects from metabolic syndrome-associated cancer. *Nature communications*, 1, p.3.

Hirota, K. *et al.*, 1999. Distinct roles of thioredoxin in the cytoplasm and in the nucleus. A two-step mechanism of redox regulation of transcription factor NF-kappaB. *J Biol Chem*, 274(39), pp.27891–27897.

Hoeijmakers, J.H.J., 2009. DNA damage, aging, and cancer. *The New England journal of medicine*, 361(15), pp.1475–85.

Holmström, K.M. & Finkel, T., 2014. Cellular mechanisms and physiological consequences of redox-dependent signalling. *Nature reviews. Molecular cell biology*, 15(6), pp.411–21.

Houtkooper, R.H., Williams, R.W. & Auwerx, J., 2010. Metabolic networks of longevity. *Cell*, 142(1), pp.9–14.

Howitz, K.T. *et al.*, 2003. Small molecule activators of sirtuins extend Saccharomyces cerevisiae lifespan. *Nature*, 425(6954), pp.191–6.

Hwang, J. *et al.*, 2014. The structural basis for the negative regulation of thioredoxin by thioredoxin-interacting protein. *Nature communications*, 5, p.2958.

Iakova, P., Awad, S.S. & Timchenko, N.A., 2003. Aging reduces proliferative capacities of liver by switching pathways of C/EBPalpha growth arrest. *Cell*, 113(4), pp.495–506.

Ikarashi, M. *et al.*, 2002. Vitamin D3 up-regulated protein 1 (VDUP1) expression in gastrointestinal cancer and its relation to stage of disease. *Anticancer Res*, 22(6C), pp.4045–4048.

Ingram, D.K. *et al.*, 2006. Calorie restriction mimetics: an emerging research field. *Aging Cell*, 5(2), pp.97–108.

Ingram, D.K. *et al.*, 1990. Dietary restriction and aging: the initiation of a primate study. *Journal of gerontology*, 45(5), pp.B148–63.

Jackson, S.H. *et al.*, 2004. T cells express a phagocyte-type NADPH oxidase that is activated after T cell receptor stimulation. *Nat Immunol*, 5(8), pp.818–827.

Janzen, V. *et al.*, 2006. Stem-cell ageing modified by the cyclin-dependent kinase inhibitor p16INK4a. *Nature*, 443(7110), pp.421–6.

Jaskelioff, M. *et al.*, 2011. Telomerase reactivation reverses tissue degeneration in aged telomerase-deficient mice. *Nature*, 469(7328), pp.102–6.

Jeon, J.H. *et al.*, 2005. Tumor suppressor VDUP1 increases p27(kip1) stability by inhibiting JAB1. *Cancer Res*, 65(11), pp.4485–4489.

Jin, K., 2010. Modern Biological Theories of Aging. *Aging and disease*, 1(2), pp.72–74.

Johnson, S.C., Rabinovitch, P.S. & Kaeberlein, M., 2013. mTOR is a key modulator of ageing and age-related disease. *Nature*, 493(7432), pp.338–45.

Jones, M.A. & Grotewiel, M., 2011. Drosophila as a model for age-related impairment in locomotor and other behaviors. *Experimental gerontology*, 46(5), pp.320–5.

Jung, H. *et al.*, 2013. TXNIP maintains the hematopoietic cell pool by switching the function of p53 under oxidative stress. *Cell metabolism*, 18(1), pp.75–85.

Junn, E. *et al.*, 2000. Vitamin D3 up-regulated protein 1 mediates oxidative stress via suppressing the thioredoxin function. *J Immunol*, 164(12), pp.6287–6295.

Kaeberlein, M., McVey, M. & Guarente, L., 1999. The SIR2/3/4 complex and SIR2 alone promote longevity in Saccharomyces cerevisiae by two different mechanisms. *Genes & development*, 13(19), pp.2570–80.

Kallis, G.B. & Holmgren, A., 1980. Differential reactivity of the functional sulfhydryl groups of cysteine-32 and cysteine-35 present in the reduced form of thioredoxin from Escherichia coli. *J Biol Chem*, 255(21), pp.10261–10265.

Kaminski, M. *et al.*, 2007. Novel role for mitochondria: protein kinase Ctheta-dependent oxidative signaling organelles in activation-induced T-cell death. *Mol Cell Biol*, 27(10), pp.3625–3639.

Kaminski, M.M. *et al.*, 2010. Mitochondrial reactive oxygen species control T cell activation by regulating IL-2 and IL-4 expression: mechanism of ciprofloxacin-mediated immunosuppression. *J Immunol*, 184(9), pp.4827–4841.

Kamiński, M.M. *et al.*, 2012. Manganese superoxide dismutase: a regulator of T cell activation-induced oxidative signaling and cell death. *Biochimica et biophysica acta*, 1823(5), pp.1041–52.

Kamiński, M.M. *et al.*, 2013. Mitochondria as oxidative signaling organelles in T-cell activation: Physiological role and pathological implications. *Archivum Immunologiae et Therapiae Experimentalis*, 61(5), pp.367–384.

Kamiński, M.M. *et al.*, 2012. T cell Activation Is Driven by an ADP-Dependent Glucokinase Linking Enhanced Glycolysis with Mitochondrial Reactive Oxygen Species Generation. *Cell Reports*, 2(5), pp.1300–1315.

Kanfi, Y. *et al.*, 2008. Regulation of SIRT1 protein levels by nutrient availability. *FEBS letters*, 582(16), pp.2417–23.

Kanfi, Y. *et al.*, 2012. The sirtuin SIRT6 regulates lifespan in male mice. *Nature*, 483(7388), pp.218–221.

Kanzok, S.M. *et al.*, 2001. Substitution of the thioredoxin system for glutathione reductase in Drosophila melanogaster. *Science (New York, N.Y.)*, 291(5504), pp.643–6.

Kapahi, P. *et al.*, 2004. Regulation of lifespan in Drosophila by modulation of genes in the TOR signaling pathway. *Current biology : CB*, 14(10), pp.885–90.

Karlenius, T.C. & Tonissen, K.F., 2010. Thioredoxin and Cancer: A Role for Thioredoxin in all States of Tumor Oxygenation. *Cancers*, 2(2), pp.209–32.

Kawahara, N. *et al.*, 1996. Enhanced coexpression of thioredoxin and high mobility group protein 1 genes in human hepatocellular carcinoma and the possible association with decreased sensitivity to cisplatin. *Cancer Res*, 56(23), pp.5330–5333.

Kawahara, T.L.A. *et al.*, 2009. SIRT6 links histone H3 lysine 9 deacetylation to NF-kappaB-dependent gene expression and organismal life span. *Cell*, 136(1), pp.62–74.

Kemnitz, J.W. *et al.*, 1994. Dietary restriction increases insulin sensitivity and lowers blood glucose in rhesus monkeys. *The American journal of physiology*, 266(4 Pt 1), pp.E540–7.

Kenyon, C. *et al.*, 1993. A C. elegans mutant that lives twice as long as wild type. *Nature*, 366(6454), pp.461–4.

Kenyon, C., 2005. The plasticity of aging: insights from long-lived mutants. *Cell*, 120(4), pp.449–460.

Kim, S.Y. *et al.*, 2007. Diverse functions of VDUP1 in cell proliferation, differentiation, and diseases. *Cell Mol Immunol*, 4(5), pp.345–351.

Koga, H., Kaushik, S. & Cuervo, A.M., 2011. Protein homeostasis and aging: The importance of exquisite quality control. *Ageing research reviews*, 10(2), pp.205–15.

Krammer, P.H. *et al.*, 2007. No life without death. *Adv Cancer Res*, 97, pp.111–138.

Krishan, A., 1975. Rapid flow cytofluorometric analysis of mammalian cell cycle by propidium iodide staining. *The Journal of cell biology*, 66(1), pp.188–93.

Krishnamurthy, J. *et al.*, 2004. Ink4a/Arf expression is a biomarker of aging. *The Journal of clinical investigation*, 114(9), pp.1299–307.

Kruegel, U. *et al.*, 2011. Elevated proteasome capacity extends replicative lifespan in Saccharomyces cerevisiae. *PLoS genetics*, 7(9), p.e1002253.

Kuilman, T. *et al.*, 2010. The essence of senescence. *Genes & development*, 24(22), pp.2463–79.

Kuningas, M. *et al.*, 2007. Haplotypes in the human Foxo1a and Foxo3a genes; impact on disease and mortality at old age. *Eur J Hum Genet*, 15(3), pp.294–301.

Kwon, J. *et al.*, 2010. The nonphagocytic NADPH oxidase Duox1 mediates a positive feedback loop during T cell receptor signaling. *Sci Signal*, 3(133), p.ra59.

Ladenstein, R. *et al.*, 1979. Structure analysis and molecular model of the selenoenzyme glutathione peroxidase at 2.8 Å resolution. *Journal of Molecular Biology*, 134(2), pp.199–218.

Laemmli, U.K., 1970. Cleavage of structural proteins during the assembly of the head of bacteriophage T4. *Nature*, 227(5259), pp.680–5.

Landis, G.N. & Tower, J., 2005. Superoxide dismutase evolution and life span regulation. *Mech Ageing Dev*, 126(3), pp.365–379.

Lane, M.A. *et al.*, 1992. Dietary restriction in nonhuman primates: progress report on the NIA study. *Annals of the New York Academy of Sciences*, 673, pp.36–45.

Lansdorp, P.M. *et al.*, 1994. Age-related decline in proliferative potential of purified stem cell candidates. *Blood Cells*, 20(2-3), pp.371–376.

Laplante, M. & Sabatini, D.M., 2012. mTOR signaling in growth control and disease. *Cell*, 149(2), pp.274–93.

Larson, K. *et al.*, 2012. Heterochromatin formation promotes longevity and represses ribosomal RNA synthesis. *PLoS genetics*, 8(1), p.e1002473.

Larsson, N.-G., 2010. Somatic mitochondrial DNA mutations in mammalian aging. *Annual review of biochemistry*, 79, pp.683–706.

Lavasani, M. *et al.*, 2012. Muscle-derived stem/progenitor cell dysfunction limits healthspan and lifespan in a murine progeria model. *Nature communications*, 3, p.608.

Lee, B.-H. *et al.*, 2010. Enhancement of proteasome activity by a small-molecule inhibitor of USP14. *Nature*, 467(7312), pp.179–84.

Lee, I.H. *et al.*, 2008. A role for the NAD-dependent deacetylase Sirt1 in the regulation of autophagy. *Proceedings of the National Academy of Sciences of the United States of America*, 105(9), pp.3374–9.

Lee, S. *et al.*, 2014. Thioredoxin-interacting protein regulates protein disulfide isomerases and endoplasmic reticulum stress. *EMBO molecular medicine*, 6(6), pp.732–43.

Lerner, A.G. *et al.*, 2012. IRE1α induces thioredoxin-interacting protein to activate the NLRP3 inflammasome and promote programmed cell death under irremediable ER stress. *Cell metabolism*, 16(2), pp.250–64.

Levendusky, M.C. *et al.*, 2009. Expression and regulation of vitamin D3 upregulated protein 1 (VDUP1) is conserved in mammalian and insect brain. *J Comp Neurol*, 517(5), pp.581–600.

Linford, N.J. *et al.*, 2013. Measurement of lifespan in Drosophila melanogaster. *Journal of visualized experiments : JoVE*, (71).

Linton, P.J. & Dorshkind, K., 2004. Age-related changes in lymphocyte development and function. *Nat Immunol*, 5(2), pp.133–139.

Loeb, J. & Northrop, J.H., 1916. Is There a Temperature Coefficient for the Duration of Life? *Proceedings of the National Academy of Sciences of the United States of America*, 2(8), pp.456–7.

López-Otín, C. *et al.*, 2013. The hallmarks of aging. *Cell*, 153(6), pp.1194–217.

Lord, C.J. & Ashworth, A., 2012. The DNA damage response and cancer therapy. *Nature*, 481(7381), pp.287–94.

Lu, J. & Holmgren, A., 2014. The thioredoxin antioxidant system. *Free radical biology & medicine*, 66, pp.75–87.

Magwere, T., Chapman, T. & Partridge, L., 2004. Sex Differences in the Effect of Dietary Restriction on Life Span and Mortality Rates in Female and Male Drosophila Melanogaster. *The Journals of Gerontology Series A: Biological Sciences and Medical Sciences*, 59(1), pp.B3–B9.

Mandalaywala, N. V *et al.*, 2008. The tumor suppressor, vitamin D3 up-regulated protein 1 (VDUP1), functions downstream of REPO during Drosophila gliogenesis. *Dev Biol*, 315(2), pp.489–504.

Masoro, E.J., 2005. Overview of caloric restriction and ageing. *Mech Ageing Dev*, 126(9), pp.913–922.

Masutani, H. *et al.*, 2012. Thioredoxin binding protein (TBP)-2/Txnip and α-arrestin proteins in cancer and diabetes mellitus. *Journal of clinical biochemistry and nutrition*, 50(1), pp.23–34.

McCarty, M.F., 2004. Chronic activation of AMP-activated kinase as a strategy for slowing aging. *Med Hypotheses*, 63(2), pp.334–339.

McLennan, H.R. & Degli Esposti, M., 2000. The contribution of mitochondrial respiratory complexes to the production of reactive oxygen species. *J Bioenerg Biomembr*, 32(2), pp.153–162.

Melov, S. *et al.*, 1999. Mitochondrial disease in superoxide dismutase 2 mutant mice. *Proceedings of the National Academy of Sciences of the United States of America*, 96(3), pp.846–51.

Migliaccio, E. *et al.*, 1999. The p66shc adaptor protein controls oxidative stress response and life span in mammals. *Nature*, 402(6759), pp.309–13.

Miller, R.A. *et al.*, 2011. Rapamycin, but not resveratrol or simvastatin, extends life span of genetically heterogeneous mice. *The journals of gerontology. Series A, Biological sciences and medical sciences*, 66(2), pp.191–201.

Miller, R.A., 1996. The aging immune system: primer and prospectus. *Science*, 273(5271), pp.70–74.

Minn, A.H., Hafele, C. & Shalev, A., 2005. Thioredoxin-interacting protein is stimulated by glucose through a carbohydrate response element and induces beta-cell apoptosis. *Endocrinology*, 146(5), pp.2397–2405.

Miquel, J. *et al.*, 1980. Mitochondrial role in cell aging. *Experimental gerontology*, 15(6), pp.575–91.

Mizushima, N. *et al.*, 2008. Autophagy fights disease through cellular self-digestion. *Nature*, 451(7182), pp.1069–75.

Morrison, J.A. *et al.*, 2014. Thioredoxin interacting protein (TXNIP) is a novel tumor suppressor in thyroid cancer. *Molecular cancer*, 13, p.62.

Morrow, G. *et al.*, 2004. Overexpression of the small mitochondrial Hsp22 extends Drosophila life span and increases resistance to oxidative stress. *FASEB journal : official publication of the Federation of American Societies for Experimental Biology*, 18(3), pp.598–9.

Morselli, E. *et al.*, 2010. Caloric restriction and resveratrol promote longevity through the Sirtuin-1-dependent induction of autophagy. *Cell death & disease*, 1, p.e10.

Moskalev, A.A. *et al.*, 2013. The role of DNA damage and repair in aging through the prism of Koch-like criteria. *Ageing research reviews*, 12(2), pp.661–84.

Mostoslavsky, R. *et al.*, 2006. Genomic instability and aging-like phenotype in the absence of mammalian SIRT6. *Cell*, 124(2), pp.315–29.

Muqit, M.M.K. & Feany, M.B., 2002. Modelling neurodegenerative diseases in Drosophila: a fruitful approach? *Nature reviews. Neuroscience*, 3(3), pp.237–43.

Murphy, M.P., 2009. How mitochondria produce reactive oxygen species. *The Biochemical journal*, 417(1), pp.1–13.

Nakamura, H. *et al.*, 1992. Expression and growth-promoting effect of adult T-cell leukemia-derived factor. A human thioredoxin homologue in hepatocellular carcinoma. *Cancer*, 69(8), pp.2091–2097.

Nelson, G. *et al.*, 2012. A senescent cell bystander effect: senescence-induced senescence. *Aging cell*, 11(2), pp.345–9.

Nishiyama, A. *et al.*, 1999. Identification of thioredoxin-binding protein-2/vitamin D(3) up-regulated protein 1 as a negative regulator of thioredoxin function and expression. *J Biol Chem*, 274(31), pp.21645–21650.

Nisoli, E. *et al.*, 2005. Calorie restriction promotes mitochondrial biogenesis by inducing the expression of eNOS. *Science (New York, N.Y.)*, 310(5746), pp.314–7.

Oka, S. *et al.*, 2006. Impaired fatty acid utilization in thioredoxin binding protein-2 (TBP-2)-deficient mice: a unique animal model of Reye syndrome. *FASEB J*, 20(1), pp.121–123.

Orr, W.C. & Sohal, R.S., 1994. Extension of life-span by overexpression of superoxide dismutase and catalase in Drosophila melanogaster. *Science*, 263(5150), pp.1128–1130.

Orsini, F. *et al.*, 2004. The life span determinant p66Shc localizes to mitochondria where it associates with mitochondrial heat shock protein 70 and regulates trans-membrane potential. *The Journal of biological chemistry*, 279(24), pp.25689–95.

Ortega-Molina, A. *et al.*, 2012. Pten positively regulates brown adipose function, energy expenditure, and longevity. *Cell metabolism*, 15(3), pp.382–94.

Osborne, T.B., Mendel, L.B. & Ferry, E.L., 1917. The Effect of Retardation of Growth Upon the Breeding Period and Duration of Life of Rats. *Science*, 45(1160), pp.294–295.

Oslowski, C.M. *et al.*, 2012. Thioredoxin-interacting protein mediates ER stress-induced β cell death through initiation of the inflammasome. *Cell metabolism*, 16(2), pp.265–73.

Ozgenc, A. & Loeb, L.A., 2006. Werner Syndrome, aging and cancer. *Genome Dyn*, 1, pp.206–217.

Parikh, H. *et al.*, 2007. TXNIP regulates peripheral glucose metabolism in humans. *PLoS Med*, 4(5), p.e158.

Patwari, P. *et al.*, 2006. The interaction of thioredoxin with Txnip. Evidence for formation of a mixed disulfide by disulfide exchange. *J Biol Chem*, 281(31), pp.21884–21891.

Patwari, P. *et al.*, 2009. Thioredoxin-independent regulation of metabolism by the alpha-arrestin proteins. *J Biol Chem*, 284(37), pp.24996–25003.

Pearson, K.J. *et al.*, 2008. Resveratrol delays age-related deterioration and mimics transcriptional aspects of dietary restriction without extending life span. *Cell Metab*, 8(2), pp.157–168.

Pellicena-Pallé, A., Stitzinger, S.M. & Salz, H.K., 1997. The function of the Drosophila thioredoxin homologue encoded by the deadhead gene is redox-dependent and blocks the initiation of development but not DNA synthesis. *Mechanisms of development*, 62(1), pp.61–5.

Pfaffl, M.W., 2001. A new mathematical model for relative quantification in real-time RT-PCR. *Nucleic acids research*, 29(9), p.e45.

Piper, M.D.W. *et al.*, 2011. Dietary Restriction and Aging: A Unifying Perspective. *Cell Metabolism*, 14(2), pp.154–160.

Powers, E.T. *et al.*, 2009. Biological and chemical approaches to diseases of proteostasis deficiency. *Annual review of biochemistry*, 78, pp.959–91.

Qiao, S. *et al.*, 2015. A REDD1/TXNIP pro-oxidant complex regulates ATG4B activity to control stress-induced autophagy and sustain exercise capacity. *Nature communications*, 6, p.7014.

Rämet, M. *et al.*, 2002. Functional genomic analysis of phagocytosis and identification of a Drosophila receptor for E. coli. *Nature*, 416(6881), pp.644–8.

Ran, F.A. *et al.*, 2013. Genome engineering using the CRISPR-Cas9 system. *Nature protocols*, 8(11), pp.2281–308.

Van Remmen, H. *et al.*, 2003. Life-long reduction in MnSOD activity results in increased DNA damage and higher incidence of cancer but does not accelerate aging. *Physiological genomics*, 16(1), pp.29–37.

Rena, G., Pearson, E.R. & Sakamoto, K., 2013. Molecular mechanism of action of metformin: old or new insights? *Diabetologia*, 56(9), pp.1898–906.

Renner, O. & Carnero, A., 2009. Mouse models to decipher the PI3K signaling network in human cancer. *Current molecular medicine*, 9(5), pp.612–25.

Rera, M. *et al.*, 2011. Modulation of longevity and tissue homeostasis by the Drosophila PGC-1 homolog. *Cell metabolism*, 14(5), pp.623–34.

Ressler, S. *et al.*, 2006. p16INK4A is a robust in vivo biomarker of cellular aging in human skin. *Aging cell*, 5(5), pp.379–89.

Rhee, S.G. *et al.*, 2001. Peroxiredoxin, a novel family of peroxidases. *IUBMB life*, 52(1-2), pp.35–41.

Rodgers, J.T. *et al.*, 2005. Nutrient control of glucose homeostasis through a complex of PGC-1alpha and SIRT1. *Nature*, 434(7029), pp.113–8.

Rogina, B., 2011. For the special issue: aging studies in Drosophila melanogaster. *Experimental gerontology*, 46(5), pp.317–9.

Rogina, B. & Helfand, S.L., 2004. Sir2 mediates longevity in the fly through a pathway related to calorie restriction. *Proceedings of the National Academy of Sciences of the United States of America*, 101(45), pp.15998–6003.

Rossi, D.J. *et al.*, 2007. Deficiencies in DNA damage repair limit the function of haematopoietic stem cells with age. *Nature*, 447(7145), pp.725–9.

Röth, D., Krammer, P.H. & Gülow, K., 2014. Dynamin related protein 1-dependent mitochondrial fission regulates oxidative signalling in T cells. *FEBS Letters*, 588(9), pp.1749–1754.

Rothgiesser, K.M. *et al.*, 2010. SIRT2 regulates NF-κB dependent gene expression through deacetylation of p65 Lys310. *Journal of cell science*, 123(Pt 24), pp.4251–8.

Rubinsztein, D.C., Mariño, G. & Kroemer, G., 2011. Autophagy and aging. *Cell*, 146(5), pp.682–95.

Salminen, A. & Kaarniranta, K., 2009. SIRT1: regulation of longevity via autophagy. *Cellular signalling*, 21(9), pp.1356–60.

Salminen, A., Kaarniranta, K. & Kauppinen, A., 2012. Inflammaging: disturbed interplay between autophagy and inflammasomes. *Aging*, 4(3), pp.166–75.

Salz, H.K. *et al.*, 1994. The Drosophila maternal effect locus deadhead encodes a thioredoxin homolog required for female meiosis and early embryonic development. *Genetics*, 136(3), pp.1075–86.

Sanger, F., Nicklen, S. & Coulson, A.R., 1977. DNA sequencing with chain-terminating inhibitors. *Proceedings of the National Academy of Sciences of the United States of America*, 74(12), pp.5463–7.

Sass, S., 2010. *The control of stress resistance in aged cells*. University of Heidelberg.

Savitsky, K. *et al.*, 1995. A single ataxia telangiectasia gene with a product similar to PI-3 kinase. *Science*, 268(5218), pp.1749–1753.

Saxena, G., Chen, J. & Shalev, A., 2010. Intracellular shuttling and mitochondrial function of thioredoxin-interacting protein. *J Biol Chem*, 285(6), pp.3997–4005.

Schneider, I., 1972. Cell lines derived from late embryonic stages of Drosophila melanogaster. *Journal of embryology and experimental morphology*, 27(2), pp.353–365.

Schroder, K., Zhou, R. & Tschopp, J., 2010. The NLRP3 inflammasome: a sensor for metabolic danger? *Science*, 327(5963), pp.296–300.

Schulze, P.C. *et al.*, 2004. Hyperglycemia promotes oxidative stress through inhibition of thioredoxin function by thioredoxin-interacting protein. *J Biol Chem*, 279(29), pp.30369–30374.

Schwarze, S.R., Weindruch, R. & Aiken, J.M., 1998. Oxidative stress and aging reduce COX I RNA and cytochrome oxidase activity in Drosophila. *Free Radic Biol Med*, 25(6), pp.740–747.

Selman, C. *et al.*, 2009. Ribosomal protein S6 kinase 1 signaling regulates mammalian life span. *Science*, 326(5949), pp.140–144.

Sena, L.A. & Chandel, N.S., 2012. Physiological roles of mitochondrial reactive oxygen species. *Molecular cell*, 48(2), pp.158–67.

Shao, L. *et al.*, 2011. Reactive oxygen species and hematopoietic stem cell senescence. *International journal of hematology*, 94(1), pp.24–32.

Sharp, Z.D., 2011. Aging and TOR: interwoven in the fabric of life. *Cellular and molecular life sciences : CMLS*, 68(4), pp.587–97.

Sharpless, N.E. & DePinho, R.A., 2007. How stem cells age and why this makes us grow old. *Nat Rev Mol Cell Biol*, 8(9), pp.703–713.

Sheth, S.S. *et al.*, 2006. Hepatocellular carcinoma in Txnip-deficient mice. *Oncogene*, 25(25), pp.3528–3536.

Sheth, S.S. *et al.*, 2005. Thioredoxin-interacting protein deficiency disrupts the fasting-feeding metabolic transition. *J Lipid Res*, 46(1), pp.123–134.

Siebold, A.P. *et al.*, 2010. Polycomb Repressive Complex 2 and Trithorax modulate Drosophila longevity and stress resistance. *Proceedings of the National Academy of Sciences of the United States of America*, 107(1), pp.169–74.

Slack, C. *et al.*, 2011. dFOXO-independent effects of reduced insulin-like signaling in Drosophila. *Aging cell*, 10(5), pp.735–48.

Slack, C. *et al.*, 2015. The Ras-Erk-ETS-Signaling Pathway Is a Drug Target for Longevity. *Cell*, 162(1), pp.72–83.

Sohal, R.S. *et al.*, 1994. Effect of age and caloric restriction on DNA oxidative damage in different tissues of C57BL/6 mice. *Mech Ageing Dev*, 76(2-3), pp.215–224.

Sohal, R.S. & Weindruch, R., 1996. Oxidative stress, caloric restriction, and aging. *Science*, 273(5271), pp.59–63.

Sousounis, K., Baddour, J.A. & Tsonis, P.A., 2014. Aging and regeneration in vertebrates. *Current topics in developmental biology*, 108, pp.217–46.

Speakman, J.R. & Mitchell, S.E., 2011. Caloric restriction. *Molecular aspects of medicine*, 32(3), pp.159–221.

Stadtman, E.R., 1992. Protein oxidation and aging. *Science*, 257(5074), pp.1220–1224.

Stuart, J.A. *et al.*, 2014. A midlife crisis for the mitochondrial free radical theory of aging. *Longevity & healthspan*, 3(1), p.4.

Sun, H.-Y. *et al.*, 2015. Age-related changes in mitochondrial antioxidant enzyme Trx2 and TXNIP-Trx2-ASK1 signal pathways in the auditory cortex of a mimetic aging rat model: changes to Trx2 in the auditory cortex. *The FEBS journal*, 282(14), pp.2758–74.

Sun, J. *et al.*, 2002. Induced overexpression of mitochondrial Mn-superoxide dismutase extends the life span of adult Drosophila melanogaster. *Genetics*, 161(2), pp.661–72.

Svensson, M.J. *et al.*, 2003. The ThioredoxinT and deadhead gene pair encode testis- and ovary-specific thioredoxins in Drosophila melanogaster. *Chromosoma*, 112(3), pp.133–43.

Svensson, M.J. & Larsson, J., 2007. Thioredoxin-2 affects lifespan and oxidative stress in Drosophila. *Hereditas*, 144(1), pp.25–32.

Tatar, M. *et al.*, 2001. A mutant Drosophila insulin receptor homolog that extends life-span and impairs neuroendocrine function. *Science (New York, N.Y.)*, 292(5514), pp.107–10.

Tebay, L.E. *et al.*, 2015. Mechanisms of activation of the transcription factor Nrf2 by redox stressors, nutrient cues, and energy status and the pathways through which it attenuates degenerative disease. *Free radical biology & medicine*.

Tissenbaum, H.A. & Guarente, L., 2001. Increased dosage of a sir-2 gene extends lifespan in Caenorhabditis elegans. *Nature*, 410(6825), pp.227–30.

Tomaru, U. *et al.*, 2012. Decreased proteasomal activity causes age-related phenotypes and promotes the development of metabolic abnormalities. *The American journal of pathology*, 180(3), pp.963–72.

Trifunovic, A. *et al.*, 2005. Somatic mtDNA mutations cause aging phenotypes without affecting reactive oxygen species production. *Proceedings of the National Academy of Sciences of the United States of America*, 102(50), pp.17993–8.

Tsuda, A. *et al.*, 2010. Spectroscopic visualization of sound-induced liquid vibrations using a supramolecular nanofibre. *Nat Chem*, 2(11), pp.977–983.

Tsuda, M. *et al.*, 2010. Loss of Trx-2 enhances oxidative stress-dependent phenotypes in Drosophila. *FEBS letters*, 584(15), pp.3398–401.

Valko, M. *et al.*, 2007. Free radicals and antioxidants in normal physiological functions and human disease. *Int J Biochem Cell Biol*, 39(1), pp.44–84.

Villeponteau, B., 1997. The heterochromatin loss model of aging. *Experimental gerontology*, 32(4-5), pp.383–94.

Viña, J. *et al.*, 1992. Effect of aging on glutathione metabolism. Protection by antioxidants. *EXS*, 62, pp.136–44.

Waldmann, H. & Lefkovits, I., 1984. Limiting dilution analysis of cells of the immune system II: What can be learnt? *Immunology today*, 5(10), pp.295–8.

Walker, G.A. & Lithgow, G.J., 2003. Lifespan extension in C. elegans by a molecular chaperone dependent upon insulin-like signals. *Aging cell*, 2(2), pp.131–9.

Wang, C. *et al.*, 2009. DNA damage response and cellular senescence in tissues of aging mice. *Aging cell*, 8(3), pp.311–23.

Wang, L. & Jones, D.L., 2011. The effects of aging on stem cell behavior in Drosophila. *Experimental gerontology*, 46(5), pp.340–4.

Wang, M. *et al.*, 2010. Involvement of NADPH oxidase in age-associated cardiac remodeling. *Journal of Molecular and Cellular Cardiology*, 48(4), pp.765–772.

Wang, Y., De Keulenaer, G.W. & Lee, R.T., 2002. Vitamin D(3)-up-regulated protein-1 is a stress-responsive gene that regulates cardiomyocyte viability through interaction with thioredoxin. *J Biol Chem*, 277(29), pp.26496–26500.

Watanabe, R. *et al.*, 2010. Anti-oxidative, anti-cancer and anti-inflammatory actions by thioredoxin 1 and thioredoxin-binding protein-2. *Pharmacol Ther*, 127(3), pp.261–270.

Westerheide, S.D. *et al.*, 2009. Stress-inducible regulation of heat shock factor 1 by the deacetylase SIRT1. *Science*, 323(5917), pp.1063–1066.

Weyand, C.M. *et al.*, 2009. Rejuvenating the immune system in rheumatoid arthritis. *Nat Rev Rheumatol*, 5(10), pp.583–588.

Weyand, C.M., Yang, Z. & Goronzy, J.J., 2014. T-cell aging in rheumatoid arthritis. *Current opinion in rheumatology*, 26(1), pp.93–100.

Whisler, R.L. *et al.*, 1998. Phosphorylation and coupling of zeta-chains to activated T-cell receptor (TCR)/CD3 complexes from peripheral blood T-cells of elderly humans. *Mech Ageing Dev*, 105(1-2), pp.115–135.

Whisler, R.L. *et al.*, 1991. Signal transduction in human B cells during aging: alterations in stimulus-induced phosphorylations of tyrosine and serine/threonine substrates and in cytosolic calcium responsiveness. *Lymphokine Cytokine Res*, 10(6), pp.463–473.

Whisler, R.L., Beiqing, L. & Chen, M., 1996. Age-related decreases in IL-2 production by human T cells are associated with impaired activation of nuclear transcriptional factors AP-1 and NF-AT. *Cell Immunol*, 169(2), pp.185–195.

Wilkinson, J.E. *et al.*, 2012. Rapamycin slows aging in mice. *Aging cell*, 11(4), pp.675–82.

Willcox, B.J. *et al.*, 2008. FOXO3A genotype is strongly associated with human longevity. *Proc Natl Acad Sci U S A*, 105(37), pp.13987–13992.

Williams, M.D. *et al.*, 1998. Increased Oxidative Damage Is Correlated to Altered Mitochondrial Function in Heterozygous Manganese Superoxide Dismutase Knockout Mice. *Journal of Biological Chemistry*, 273(43), pp.28510–28515.

Williamson, J.R., 1986. Role of inositol lipid breakdown in the generation of intracellular signals. State of the art lecture. *Hypertension*, 8(6 Pt 2), pp.II140–56.

Wood, J.G. *et al.*, 2004. Sirtuin activators mimic caloric restriction and delay ageing in metazoans. *Nature*, 430(7000), pp.686–689.

Wood, Z.A. *et al.*, 2003. Structure, mechanism and regulation of peroxiredoxins. *Trends in Biochemical Sciences*, 28(1), pp.32–40.

Wu, N. *et al.*, 2013. AMPK-dependent degradation of TXNIP upon energy stress leads to enhanced glucose uptake via GLUT1. *Molecular cell*, 49(6), pp.1167–75.

Wu, Z. *et al.*, 1999. Mechanisms Controlling Mitochondrial Biogenesis and Respiration through the Thermogenic Coactivator PGC-1. *Cell*, 98(1), pp.115–124.

Xie, J., Zhang, X. & Zhang, L., 2013. Negative regulation of inflammation by SIRT1. *Pharmacological Research*, 67(1), pp.60–67.

Yang, X., Young, L.H. & Voigt, J.M., 1998. Expression of a vitamin D-regulated gene (VDUP-1) in untreated- and MNU-treated rat mammary tissue. *Breast cancer research and treatment*, 48(1), pp.33–44.

Yoshihara, E., Fujimoto, S., *et al.*, 2010. Disruption of TBP-2 ameliorates insulin sensitivity and secretion without affecting obesity. *Nature communications*, 1, p.127.

Yoshihara, E., Chen, Z., *et al.*, 2010. Thiol redox transitions by thioredoxin and thioredoxin-binding protein-2 in cell signaling. *Methods in enzymology*, 474, pp.67–82.

Yoshihara, E. *et al.*, 2014. Thioredoxin/Txnip: redoxisome, as a redox switch for the pathogenesis of diseases. *Frontiers in immunology*, 4, p.514.

Yoshioka, J. *et al.*, 2007. Targeted deletion of thioredoxin-interacting protein regulates cardiac dysfunction in response to pressure overload. *Circ Res*, 101(12), pp.1328–1338.

Yu, F.X. & Luo, Y., 2009. Tandem ChoRE and CCAAT motifs and associated factors regulate Txnip expression in response to glucose or adenosine-containing molecules. *PLoS One*, 4(12), p.e8397.

Zhang, C. & Cuervo, A.M., 2008. Restoration of chaperone-mediated autophagy in aging liver improves cellular maintenance and hepatic function. *Nature medicine*, 14(9), pp.959–65.

Zhang, G. *et al.*, 2013. Hypothalamic programming of systemic ageing involving IKK-β, NF-κB and GnRH. *Nature*, 497(7448), pp.211–6.

Zhang, P. *et al.*, 2010. The ubiquitin ligase itch regulates apoptosis by targeting thioredoxin-interacting protein for ubiquitin-dependent degradation. *J Biol Chem*, 285(12), pp.8869–8879.

Zhang, Y. *et al.*, 2009. Mice deficient in both Mn superoxide dismutase and glutathione peroxidase-1 have increased oxidative damage and a greater incidence of pathology but no reduction in longevity. *The journals of gerontology. Series A, Biological sciences and medical sciences*, 64(12), pp.1212–20.

Zhang, Z. *et al.*, 2010. Roles of SIRT1 in the acute and restorative phases following induction of inflammation. *The Journal of biological chemistry*, 285(53), pp.41391–401.

Zhou, R. *et al.*, 2010. Thioredoxin-interacting protein links oxidative stress to inflammasome activation. *Nat Immunol*, 11(2), pp.136–140.

Zou, S. *et al.*, The prolongevity effect of resveratrol depends on dietary composition and calorie intake in a tephritid fruit fly. *Experimental gerontology*, 44(6-7), pp.472–6.

LIST OF FIGURES

LIST OF TABLES

ABBREVIATIONS

ADP	Adenosine diphosphate
ADPGK	ADP-dependent glucokinase
AMP	Adenosine monophosphate
AMPK	AMP-activated protein kinase
APS	Ammoniumpersulfate
ASK1	Apoptosis signal-regulating kinase 1
A-T	Ataxia telangiectasia
ATM	Ataxia telangiectasia mutated
ATP	Adenosine triphosphate
BLAST	Basic Local Alignment Search Tool
CD95L	Cluster of differentiation 95 ligand
CDK	Cyclin-dependent kinase
CDKN1B	Cyclin-dependent kinase inhibitor 1B
cDNA	Copy DNA
ChoRE	Carbohydrate response elements
Ci	Cubitus interruptus
CIP	Calf intestine phosphatase
COP9	Constitutive photomorphogenesis 9
COPS5	COP9 signalosome subunit 5
COX1	Cyclooxygenase 1
CR	Caloric restriction
CSA	Cockayne syndrome type A
CSB	Cockayne syndrome type B
Cyt c	Cytochrome c
DAG	Diacylglycerol
DHD	Deadhead
DMSO	Dimethylsulfoxide
DNA	Deoxyribonucleic acid
dNTP	deoxynucleoside
DR	Dietary restriction
Drp1	Dynamin-related protein 1

Duox1	Dual oxidase 1
ECL	Enhanced chemiluminescence
ELISA	Enzyme-linked immunosorbent assay
ER	Endoplasmatic reticulum
ERK	extracellular-signal-regulated kinase
ETC	Electron transport chain
ETS	E-twenty six
EV	Empty vector
$FADH_2$	Flavin adenine dinucleotide
FCHL	Familial combined hyperlipidemia
FCS	Fetal calf serum
FGF2	Fibroblast growth factor 2
FOXO	Forkhead box O
FSC	Forward scatter
GnRH	Gonadotropin-releasing hormone
Gpx	Glutathione peroxidase
GSH	Glutathione
H_2DCFDA	2'-7'- dichlorodihydrofluorescein diacetate
HGPS	Hutchinson-Gilford progeria syndrome
Hh	Hedgehog
HRP	Horseradish peroxidase
HSF	Heat shock factor
HSP70	Heat shock protein 70
Ig	Immune globulin
IGF-1	Insulin-like growth factor 1
IIS	insulin and IGF-1 signaling pathway
IL	Interleukin
IP_3	Inositol-1,4,5- trisphosphate
iPSC	Induced pluripotent stem cells
IRE1α	Inositol-requiring enzyme 1α
kDa	Kilo Dlaton
LAMP2a	Lysosome-associated membrane protein 2
LAT	Linke of activated T cells
LB	Lysogene broth

LPC	Laminar precursor cells
MDM2	Mouse double minute 2
MEK	Mitogen/extracellular signal-regulated kinase
MFI	Mean fluorescence intensity
MFRTA	Mitochondrial free radical theory of aging
Mlx	Max-like protein
MnSOD	Manganese superoxide mismutase
mRNA	Messenger ribonucleic acid
mtDNA	Mitochondrial DNA
NAD	Nicotinamide adenine dinucleotide
NADH	Nicotinamide adenine dinucleotide
NADPH	Nicotinamide adenine dinucleotide phosphate
NCBI	National Center for Biotechnology Information
NF-Y	Nuclear factor Y
NF-κB	Nuclear factor kappa-light-chain-enhancer of activated B cells
NLRP3	NOD-like receptor family pyrin domain containing 3
NOD	Non-obese diabetic
NOX	NADPH oxidases NOX
Nrf2	Nuclear factor-erythroid 2 p45-related factor 2
OD	Optical density
PAGE	Polyacylamide gel electrophoresis
PBS	Phosphate-buffered saline
PCR	Polymerase chain reaction
PDI	Peptide disulfide isomerases
PERK	Protein kinase RNA-like endoplasmic reticulum kinase
PGC-1α	PPARγ coactivator 1α
PI	Propidium iodide
PI3K	Phosphatidylinositol-3-kinase
PKB	Protein kinase B
PKCθ	Protein kinase C θ
PLCγ1	phospholipase Cγ1
PMX 464	4-(2-Benzothiazolyl)-4-hydroxy-2,5-cyclohexadien-1-one
PNK	Polynucleotide kinase
PPARγ	peroxisome proliferator-activated receptor γ

PQ	Paraquat
PVDF	Polyvinylidene fluoride
Q	Ubiquinone
qRT-PCR	Quantitative real time PCR
RA	Rheumatoid arthritis
REDD1	Regulated in development and DNA damage responses 1
REPO	Reverse polarity
rH	Relative humidity
RIPA	Radioimmunoprecipitation assay lysis buffer
RNA	Ribonucleic acid
RNS	Reactive nitrogen species
ROS	Reactive oxygen species
rpm	Rounds per minute
RT	Room temperature
S6K1	S6 protein kinase 1
SD	Standard deviation
SDS	Sodiumdodecylsulfate
SEM	Standard error of the mean
shRNA	Short hairpin RNA
SIR	Silent information regulator
SOD	Superoxide dismutase
SSC	Sideward scatter
STAC	Sirtuin-activating compounds
TCR	T cell receptor
TEMED	Tetramethylethylenediamine
T_m	Melting temperature
TNFα	Tumor necrosis factor α
TOR	Target of rapamycin
Trx	Thioredoxin
TrxR	Thioredoxin reductase
TrxT	Thioredoxin T
TXNIP	Thioredoxin-interacting protein
UAS	Upstream activator sequence
UPR	Unfolded protein response

UT	untransfected
VDRC	Vienna Drosophila Research Center
VDUP1	vitamin D_3-upregulated protein 1
WRN	Werner syndrome
WT	wildtype
ZAP70	Zeta chain-associated protein kinase 70
α-	Anti-
γ-GCS	γ-glutamyl cysteine synthetase

APPENDIX

A

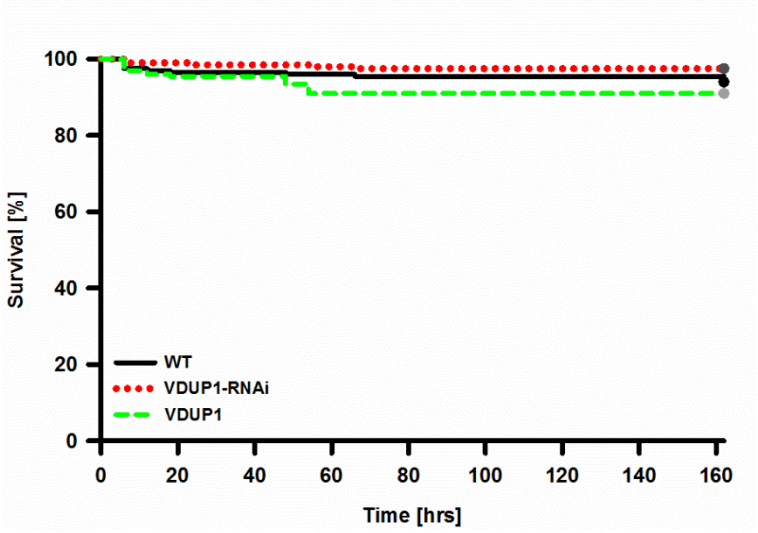

B

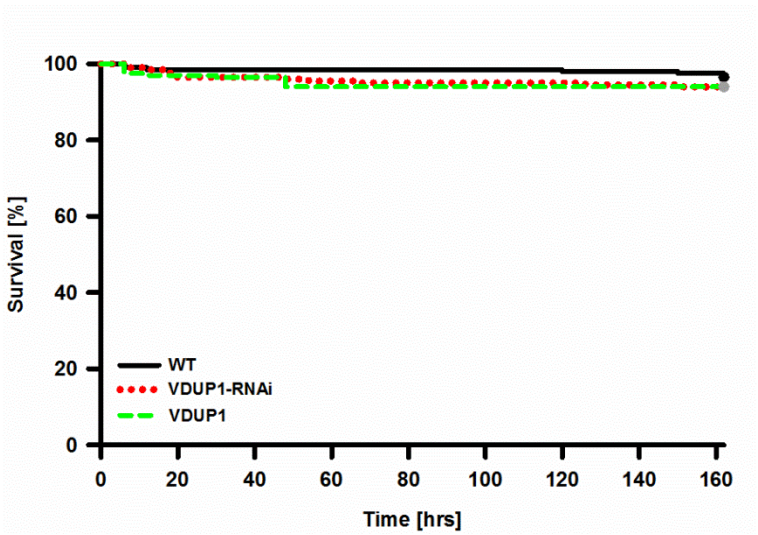

Supplementary Figure 1: Sucrose treatment had no effect on survival.
Male **(A)** or female **(B)** flies were transferred to vials containing 5 % sucrose. Flies were monitored for 160 hrs and dead flies were recorded every 6-12 hrs. Survival differences between groups were tested in each sex using log-rank test and showed no statistical significance ($p>0.05$).

Supplementary table 1: Comparison of human and *Drosophila* homologs.

Human	*Drosophila*
Trx(1)	TRX-2
Trx2	No homologue
TXNIP	VDUP-1